Evidence of euxinia in the Norian of western Canada: Implications to halobiid and monotid paleoecology and the sedimentology of the Pardonet formation.

by

Riley Cole Morton

A thesis submitted in partial fulfillment of the requirements for the degree of

Master of Science

Earth and Atmospheric Sciences
University of Alberta

ABSTRACT

The Norian Pardonet formation tops a well-studied Triassic stratigraphy in Western Canada which can be viewed in outcrop along the shores of Williston Lake, B. C. The Pardonet itself, however, has remained rather enigmatic. The formation is composed of dominantly fine-grained, organic-rich limestone and shale complicated by the occurrence of dense, monospecific bivalve shell-beds. Most studies on the Pardonet have focussed on its biostratigraphy thanks to its abundance of biostratigraphically useful fossil taxa including ammonoids, conodonts, bivalves, and ichthyoliths. From a sedimentological perspective, the formation appears to have been deposited in deep water by dominantly pelagic deposition with more minor bioclastic debris-flows. High TOC and lack of bioturbation have led to the belief that the Pardonet was deposited in anoxic bottom-waters. Such a situation, however, seems inconsistent with the abundance of fossil material, especially the bivalves which do not appear to have been transported, even in shell-bed accumulations. Further, multiple genera can be observed replacing earlier forms meaning multiple species were able to exploit this deep, anoxic benthic environment. Some researchers have proposed that the bivalve taxa present were adapted to low-oxygen conditions but this hypothesis has never been tested in the Pardonet formation.

Pyrite framboid size distributions and trace metal indices (Mo/U, V/Cr, V(V+Ni)) are applied as geochemical paleo-redox proxies in order to help resolve some of the questions outlined above. Firstly, to determine if the Pardonet was truly deposited in persistently anoxic water and if so, were the bivalves able to survive in such conditions. In addition, the sedimentology is reassessed in greater detail to refine the interpretations of the depositional environment. Given a reinterpreted depositional system and geochemical data, some inferences can be made about the studied intervals' position in a sequence stratigraphic scheme.

All applied proxies agree that the studied intervals were, indeed, deposited in persistent anoxic conditions with varying degrees of euxinia. There is some evidence for brief reoxygenation events but not long enough to produce observable facies changes. In many cases, bivalves are confirmed to be autochthonous and therefore survived in low-oxygen waters. The distribution of autochthonous shell material is controlled by the degree of euxinia, suggesting there was a limit to the tolerance of reducing conditions for the bivalves. Reexamination of sedimentological features, especially the observation of allochthonous shell material in euxinic facies, reveals that the Pardonet represents deposits of multiple aspects of a bioclastic turbidite system with more minor pelagic deposition. Applying models of sequence stratigraphy in turbidite systems and chemostratigraphy allows an interpretation that the upper Pardonet saw a regression followed by transgression resulting in facies changes from bioclastic turbidites to suboxic pelagic deposition followed by pelagic deposition in euxinic water.

PREFACE

This thesis is an original work by Riley Morton. No part of this thesis has been previously published.

DEDICATION

This thesis is dedicated to my loving wife, Nicolette Morton, and my daughters, Alexandra Elizabeth, Lilith Anne, Charlotte June, and Madeline Hope. Without their endless love, support, patience, and hard work this thesis would not have come to fruition.

This thesis is also dedicated to my son Atticus Jesper, who was born during the course of this research but sadly had to leave us before it was finished. He is loved by all of us, deeply missed and thanked for giving me much needed distraction from writing.

"Species come and go, but the earth stands forever fast"

- *Embody the Invisible, Anders Fridén, In Flames.*

ACKNOWLEDGMENTS

I'd like to thank the Geological Survey of Canada, Natural Resources Canada for funding this research and providing me the means to take it on through the Research Affiliates Program. In particular, Dr. Martyn Golding for guidance and encouragement as well as assisting in the field and processing and identifying conodont samples. Thank you to my supervisor, Dr. John-Paul Zonneveld for his guidance, understanding, and companionship. Thank you to Dr. Zhiquan Li for his invaluable assistance in digesting and analyzing my samples with the ICP mass spectrometer as well as to Dr. Kurt Konhauser for very helpful consultations on the direction of this project. An additional thanks to Dr. Murray Gingras for his advice and friendship. To Arzu Açikelli, a thanks for being as reliably exceptional as a field hand as she is a friend. And to the entire Ichnology Research Group, I was made to feel welcome from the first day I worked with the group as an undergrad and I am thankful for that. The culture in the Department of Earth and Atmospheric Sciences is so supportive and there are too many people to list that I am proud to call my friends: students, alumni, faculty, and support staff alike.

TABLE OF CONTENTS

LIST OF TABLES

LIST OF FIGURES

Figure 2.5: Thin-section photomicrograph of BF1 stained with alizarin red. White arrow points to a calcite filled test of some shallow water animal. Calcite lineaments creating lamination in the matrix are *Halobia sp.* shells concordant to bedding. Matrix is composed of organic matter, pyrite, and mud-sized carbonate giving it its dark appearance. Sample SA-1605-BBR-073 from Black Bear Ridge, 25.4 m below top.Scale is 500 µm.

Figure 2.6: BF2 in outcrop, lateral view. Crinkled breaks between beds are caused by densely packed *Halobia.* Photograph from Brown Hill, 45.5 m above base. Rock hammer is 33 cm in length.

Figure 2.7: BF2 in outcrop, lateral view. Crinkled lamination is caused by densely packed *Monotis*. Photograph taken at Black Bear Ridge, 29.5 m below top. Ruler is 1.5 m long.

Figure 2.8: BF2 in outcrop. Above the scale bar, wavy or 'crinkly' lamination is apparent in lateral view. In the bedding plane below the scale bar, ribs of *Monotis* sp. shells can be seen. Photograph taken at Brown Hill, 63 m above base.

Figure 2.9: BF2 in bedding-plane view with abundant, overlapping *Monotis subcircularis*. Photograph taken at Black Bear Ridge, 0.5 m below top.

Figure 2.10: BF2 with abundant *Halobia sp*. Sample SA-PA-1605-47 from Pardonet Hill, 27 m above base. A) Ribs are apparent on bedding plane but much less apparent than in BF2 composed of monotids (Figure 2.9). Scale is 1 cm. B) Thin-section photomicrograph showing dense packing of *Halobia* shells scale is 500 µm.

Figure 2.11: Thin-section photomicrograph of BF2. The sample is dominantly composed of *Monotis sp.* shells concordant to bedding. Sample SA-1605-BH-017 from Brown Hill, 52.9 m above base. Scale is 500 µm

Figure 2.12: BF3 in outcrop overlain by BF5. Photograph taken at Brown Hill, 40 m above base.

Figure 2.13: BF3 in outcrop, lateral view. A small-scale reverse fault, marked by the black line, is an example of fractures that are commonly observed in the Pardonet formation in the Rocky Mountain Foothills. Photograph taken at Brown Hill, 57.5 m above base. Rock hammer is 33 cm.

Figure 2.14: BF3 in outcrop, lateral view. Photograph taken at Black Bear Ridge, 35 m below top. Ruler is 1.5 m in length.

Figure 2.15: BF3 in outcrop overlying BF5, lateral view. Black arrows indicate two large concretions. These are very common in the thinner bedded units of the Pardonet formation and are commonly more fossiliferous than surrounding strata. Photograph taken at Brown Hill, 50.5 m above base. Rock hammer is 33 cm in length.

Figure 2.16: *Eomonotis pinensis* preserved in BF3. Photographs taken at Brown Hill in bedding plane view, 53.5 m above base. Scale card is 7 cm. A) Abundant *E. pinensis* in several beds always concordant to bedding and approximately equal proportions convex-up and concave-up orientations. White arrow indicates the position of B. B) Close association of right and left valves with hingelines aligned indicates this specimen was not transported post-mortem.

Figure 2.17: *Monotis subcircularis* in BF3. These specimens are small for this species but are also among the oldest *Monotis* observed at Black Bear Ridge, 35.6 m above base. Scale is 5 cm.

Figure 2.18: Thin-section photomicrograph of BF3. White arrows indicate thin *Halobia sp.* shells concordant to bedding. White angular grains are quartz silt. Matrix is composed of organic matter, pyrite, and mud-sized carbonate giving it a dark appearance. Sample SA-1605-BBR-076 from Black Bear Ridge, 53.4 m below top. Scale is 500 μm.

Figure 2.19: BF4 in outcrop, lateral view. Crinkled breaks between beds is caused by dense *Halobia sp.* on bedding contacts. BF4 superficially resembles BF2 in outcrop but is typically more recessive and thinner bedded. Thicker beds above are BF1. Photograph taken at Brown Hill, 49.7 m above base. Rock hammer is 33 cm in length.

Figure 2.20: BF4 in outcrop, lateral view. Crinkled breaks between beds is caused by dense *Halobia sp.* on bedding contacts. BF4 superficially resembles BF2 in outcrop but is distinctly more fissile. Photograph taken at Black Bear Ridge, 43.5 m below top. Ruler segments are 30 cm.

Figure 2.21: BF4 in outcrop, lateral view. Crinkled breaks between beds is caused by dense *Monotis sp.* on bedding contacts. These beds are conspicuously similar to BF4 in the *Halobia* interval (Figure 2.19, 2.20). Photograph taken at Black Bear Ridge, 12 m below the top. Ruler segments are 30

Figure 2.22: BF4 with fragments of *Halobia sp.*on the bedding plane. Sample is from BH-22-2-2.50 from Brown Hill, 48 m above base. Note that this sample occurs above the first appearance of *Eomonotis*. This species survived into the *Eomonotis* interval (McRoberts, 2010; 2011).

Figure 2.23: BF4 with abundant monotids. These shells are much smaller than expected for monotids, however, this sample is from about 30 m above the last appearance of *Eomonotis pinensis* at Black Bear Ridge, 9 m below the top. Scale is 1 cm.

Figure 2.24: Thin section photomicrograph of BF4. White arrows indicate shells fragments of *Halobia sp.* Note that there is much more detritus when compared to thin sections of the other facies. Sample SA-1605-BBR-081 from Black Bear Ridge, 116.1 m above the base. Scale is 500 μm.

Figure 2.25: BF5 in outcrop at Brown Hill, 59.5 m above the base. Recessive beds in between are the only example of BF6 observed outside of the upper portion of Black Bear Ridge. BF2 overlays.

Figure 2.26: *Monotis subcircularis* preserved in 3 dimensions on a bedding plane in BF5. Photograph taken at Black Bear Ridge, 1.6 m below the top.

Figure 2.27: Sample BBR-22-2-40.95F from Black Bear Ridge, 11.6 m below top: *Monotis subcircularis* in BF5. Scale is 5 cm. A) One large isolated shell in 3 dimensions on the bedding plane and several larger shells exposed towards the bottom of the photograph. B) Exposed on a lower bedding plane is a lag of very small individuals.

Figure 2.28: Concentration of small *Monotis subcircularis* exposed on a bedding plane in BF5. Photograph taken at Black Bear Ridge, 16. 2 m below the top. Scale card is 7 cm.

Figure 2.29: Impression of *Eomonotis pinensis* on the sole of bed, BF5. Note the variability in size and dominantly convex-up orientation. Sample BH-22-2-11.65F from Brown Hill, 57.2 m above the base. Scale is 3 cm.

Figure 2.30: Sample PH-22-2-5.00F from Juvavites Cove, 5 m above creek (UTM: 49772 E, 6213150 N, 10V). Scale is 1 cm. A) *Halobia sp.* is apparent on upper bedding plane and resembles the expression of BF2 in the *Halobia* interval (Figure 2.10). B) Impressions of small *Halobia* on the sole of the sample. This sample establishes a criterion of recognition of BF5 in the *Halobia* interval.

Figure 2.31: Sample SA-BH-1605-015 from Brown Hill, 45.3 m above the base. This sample is an example of how BF5 can be expressed in the Halobia interval. A) *Halobia sp.* is obviously abundant in this sample. Note the inflation preserved in the umbo area (black arrow) Scale is 3 cm. B) Thin-section photomicrograph shows that shell is, in fact, not the dominant the dominant component of this rock. Scale is 500 μm.

Figure 2.32: Thin-section photomicrograph of BF5. Note the single large *Monotis sp.* shell (white arrow) and the large silt grain size compared to other thin sections. Sample SA-1605-BH-019 from Brown Hill, 65.5 m above base. Scale is 500 μm.

Figure 2.33: BF6 in outcrop. Prominent bed stratigraphically underlying is BF5. Photograph taken at Black Bear Ridge, 20.3 m below the top. Ruler is 150 cm in length.

Figure 2.34: BF6 in outcrop, bedding-plane view. Abundant but small *Monotis sp.* exposed. In contrast to BF5, no adult size shells are observed. Photograph taken at Black Bear Ridge, 17.5 m below top. Segments on Jacob's staff are 10 cm.

Figure 2.35: BF6 in outcrop, bedding-plane view. Solitary, juvenile monotid. Photograph taken at Black Bear Ridge, 18.7 m below top. Scale card is 7 cm.

Figure 2.36: BF6 in outcrop. Abundant shell fragments on bedding plane. Photograph taken at Black Bear Ridge, 7 m below the top. Scale card is 7 cm.

Figure 2.37: BF6 in outcrop, Black Bear Ridge, 7 m below the top. A) Scattered shell material on bedding planes. White box is the location of B. Scale card 7 cm. B) Shell material is fragments or small individuals. Scale 3 cm.

Figure 2.38: Thin-section photomicrograph of BF6. Single shell fragment indicated by white arrow. The rock is dominantly composed of fine-grained silt, carbonate, and organic matter. Sample SA-1605-BBR-090 from Black Bear Ridge, 88.9 m above the base. Scale is 500 µm.

Figure 2.39: Box plots comparing redox proxy data between the 6 facies. A) Box plots represent the distribution of the average framboid diameters per sample from each facies. B) Box plots display the distribution of the variance in framboid diameter for each sample compared between facies. C) U_{XS} distributions are plotted for each facies. D) Mo_{XS} distributions shown for each facies.

CHAPTER 3

Figure 3.1: Mean versus standard deviation cross-plot of framboid distributions per sample. Euxinic-dysoxic boundary defined following Wilkin et al. (1996).

Figure 3.2: Brown Hill section litholog demonstrating stratigraphic distribution of observed facies aligned with multiple geochemical logs of redox proxy data. 0 m on the logs is 45.5 m above the basal contact with the Baldonnel formation. The top is the end of outcrop exposure at Brown Hill.Timescale on left calibrated with conodont and bivalve sample identifications, ammonoid zones assumed based on previously published correlations to conodont and bivalve zonations.

Figure 3.3: Black Bear Ridge section litholog demonstrating stratigraphic distribution of observed facies aligned with multiple geochemical logs of redox proxy data. 0 m on the logs is 52.5 m below the top contact with the Fernie formation (top of logs). Timescale on left calibrated with conodont and bivalve sample identifications, ammonoid zones assumed based on previously published correlations to conodont and bivalve zonations. Note that the vertical scale is much larger than in Figure 3.2 and sample density is less.

Figure 3.4: Cross-plot of U_{XS} against Mo_{XS}. Data shows an increasing Mo:U ratio relative to the ratio observable in modern open marine sea-water. Fields outlined define the expected ranges data should fall in based on degree of basin restriction. Sea-water ratios and data fields defined after Algeo & Tribovillard (2009) and Tribovillard et al. (2012).

Figure 3.5: Redox sensitive trace metals, U (A, C) and Mo (B, D) plotted against detrital proxies, Al (A, B) and Ti (C, D). R^2 values indicated next to line-of-best-fit.

CHAPTER 4

Figure 4.1: Cartoon illustrating the idealized sequence of facies produced by the interpreted carbonate turbidites. Sequence grades from FA1, proximal carbonate turbidites, to FA3, distal carbonate turbidites in euxinic bottom waters. I) Traction carpet composed of ooids. Common at bases of BF1. II) Ichthysaur bone in silty micrite matrix. An expression of BF1. Other clasts also common. III) Abundant ammonoids and dense bivalves. An expression of BF1. IV) Bivalve laminite, BF2. V) Detritus rich, dark-gray limestone with abundant small and fragmentary bivalves, BF4. VI) Pelagic settling of small shell material, organic matter, and fine-grained sediment with H_2S present in the water column, BF6.

Figure 4.2: Illustration of the sequence of events interpreted to lead to the formation of BF5. 1) A population of flat-clams live on a soupy, fine-grained substrate. Being r-selected taxa, the population is dominated by juveniles with relatively few adult-sized individuals. 2) A waning turbidity current passes over the substrate. The flattened morphology of the juveniles allows them to be entrained by the current while adults are overturned into a more hydrodynamically stable position. 3) Adults are buried by fine-grained sediment carried by the turbidity current. Juveniles are deposited in a lag as the current loses energy and are in turn buried by more fine-grained sediment. Once the current has settled a new population is established on top of the fine-grained sediment. In the absence of passing currents, pelagic deposition dominates and most flat-clams reach adult size, allowing the formation of BF3.

Figure 4.3: Correlation between Black Bear Ridge (BBR) and Brown Hill (BH). Solid lines mark boundaries between facies associations. Two of these surfaces can be correlated between the two sections. Datum is arbitrarily picked on one of these surfaces (29 m below the top of the Pardonet at BBR; 60.9 m above the top of the Baldonnel formation at BH). Dashed lines indicate biostratigraphic turnovers between *Halobia* and *Eomonotis (H./E.)* and *Eomonotis* and *Monotis (E./M.)*.

Figure 4.4: Three well cross-section of the Pardonet formation in the subsurface Southeast of Williston Lake. Datum is the top of the Baldonnel formation. The Pardonet can be divided into four units in the subsurface based on log responses. P1 is identified by the high-gamma response. P2 has a lower and more constant log signature. P3 appears less organized with a low but serrated signature and, finally, P4 is identified by the chaotic appearance of the sonic log. P4 is truncated by the sub-Jurassic unconformity to the East. After Barss & Montandon (1981).

CHAPTER 1: INTRODUCTION

Triassic 'flat-clams'

Deep-water, pelagic successions of Triassic rocks around the world are dominated by a series of pteriomorph bivalves that share a flattened morphology (McRoberts, 2010). Commonly referred to as 'flat clams,' these fossils have long been recognized for their biostratigraphic utility that arises from their widespread distribution and high turnover rates (De Capoa Bonardi, 1984, Palubotko, 1986, McRoberts, 1997, Zakharov et al., 1997, Yin, 2003). The Norian stage of the Upper Triassic saw the sequential turnover from *Halobia* in the lower to middle Norian, to *Eomonotis* in the upper middle Norian, followed by *Monotis* in the upper Norian (McRoberts, 2010). All three of these genera are known to occur in laterally-extensive, densely-abundant, monospecific shell accumulations that can achieve more than 2 m in thickness (McRoberts et al., 2008). These shell accumulations are typically overwhelmingly dominated by a single bivalve taxon but may include several species within one genus.

Several different theories on the paleoecology of these bivalves have been proposed to help explain these unique facies occurrences (Gruber, 1976; Ando, 1987; Wignall & Simms, 1990; Campbell, 1994). A common theme is that these accumulations occur in sediments that were deposited under reduced-oxygen conditions (McRoberts, 2010; Del Piero et al., 2020). It has been speculated that many Triassic flat-clams may have been pseudo-planktonic, living attached to drifting seaweed, high in the oxygenated portion of the water column, and settling in reduced-oxygen bottom-waters after death (Jefferies & Minton, 1965; Tozer, 1982b; Davies, 1997a, 1997b; McRoberts, 1997). The extreme abundance and lack of definitive evidence of attachment structures leave this theory less plausible than an *in situ,* benthic life mode (Wignall & Simms, 1990; McRoberts, 2010, 2011; Del Piero et al., 2020). In addition, bedding plane

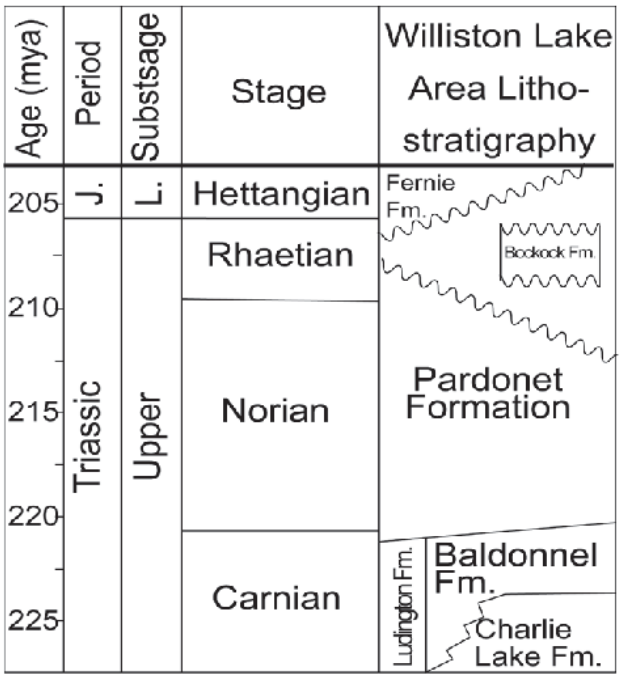

Figure 1.1: Stratigraphic column of the Late Triassic in the Peace River area. Adapted from Zonneveld (2022).

assemblages include approximately equal proportions of shells in concave-up and concave-down orientations, which would not be the case in a settling model (Zonneveld et al., 2004). Furthermore, criteria such as ornament preservation, size distribution, and the random orientation on of valves concordant to bedding planes indicate that shells in these accumulations were not likely transported significant distances (McRoberts, 2011).

Del Piero et al. (2020) proposed that *Halobia* in the Quatsino formation at Tsiko Lake, Vancouver Island, BC occur in high density in sediments interpreted as anoxic with dysoxic intervals; occur with other fossils in bioturbated sediments interpreted as moderately dysoxic; and only isolated, small shells occur in sediments interpreted as euxinic. This supports the notion that *Halobia* opportunistically colonized areas with reduced oxygen that are unfavourable to other benthos (McRoberts, 2011). This study will attempt to test if Del Piero et al. (2020)'s conclusions are consistent in a different locality while also expanding the model to include *Eomonotis* and *Monotis* as well as *Halobia*.

Geological Setting and Study Area

The Pardonet formation tops an overall deepening-upwards succession that comprises Upper Triassic (middle to upper Carnian, Norian, and Rhaetian) strata of northeastern British Columbia (BC), Canada (Davies, 1997b, Zonneveld et al., 2004; Figure 1.1). The Pardonet

overlies the vuggy carbonate limestone of the Baldonnel formation, which has been interpreted to represent a proximal carbonate ramp / shoreface depositional setting (Zonneveld and Orchard, 2002; Zonneveld et al., 2004). The Baldonnel in turn overlies a heterolithic succession of siliciclastic sandstone, fine-grained limestone, fine-grained dolomite, breccia and anhydrite of the Charlie Lake formation, which is inferred to record deposition in an intertidal to supratidal sabkha succession (Zonneveld & Orchard, 2002; Zonneveld et al., 2004).

The Pardonet formation is, in most areas unconformably overlain by the Jurassic Fernie formation; however, in the Pine Pass area, South of the Peace River, the Rhaetian Bocock formation can be observed overlying the Pardonet formation (Gibson, 1975; 1993). Deposition of the dark grey, silty, carbonaceous, bioclastic limestone, dolostone and shale of the Pardonet formation took place from the uppermost Carnian to the upper Norian (McRoberts, 2011). Like many other Late Triassic deep-water deposits, large portions of the Pardonet formation consist of accumulations of *Halobia, Eomonotis,* or *Monotis* in rock-forming abundances (Davies, 1997b, Zonneveld et al., 2004, McRoberts, 2011). The Pardonet formation has been well studied for its abundance of biostratigraphically significant fossils (eg. Tozer, 1982a; 1994; McGowan, 1991; Orchard et al., 2001a; 2001b; Orchard, 2007; Nicholls and Manabe, 2000, 2004; McRoberts, 2011) but the depositional interpretation still needs attention. Those that have considered the mode of deposition of the Pardonet limestone and shale beds generally regard them as having

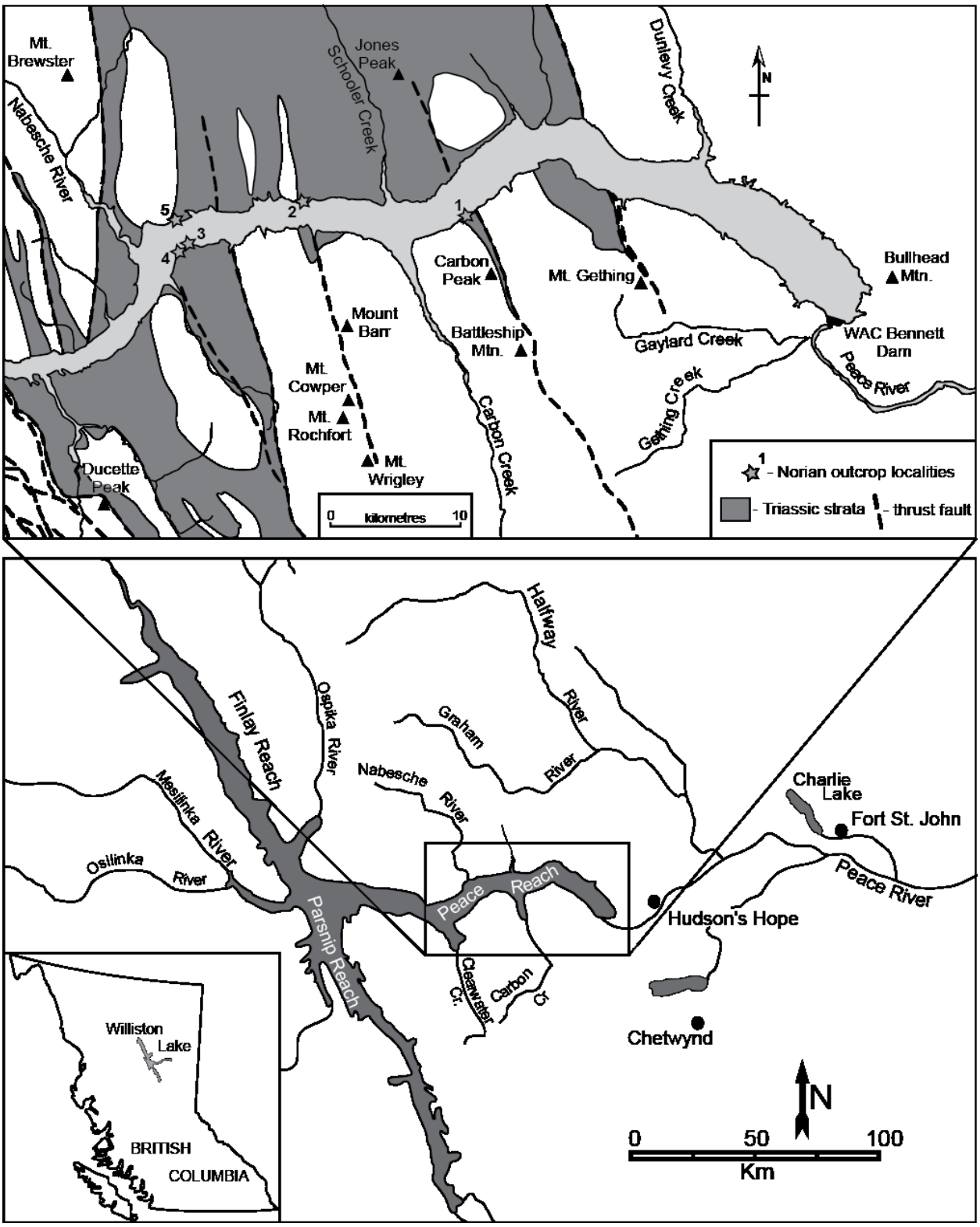

Figure 1.2: Location map of the study area. Important Late Triassic outcrop sections along Williston Lake marked with stars. 1: East Carbon Creek, 2: Brown Hill, 3: Pardonet Hill, 4:Juvavites Cove , 5: Black Bear Ridge. Modified from Zonneveld (2022).

formed in a deep, anoxic shelf environment well below storm-weather wave-base but above the carbonate compensation depth (Gibson, 1993; Davies, 1997b; Zonneveld et al., 2004; 2010; Wignall et al., 2007; Onoue et al., 2016). Much of the formation is made up of shell beds so understanding the conditions for their formation will be invaluable in resolving the internal stratigraphy and depositional system of this unit.

Triassic rocks of the Western Canadian Sedimentary Basin are well exposed along the Peace Reach of Williston Lake, BC resulting in numerous world-class fossil localities (Zonneveld, 2001; Amati et al., 2004; Blake and Zonneveld, 2004; Zonneveld et al., 2007a,b; 2010; Martindale et al., 2010; Stanley and Zonneveld, 2011; McRoberts, 2011; Figure 1.2). The first unequivocal discovery of Triassic rocks in the Peace River foothills and mountains was made by the second director of the Geological Survey of Canada, Alfred Richard Cecil Selwyn, in 1875 when he found *Monotis* west of Ne-Parle-Pas Rapids on the Peace River (Tozer, 1984). A find which was officially reported in Whiteaves (1889). McLearn, starting in 1917 followed by a 1930 report and a number of reports in the 1940's, began dividing the Triassic rock into stratigraphic units. As a product of those field reports, the Schooler Creek formation was named to encompass the Upper Triassic rocks observable along the Peace River (McLearn, 1930; 1940; 1941; 1947). Many classic Triassic outcrop sections, including the type section of the Pardonet formation, were submerged after the construction of the WAC Bennett dam on the Peace River in 1967. Fortunately, wave-erosion and annual fluctuations in lake level have exposed new sections that are easily accessed by boat (Zonneveld et al., 2010). Much refinement of the stratigraphy has occurred since the initial descriptions (Figure 1.3). The Schooler Creek Formation was subdivided into the Halfway, Charlie Lake, and Baldonnel formations while retaining the name, Schooler Creek, as a group name but the beds between the Baldonnel

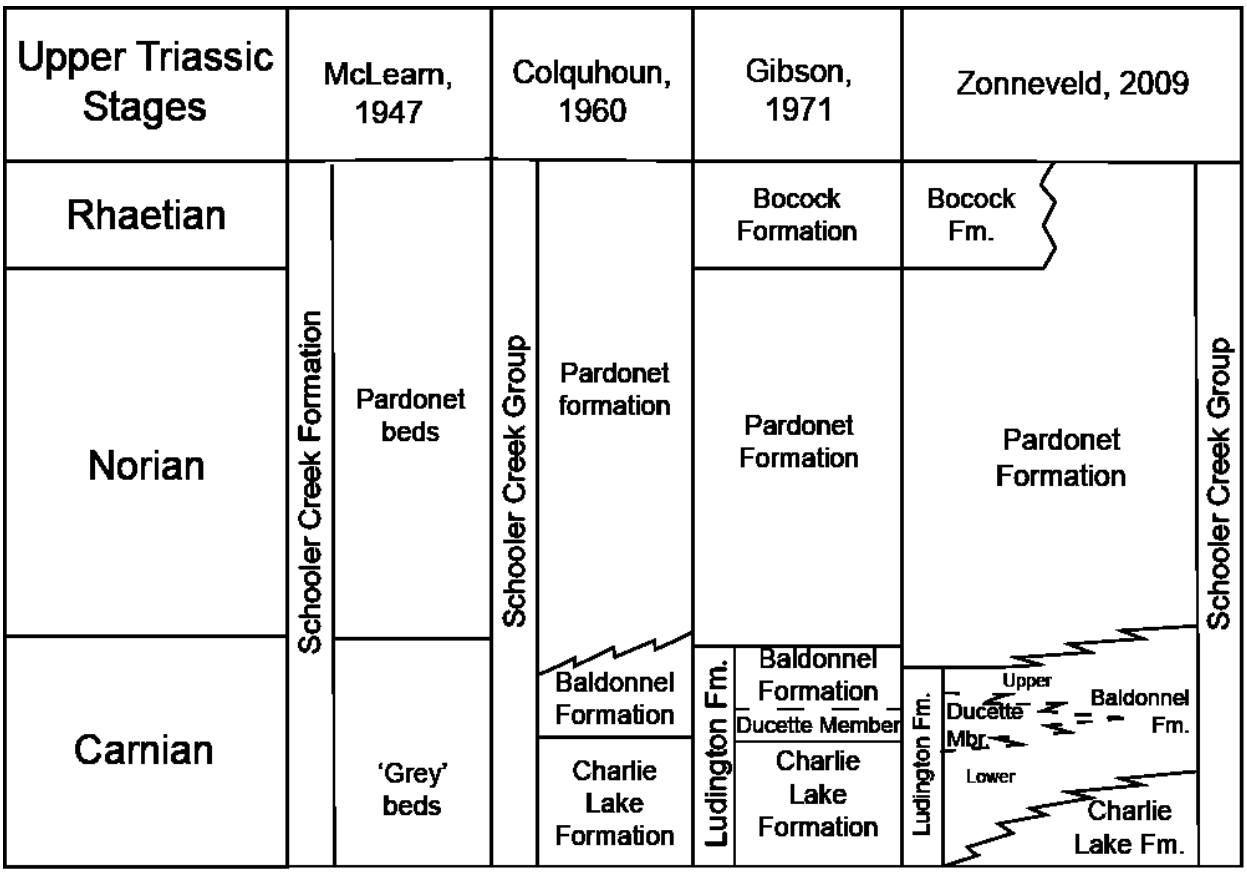

Figure 1.3: Concise stratigraphic development of the Late Triassic in the Peace River area. Adapted from Zonneveld (2022)

formation and Fernie formation were simply termed "the Pardonet beds" following McLearn (1940) (Hunt & Ratcliffe, 1959). Colquhoun (1960) followed this division of the Schooler Creek Group and elevated the status of the Pardonet beds to formation. That stratigraphy was followed by Gibson (1971) who added the Ludington formation as a lateral basinward equivalent of the Charlie Lake and Baldonnel formations which can be observed at Williston Lake, west of the Pardonet Hill East locality (Zonneveld et al., 2010). The Bocock formation was also defined as a geographically-restricted limestone of likely Rhaetian age which tops the Pardonet formation south of Williston Lake (Gibson, 1971). Detailed stratigraphic work in the Williston Lake area in the last 20 years or so has emphasized the gradational contacts between the Upper Triassic formations which can be demonstrated to interfinger implying high frequency transgression-

regression cycles across the contacts nested within the overall transgressive sequence (Zonneveld, 2022).

The Triassic succession of the Western Canadian Sedimentary Basin occurs as a wedge in the subsurface of Northwestern Alberta and Northeastern British Columbia and in outcrop in the front ranges of the Northern British Columbia Rocky Mountains (Gibson, 1993; Edwards et al., 1994; Davies, 1997a; Zonneveld et al., 2004). The Triassic strata dip to the West and are truncated by the angular sub-Jurassic unconformity such that the succession is most complete in the West but is bounded by the deformation front associated with the Rocky Mountain orogeny (Gibson, 1993; Edwards et al., 1994; Davies, 1997a). These rocks were deposited on the Western margin of Pangea just North of the tropics (Figure 1.4). This margin was long considered to be a tectonically stable, passive continental margin (Irving, 1977; Gibson, 1993; Edwards et al., 1994; Davies, 1997a; Golonka, 2007), however, recent evidence has shown that the greater Western Canada Sedimentary Basin region transitioned into a retro foreland Basin in the Early Triassic (Ferri and Zonneveld, 2008; Beranek & Mortensen, 2011; Zonneveld and Moslow, 2018; Rohais et al., 2018).

McRoberts, (2011) identified 3 distinct types of shell bed occurrences in the Pardonet formation observable at Williston Lake. All three of these types can be applied to *Halobia, Eomonotis,* and *Monotis* shell beds. Type 1 shell beds are recognizable by the occurrence of

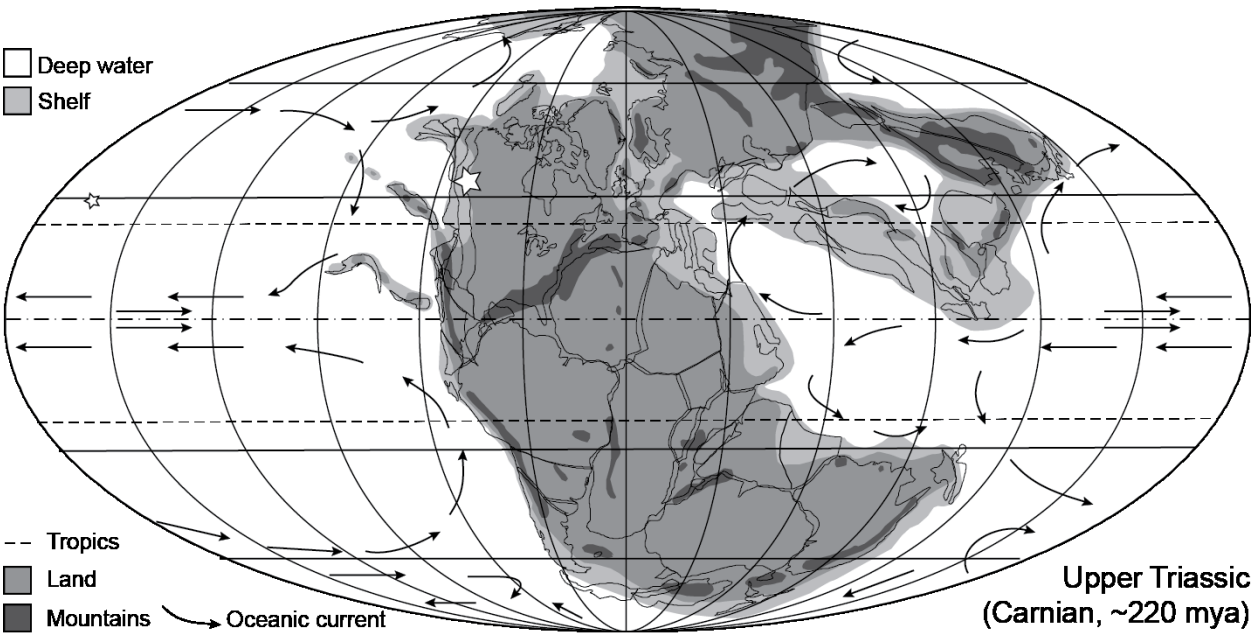

Figure 1.4: Paleogeography of the globe during the late Triassic. Approximate location of Triassic strata exposed at Williston Lake marked with a star. Exact position of terranes off the coast of Northwest Pangaea (paleo-North America) is highly debated. After Zonneveld (2022)

isolated shells of variable size, emplaced concordant to bedding, with approximately 5% of the valves deposited convex up in a matrix with a higher silt content than typical for the formation. Type 2 shell beds are high density shell beds with a low proportion of other sediment types. Shells are dominantly of adult size, overlapping, and flattened due to compaction. The high fossil content makes these shell beds very prominent in outcrop. Type 3 shell beds are identified by the occurrence of immature shells and less common adult-sized shells. Type 3 shell beds often display a bimodal size distribution. It is more common to find 3-dimensional shells in type 3 shell beds compared with type 1 and 2. McRoberts, (2011) interpreted, based on field observations, that type 1 and 2 shell beds consist of autochthonous shells while type 3 shell beds may include shells that have experienced some amount of transport.

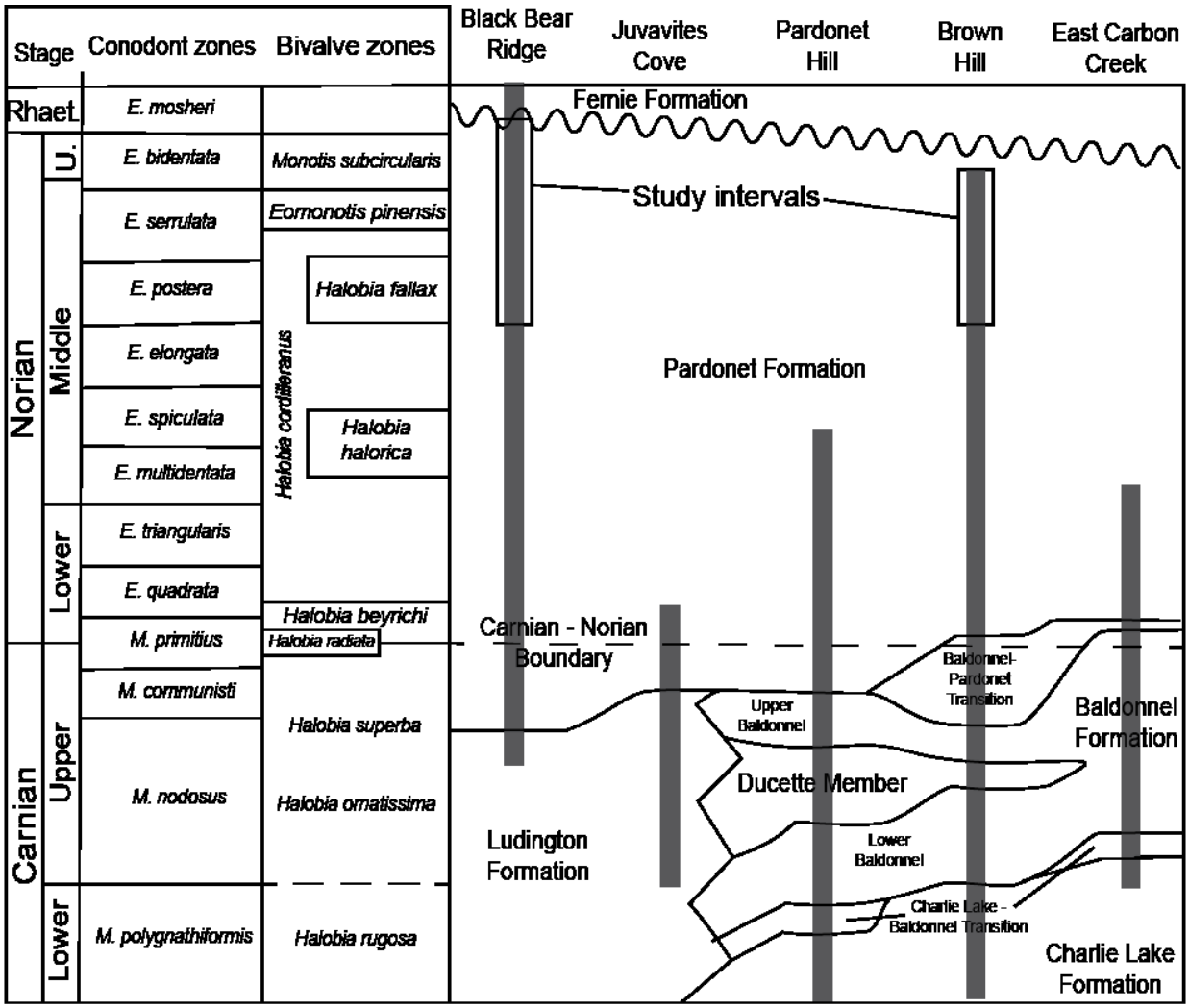

Figure 1.5: Simplified cross-section showing the stratigraphic architecture of important Late Triassic sections marked in Figure 1.2. Intervals geochemically analyzed in this study are outlined. Modified from Zonneveld et al. (2010), bivalve zonation after McRoberts (2010).

Materials and Methods

Williston Lake was visited during the 2022 field season in order to sample the Pardonet formation at East Carbon Creek, Juvavites Cove, Brown Hill and Black Bear Ridge The upper Brown Hill and Black Bear Ridge sections, where continuous outcrops can be observed through the *Halobia-Eomonotis* and *Eomonotis-Monotis* turnovers (Figure 1.5), were chosen as intervals to focus this study on. Field notes, inspection of hand samples, and thin-sections were used from all visited localities to classify the collected rock samples into six facies (Table 1). This

classification was informed by the type 1, type 2, and type 3 shell bed categories defined by McRoberts, (2011) for the Pardonet formation and are refined herein to include observations from field work for this thesis, including lithology changes associated with the different types of shell occurrences. Facies are denoted with the abbreviation 'BF' as a shorthand for biofacies in order to concisely identify the different facies in the discussion. For the purpose of this study, the term biofacies is defined as recurring combinations of sedimentological and paleoecological characters that can be identified in hand sample. In the interest of avoiding lengthy discussion of terminology, however, the term 'biofacies' will not be used further. Categorizing the samples in this way will allow comparison of geochemical data against the nature of the occurrence of the bivalves as well as changing depositional processes.

Macro-fossil samples were collected to constrain the stratigraphic height of the turnover events. *Halobia-Eomonotis* and *Eomonotis-Monotis* turnovers were noted in the field for easy correlation with published bivalve biostratigraphy of the area. Conodont samples were also collected near bivalve turnover events to help calibrate to previously published biostratigraphic logs. For clarity in biostratigraphic discussions, bivalves will only be referred to at the genus level, capitalized in italics, conodont zones will be referred to with the species name, lower case in italics, and ammonoid zones will be referred to with the species name but capitalized and non-italic. These samples also complimented the rock hand samples used in the facies descriptions presented in Chapter 2 to interpret how the occurrence of halobiids and monotids relates to facies in the Pardonet formation.

The sections of interest were sampled for geochemical analysis at 0.5 m intervals starting from the last prominent *Halobia* shell beds and ending at the top of the highest *Monotis* shell bed in a section. As much as possible, care was taken to avoid sampling fractures, excessively

weathered material, or deformed units. Additional samples were collected from unusual lithologies and intervals deemed to be of particular interest. For this study, a subset of 82 samples were selected with the goal of comparing different lithologies observed in the field. These rock samples were prepared for analysis by first cutting off any weathered surfaces or mineral veins that may give non-primary chemical signals. A small piece cut from each sample was powdered in a tungsten ring and puck mill. Cut surfaces were abraded with sandpaper to remove any trace metals introduced by the rocks saws before powdering. Another small piece was cut to be set into an epoxy puck and polished for Scanning Electron Microscope imaging.

Paleo-redox Proxies - The terms oxic, suboxic and anoxic are commonly used to describe various redox conditions of modern and ancient oceans (Wilkin et al., 1996; Wignall & Newton, 1998; Zheng et al., 2000; Tribovillard et al., 2006; 2012; Algeo & Tribovillard, 2009; Del Piero et al., 2020 La Grange et al., 2020). Some authors have defined specific dissolved oxygen ranges for each of these terms (Tyson & Pearson, 1991; Morrison et al., 1999; Revsbech et al. 2009). The paleo-redox proxies applied here cannot be used to determine the dissolved oxygen concentration in the water column at the time that the sediments were deposited so the data presented is best compared to other data points in the data set (i.e. better oxygenated or more reducing compared to another cluster). Where these redox terms are applied, they are meant to indicate the data's relative position within this dataset or relate to other studies. Where these terms are used referring to the conditions of formation of different facies or paleoecological interpretations, they should be taken to imply the inferred microbial metabolic regime with which the resident fauna existed. That is to say, oxic refers to aerobic respiration, suboxic refers to respiration where nitrate (NO_3^-) is the terminal electron acceptor, and anoxic refers to respiration with Mn(IV), Fe(III), or sulfate (SO_4^{2-}) (Konhauser, 2007, LaGrange et al., 2020).

Additionally, euxinic is used to refer to conditions where oxygen is depleted and hydrogen sulfide (H_2S) is present in the water column due to sulfate reduction (LaGrange et al., 2020).

Polished samples were analyzed with a Zeiss Sigma 300 VP-FESEM (Department of Earth and Atmospheric Sciences, University of Alberta) to find and image at least 30 pyrite framboids per sample. Samples were analyzed in variable pressure mode (approximately 45 psi) using the electron backscatter detector with the gun set to 25.00 kV. Because the machine was operated in variable pressure mode, no conductive coating was required. Framboids are readily identified using this technique due to pyrite's high molecular mass relative to other common sedimentary minerals (corresponding to high electron backscatter in the scanning electron microscope (SEM) image) and unique morphology (Figure 1.6). The presence of pyrite framboids in sediments generally indicates H_2S was periodically present in the water column (Wignall & Newton, 1998). If sediments are deposited in a euxinic water column, it is expected that framboids will have a small average diameter, about 5 µm and generally less than 7 µm, and low variation in size. When the water column is dysoxic to anoxic, anomalously large framboids may be observed meaning a higher average diameter and variance (Wilkin, et al., 1996; Wignall & Newton, 1998). It has been acknowledged that this method may underestimate the true diameter of observed framboids but it is accepted that this method still provides a reliable redox proxy (Wilkin, et al., 1996). The diameter of each framboid found in

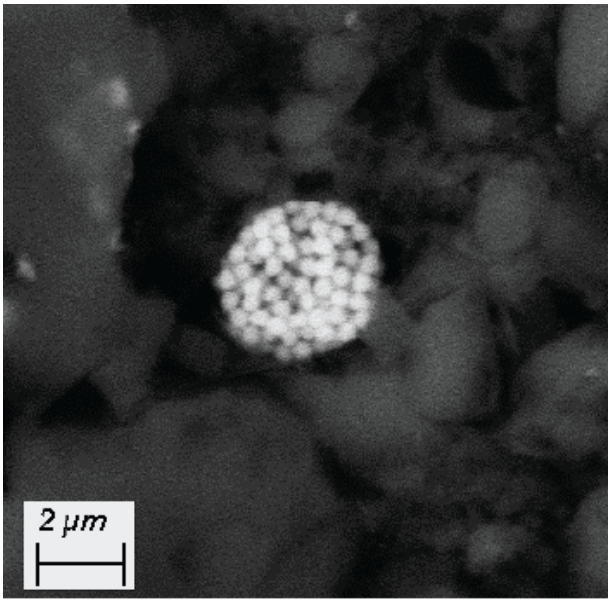

Figure 1.6: SEM backscatter image of a pyrite framboid.

the samples was digitally measured from the SEM images. Average diameters and variance was calculated for each sample then these values were compared between the six facies. This method was chosen because it appears to be more sensitive to the outliers that are expected from suboxic sediments than comparing the overall size distribution for each facies. Framboids were commonly overgrown, replaced by calcite, and sometimes amalgamated into 'polyframboids.' Care was taken to only measure the original size of the framboids when these features were observed and no measurement was taken if the original size could not be discerned. Notes were taken on the degree of modification of the framboid in each sample as these characteristics have also been associated with more oxic conditions (Wignall & Newton, 1998). Based on the size distributions, each facies were classified as euxinic or suboxic or oxic if framboids were absent in the sample.

The processes of crushing, weighing, and preparing powdered samples for solution-mode inductively coupled plasma mass spectrometry (ICP-MS) were conducted within the Department of Earth and Atmospheric Sciences at the University of Alberta. Teflon vials were thoroughly cleaned with acid and dried before the digestion. The crushed and powdered samples underwent a complete digestion process, involving a two-step heated treatment with nitric acid-hydrogen peroxide-hydrofluoric acid (HNO_3-H_2O_2-HF) digestion (Enders and Lehmann, 2012; von Gunten et al., 2017). Approximately 100 mg of powder was placed into a 50 mL acid-cleaned Teflon vial. Subsequently, 4 mL of a mixture containing 30% H_2O_2 and 70% HNO_3 was added to the sample. Initially, the vials were loosely capped to facilitate degassing before being fully sealed and heated to 130°C. In the second step, 2 mL of 70% HF was introduced, and the vials were sealed for a 3-hour treatment at 150°C.

To measure both major and trace elements, two distinct methods were employed. For major elements, 20 mL of 4.3% boric acid was added to dissolve secondary fluoride precipitates, and the vials were capped and heated at 150°C for one hour. Next, major element samples were diluted with a solution containing 2% HNO_3 and 0.5% hydrochloric acid (HCl) at a dilution factor of 10 000x. In contrast, for trace and rare earth elements (REE) measurements, the vials were left uncapped at 80°C overnight to allow the evaporation of HF, resulting in a final volume of approximately 3 mL. Prior to analysis, the solution was diluted by a factor of 5000x. Elemental abundances were determined using an Agilent 8800 ICP-MS/MS at the University of Alberta's Environmental Geochemistry Laboratory. Geostandards ShBOQ-1 and GSR-1 were employed to assess major and trace element recoveries, with concentrations for these geostandards falling within 5-10% of accepted values.

After acquiring all the geochemical data, authigenic trace metal content, defined as content not derived from terrestrial sources and was calculated with the following formula:

$$TM_{XS} = TM_{Sample} - Al_{Sample}(TM/Al)_{ShBOQ-1}$$

where TM is the element of interest (Brumsack, 2006). Enrichment factors is a more common method of normalizing data to account for variability in carbonate and biogenic silica content (Tribovillard et al., 2006). Enrichment factors are easy to understand but are problematic when analyzing rocks with low detrital content because low [Al] values in the denominator of the calculation will result in misleadingly high enrichment values (Van der Weijden, 2002; Tribovillard et al., 2006). Analyzing the excess trace metal content, circumvents that issue by focussing on the non-detrital portion rather than the ratio between the element and Al compared to the average shale values (Brumsack, 2006). Calculating excess is considered a more

appropriate index because many of the samples are limestone and also there is a high degree of variability in detrital material between facies.

The Boquilles shale (ShBOQ-1) standard (Birdwell & Wilson, 2021) was chosen to normalize the trace element data because of the high carbonate content in the Pardonet formation. The average upper continental crust (AUCC) standard (McLennan, 2001) is much more widely used in shale (Tribovillard et al., 2006; 2012; Algeo and Tribovillard, 2009) and in carbonates (Del Piero et al., 2020, Steinmann et al., 2020) because a carbonate standard only recently became available. This is particularly relevant to Mo because the reported ShBOQ-1 value for Mo is about 34 times higher than that of the AUCC (McLennan, 2001; Birdwell & Wilson, 2021). Mo_{XS} calculated using the AUCC values yielded values much greater than expected. For that reason, excess calculated using ShBOQ-1 values are reported as they are considered more reasonable.

When considering trace metal proxies, it is important to consider how post-depositional processes could alter the concentrations in the original sediments (See Steinmann et al., 2020 and references therein for discussion). Diagenesis in the Pardonet is considered to be minimal. In thin-section, it is apparent that originally aragonite shells have been recrystallized and replaced by calcite but alizarin red staining demonstrates that the formation is predominantly original limestone at least in the Williston Lake outcrops. Limestone is generally more prone to diagenetic alteration than shale which is more commonly the subject of geochemical studies. The samples gathered have consistent appearance in hand sample and thin-section meaning they should at least be comparable within the dataset. Diagenetic processes are more likely to hide a signal than create a false signal so the conclusions made from the results presented below are considered valid.

CHAPTER 2: FACIES AND RESULTS

BF1

BF1 consists of a course-grained rudstone composed dominantly of bioclasts. Two end-member expressions were observed, the first commonly grading into the second. The first expression typically contains ooids and ichthyosaur bone fragments and less commonly partially articulated ichthyosaurs, echinoid spines, ammonoids, gastropods, and an unidentified bivalve (Figs 2.1, 2.2, 2.4). Ooids, when observed, are typically concentrated toward the base of beds and overly sharp, irregular bedding contacts. The bioclastic components typically occur floating in a carbonate-mud matrix. The second expression contains many more ammonoids, which are always emplaced concordant to bedding, and *Halobia, Eomonotis,* or *Monotis* in very high density also concordant to bedding (Figs 2.3, 2.5). This expression commonly grades into BF2 or BF4. BF1 can be observed overlying any other facies.

Facies	*Description*
BF1	Bioclastic rudstone with scoured bases. Low silt content and high diversity of fossils. Flat clams are typically adult size, whole, unabraded, and deposited concordant to bedding but form more undulatory laminae than in other facies. Clasts can include bivalves, ammonoids, ichthyosaur bone, ooids, echinoid spines, and gastropods. Components can commonly be observed is sequence.
BF2	Bivalve laminate. Bivalves are densely packed and deposited concordant to bedding such that the rock appears to have a unique 'crinkly' lamination when viewed parallel to bedding. Shells are whole, unabraded, and are their size distribution is skewed towards adult sizes. Minor silt component. Equivalent to Type 2 shell beds of McRoberts, (2011)
BF3	Thinly-bedded, silty, brown floatstone with abundant, but non-overlapping, bivalves of dominantly adult size. Size distribution is more normal than in other facies. Shells are whole, unabraded, and concordant to bedding. Type 1 shell bed of McRoberts (2011)
BF4	Silty rudstone with densely packed, thin-shelled bivalves deposited concordant to bedding. Bivalves are never greater than 3 cm, have low variability in size, are unabraded, but typically appear fragmented.
BF5	Well-cemented, silty floatstone in decimetre scale beds. Isolated adult-size bivalves preserved in 3 dimensions and juveniles concentrated on some bedding planes. Shells are whole, unabraded, and deposited concordant to bedding. Fits McRoberts (2011)'s definition of Type 3 shell beds.
BF6	Thinly-bedded wackestone to floatstone with silty black or dark-grey carbonate-mud matrix. Bivalves are small with a left-skewed size distribution. Larger bivalves are typically whole, unabraded, and deposited concordant to bedding. Smaller bivalves can be more random in orientation and appear fragmentary. Considered an expression of McRoberts (2011)'s Type 3 shell beds.

Table 1: Facies descriptions.

Figure 2.1: Ooids preserved at the base of a BF1 bed, lateral view. Photograph taken at East Carbon Creek, 3.75 m above base. Scale 1 cm.

Figure 2.2: BF1 in bedding-plane view. Arrows point to large ichthyosaur vertebrae. Phosphates preserved in bone material gives it a dark appearance. Photograph taken at Brown Hill, 10.8 m above base Scale card 7 cm.

Figure 2.3: BF1 in lateral view. Recrystallized ovoid features (arrow) are ammonoids deposited concordant to bedding. Unusual crinkly lamination caused by densely packed flat-clams. Photograph taken at Black Bear Ridge, 65.7 m above base Scale 5 cm.

Figure 2.4: BF1 in outcrop, lateral view. Several ichthyosaur rib-bones can be observed in cross section (arrows). Regular spacing suggests the they were articulated at the time of deposition. Yellow dashed line at the base of the bed traces the undulatory basal surface which suggests scour. 'Crinkly' lamination above bone bed is due to a high density of *Halobia* preserved in the bed (CL). This lamination thins and pinches out to the right which suggests a secondary scour surface as indicated by the second yellow dashed line. Photograph taken at Black Bear Ridge, 44.25 m below top.

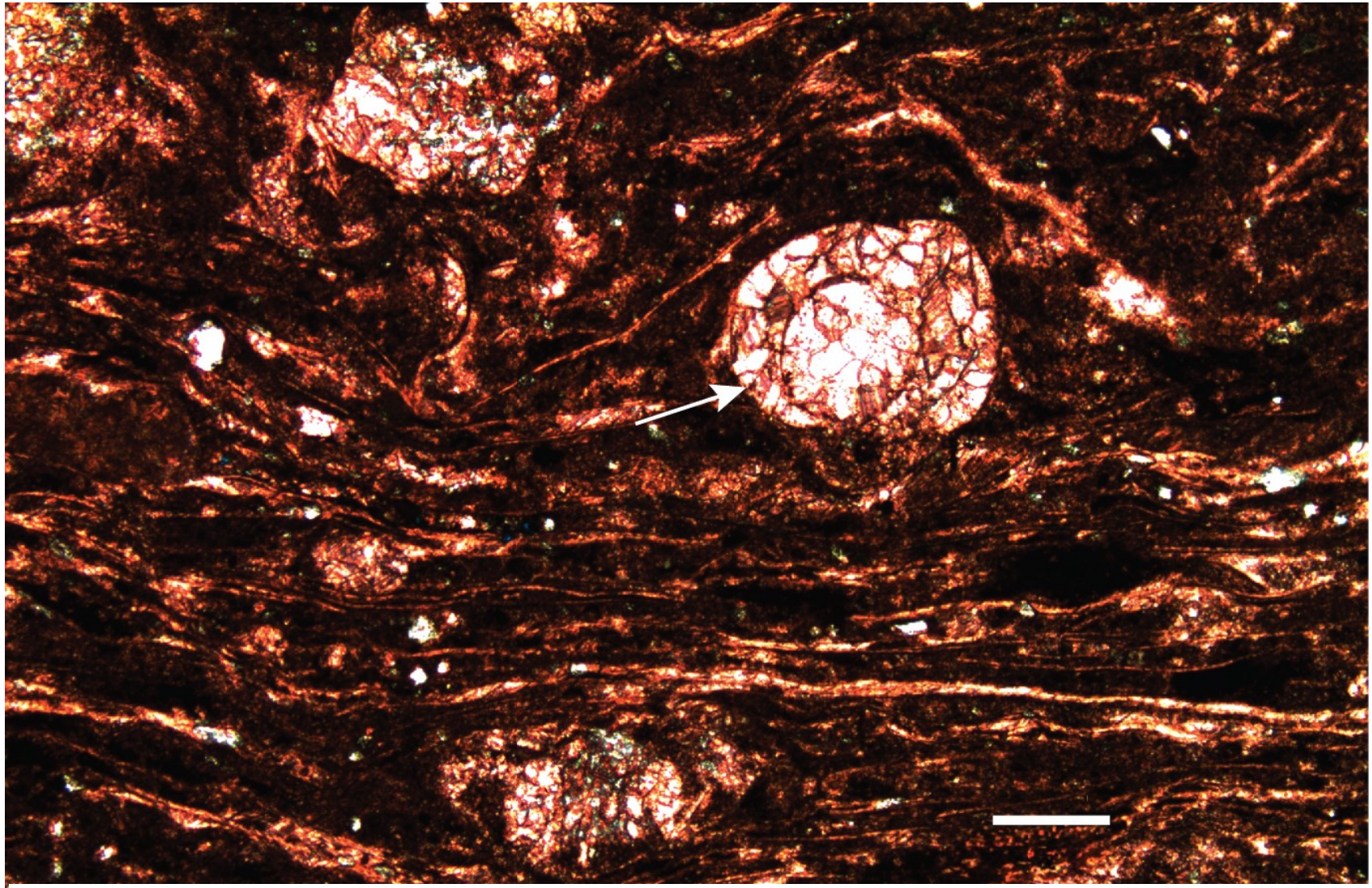

Figure 2.5: Thin-section photomicrograph of BF1 stained with alizarin red. White arrow points to a calcite filled test of some shallow water animal. Calcite lineaments creating lamination in the matrix are *Halobia sp.* shells concordant to bedding. Matrix is composed of organic matter, pyrite, and mud-sized carbonate giving it its dark appearance. Sample SA-1605-BBR-073 from Black Bear Ridge, 25.4 m below top. Scale is 500 µm.

BF2

BF2 is certainly the most conspicuous facies in the Pardonet and is commonly called a bivalve laminite in literature (Davies, 1997b; Zonneveld et al., 2004; McRoberts, 2011). BF2 typically consists of monospecific accumulations of *Halobia, Eomonotis,* or *Monotis* that are invariably deposited whole, large, unabraded but flattened, and concordant to bedding which gives the beds a unique 'crinkly' lamination in side view (Figs 2.6-2.8). This facies is prominent in outcrop due to the high fossil content. When viewed in thin-section, BF2 exhibits very little matrix although some quartz silt, organic matter, pyrite, and carbonate mud can be observed between shells. BF2 commonly gradationally overlies BF1 and is also commonly sharply overlying or underlying BF4 or BF5.

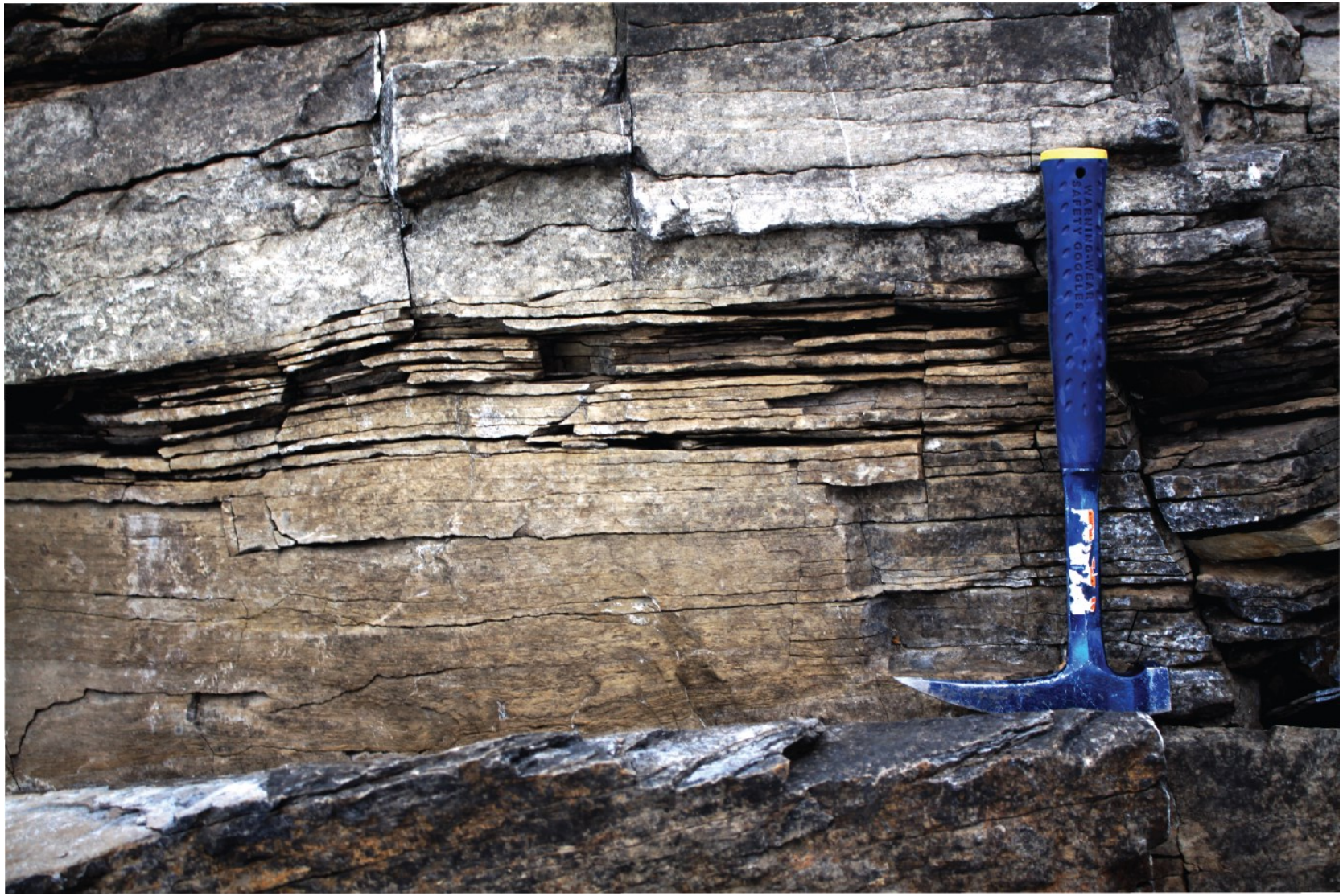

Figure 2.6: BF2 in outcrop, lateral view. Crinkled breaks between beds are caused by densely packed *Halobia.* Photograph from Brown Hill, 45.5 m above base. Rock hammer is 33 cm in length.

Figure 2.7: BF2 in outcrop, lateral view. Crinkled lamination is caused by densely packed *Monotis*. Photograph taken at Black Bear Ridge, 29.5 m below top. Ruler is 1.5 m long.

Figure 2.8: BF2 in outcrop. Above the scale bar, wavy or 'crinkly' lamination is apparent in lateral view. In the bedding plane below the scale bar, ribs of *Monotis* sp. shells can be seen. Photograph taken at Brown Hill, 63 m above base.

Figure 2.9: BF2 in bedding-plane view with abundant, overlapping *Monotis subcircularis*. Photograph taken at Black Bear Ridge, 0.5 m below top. Scale card is 7 cm

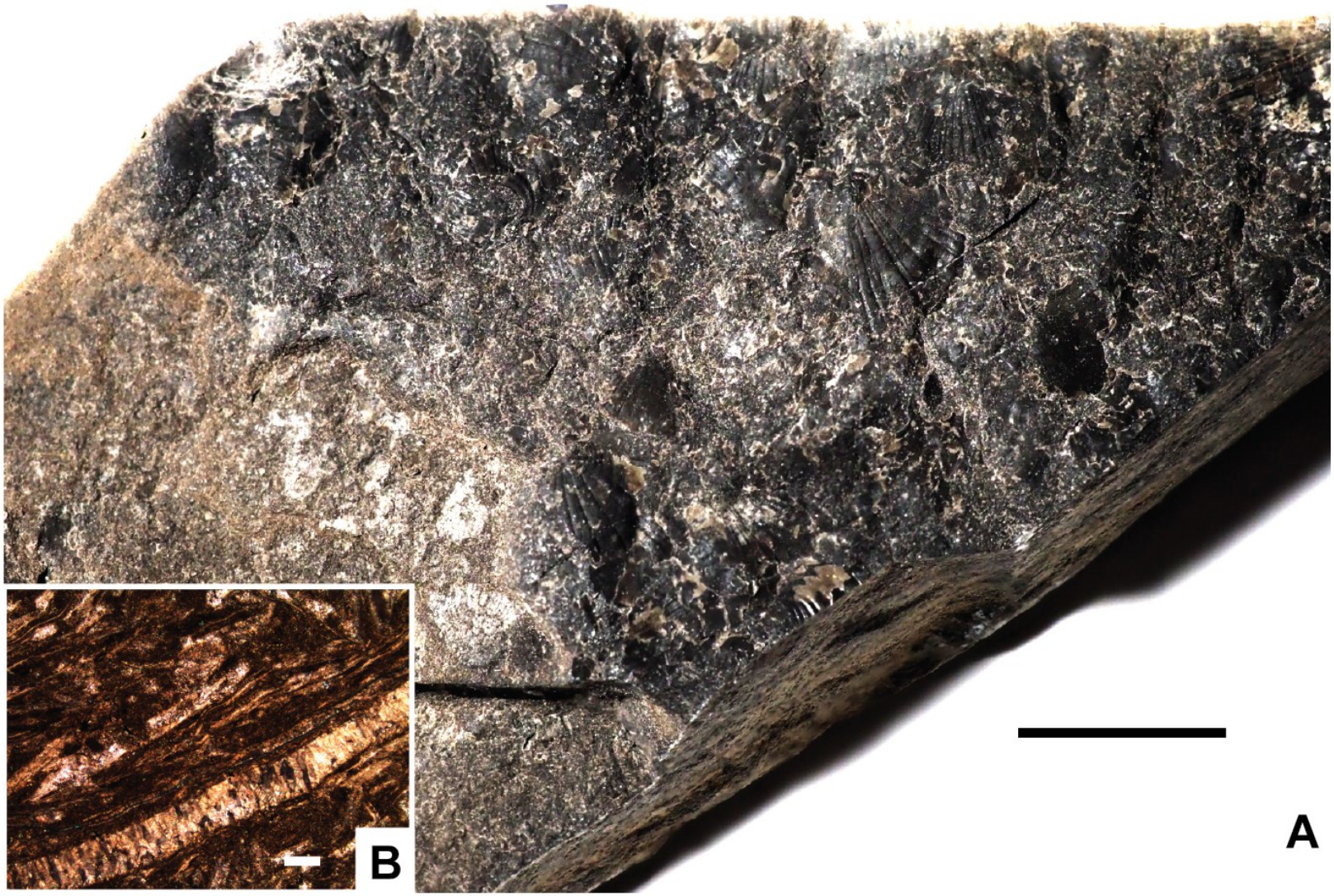

Figure 2.10: BF2 with abundant *Halobia sp*. Sample SA-PA-1605-47 from Pardonet Hill, 27 m above base. A) Ribs are apparent on bedding plane but much less apparent than in BF2 composed of monotids (Figure 2.9). Scale is 1 cm. B) Thin-section photomicrograph showing dense packing of *Halobia* shells scale is 500 µm.

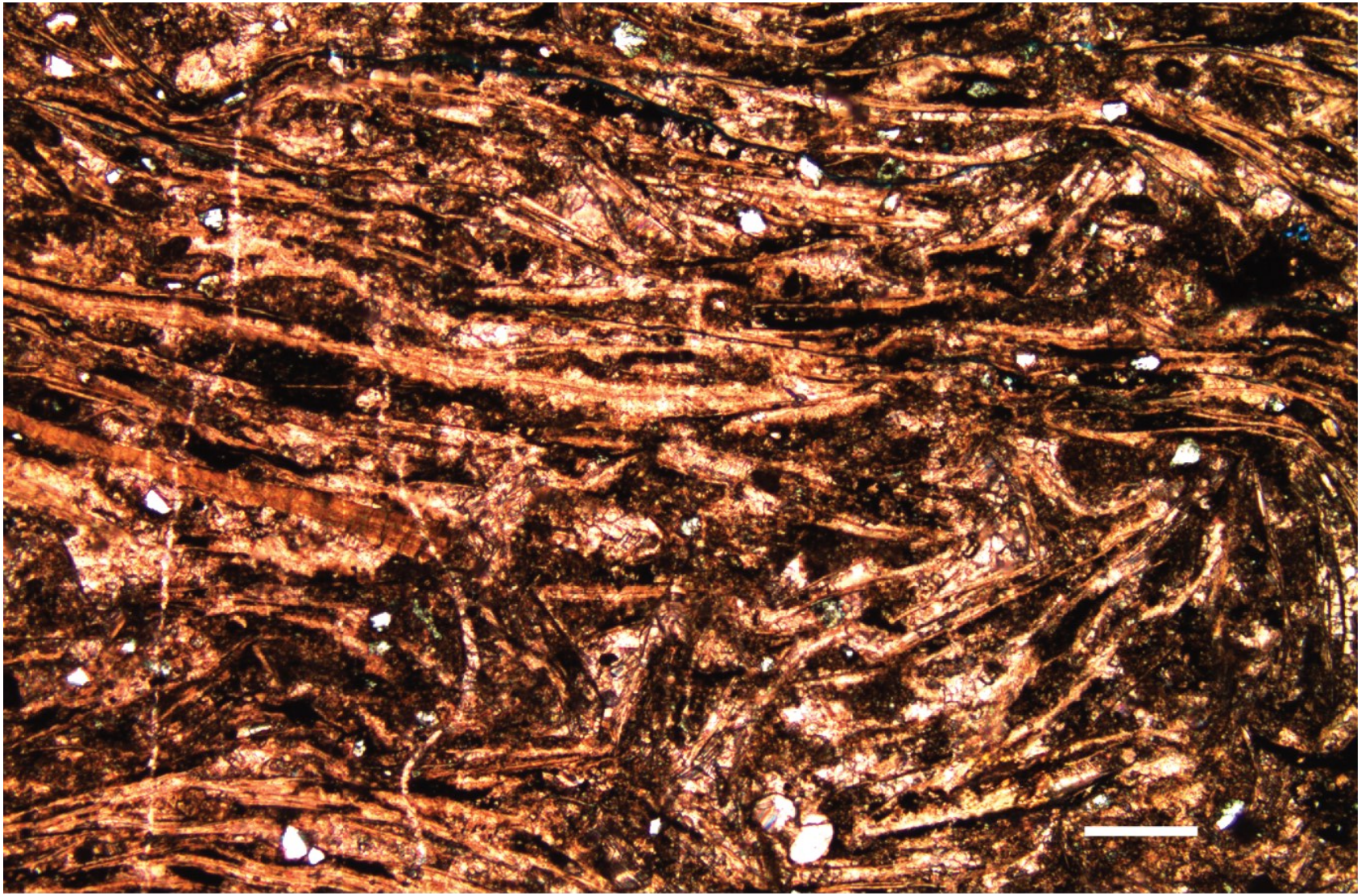

Figure 2.11: Thin-section photomicrograph of BF2. The sample is dominantly composed of *Monotis sp.* shells concordant to bedding. Sample SA-1605-BH-017 from Brown Hill, 52.9 m above base. Scale is 500 µm.

BF3

BF3 is a thinly bedded, silty floatstone with abundant but non-overlapping *Halobia, Eomonotis,* or *Monotis* that were emplaced concordant to bedding (Figs 2.15-2.18). BF3 typically appears brown in outcrop (Figs 2.12-2.15). Flat-clams are generally adult size and right and left valve pairs can be observed in association (Figure 2.16).

Figure 2.12: BF3 in outcrop overlain by BF5. Photograph taken at Brown Hill, 40 m above base.

Figure 2.13: BF3 in outcrop, lateral view. A small-scale reverse fault, marked by the black line, is an example of fractures that are commonly observed in the Pardonet formation in the Rocky Mountain foothills. Photograph taken at Brown Hill, 57.5 m above base. Rock hammer is 33 cm.

Figure 2.14: BF3 in outcrop, lateral view. Photograph taken at Black Bear Ridge, 35 m below top. Ruler is 1.5 m in length.

Figure 2.15: BF3 in outcrop overlying BF5, lateral view. Black arrows indicate two large concretions. These are very common in the thinner bedded units of the Pardonet formation and are commonly more fossiliferous than surrounding strata. Photograph taken at Brown Hill, 50.5 m above base. Rock hammer is 33 cm in length.

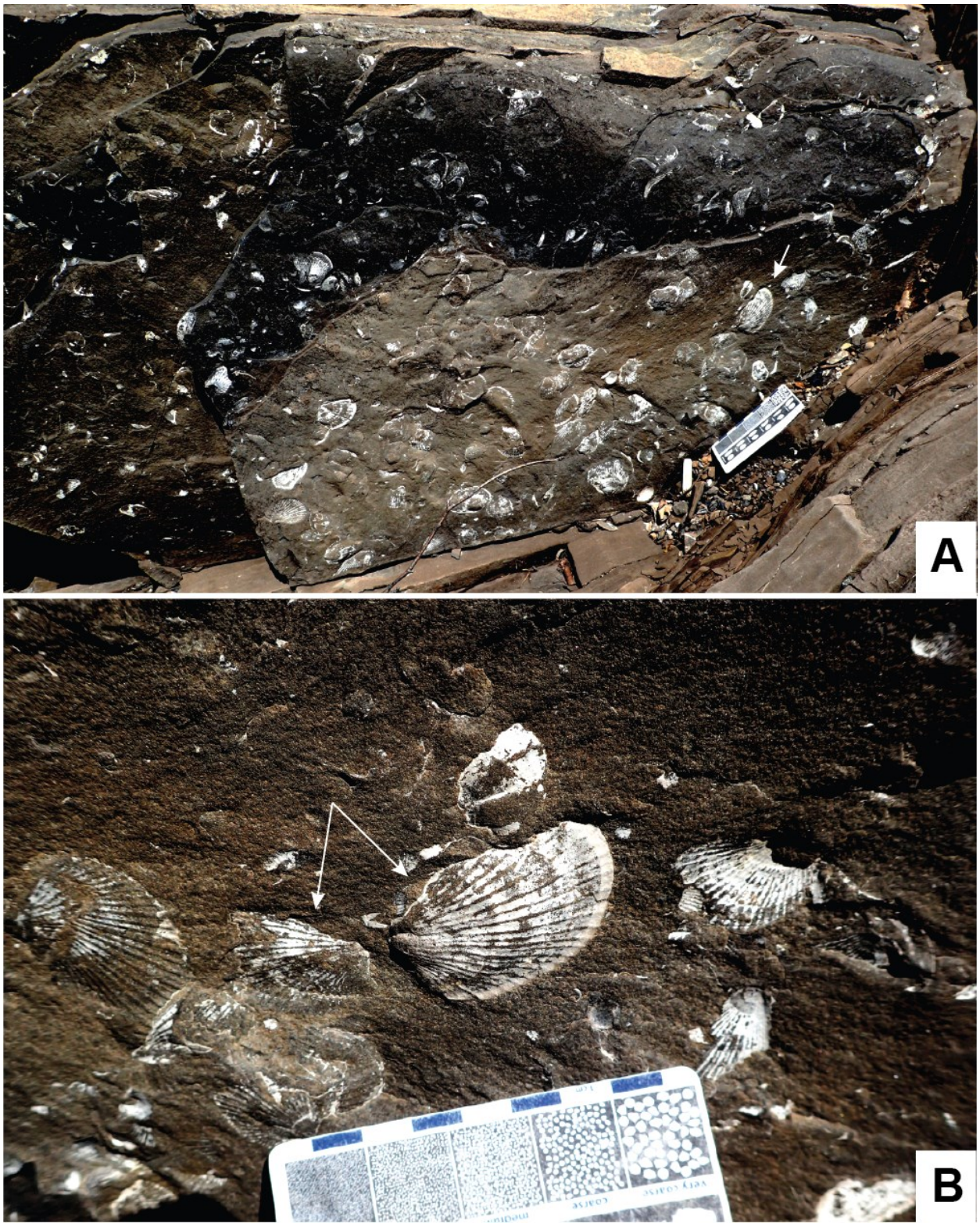

Figure 2.16: *Eomonotis pinensis* preserved in BF3. Photographs taken at Brown Hill in bedding plane view, 53.5 m above base. Scale card is 7 cm. A) Abundant *E. pinensis* in several beds always concordant to bedding and approximately equal proportions convex-up and concave-up orientations. White arrow indicates the position of B. B) Close association of right and left valves with hingelines aligned indicates this specimen was not transported

Figure 2.17: *Monotis subcircularis* in BF3. These specimens are small for this species but are also among the oldest *Monotis* observed at Black Bear Ridge, 35.6 m above base. Scale is 5 cm.

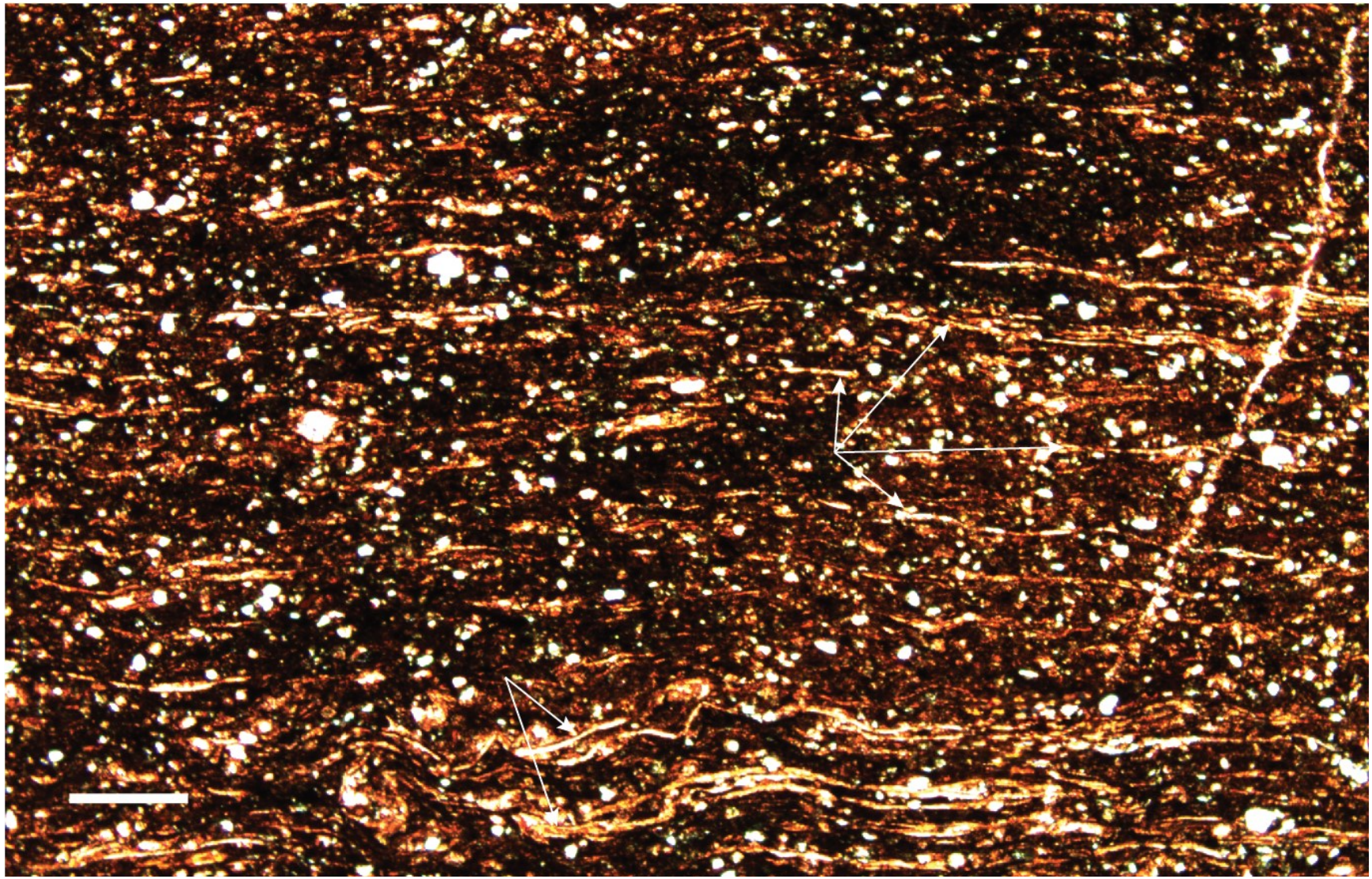

Figure 2.18: Thin-section photomicrograph of BF3. White arrows indicate thin *Halobia sp.* shells concordant to bedding. White angular grains are quartz silt. Matrix is composed of organic matter, pyrite, and mud-sized carbonate giving it a dark appearance. Sample SA-1605-BBR-076 from Black Bear Ridge, 53.4 m below top. Scale is 500 µm.

BF4

BF4 contains densely packed, flattened, whole and fragmentary halobiid or monotid bivalves deposited concordant to bedding (Figure 2.22), in a matrix containing a relatively high proportion of quartz silt and other detrital material as well as carbonate mud, organic matter, and pyrite. When viewed in thin-section, BF4 displays alternations between more shell rich and more detritus rich layers (Figure 2.24). The high shell content gives this facies a 'crinkly' lamination similar to BF2 (Figs. 2.19-2.23) In the upper Pardonet, it is notable that monotid bivavles are never full adult size in BF4 (Figure 2.23). BF4 is commonly in association with BF2 or BF6.

Figure 2.19: BF4 in outcrop, lateral view. Crinkled breaks between beds is caused by dense *Halobia sp.* on bedding contacts. BF4 superficially resembles BF2 in outcrop but is typically more recessive and thinner bedded. Thicker beds above are BF1. Photograph taken at Brown Hill, 49.7 m above base. Rock hammer is 33 cm in length.

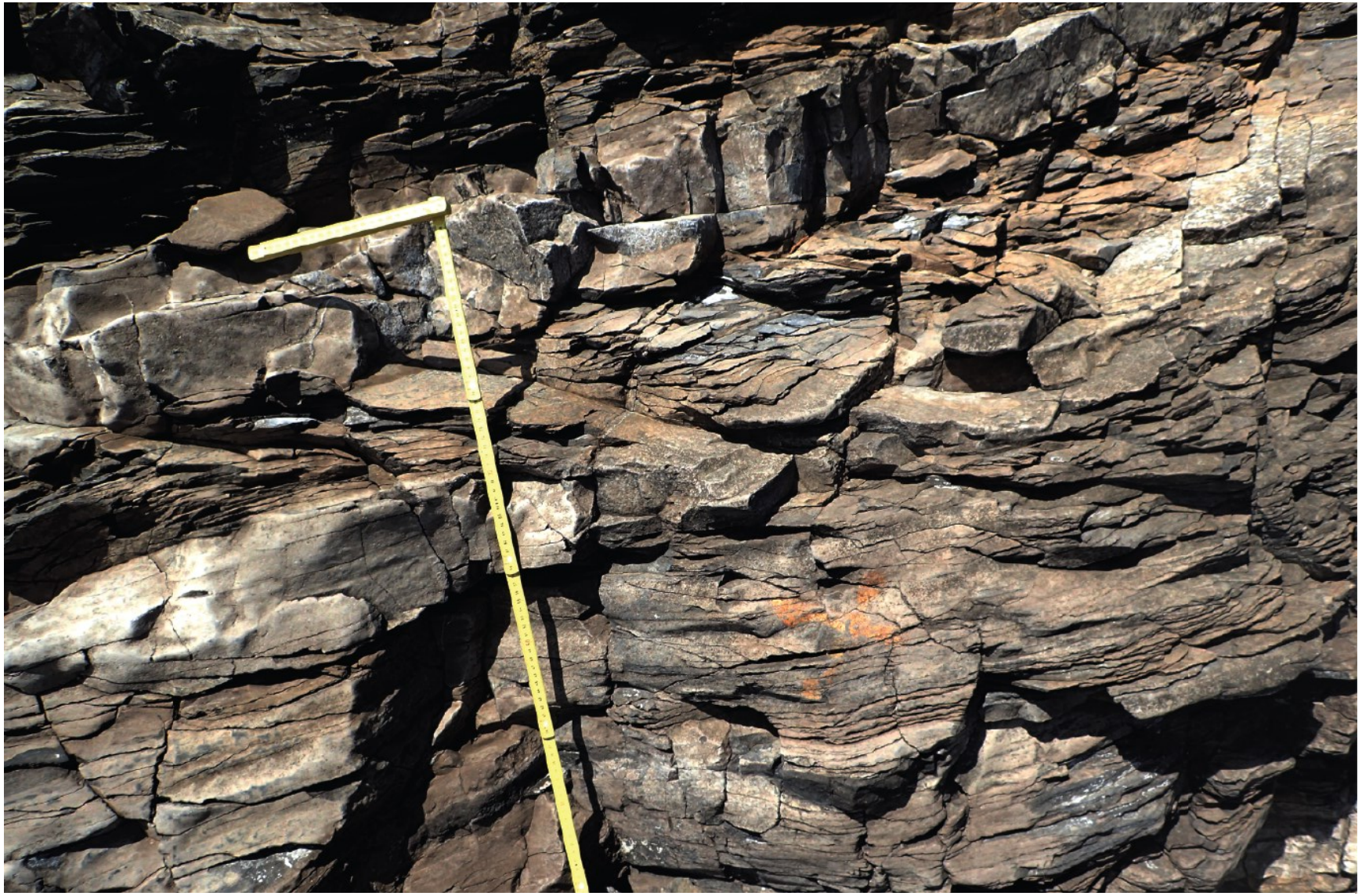

Figure 2.20: BF4 in outcrop, lateral view. Crinkled breaks between beds is caused by dense *Halobia sp.* on bedding contacts. BF4 superficially resembles BF2 in outcrop but is distinctly more fissile. Photograph taken at Black Bear Ridge, 43.5 m below top. Ruler segments are 30 cm.

Figure 2.21: BF4 in outcrop, lateral view. Crinkled breaks between beds is caused by dense *Monotis sp.* on bedding contacts. These beds are conspicuously similar to BF4 in the *Halobia* interval (Figure 2.19, 2.20). Photograph taken at Black Bear Ridge, 12 m below the top. Ruler segments are 30 cm.

Figure 2.22: BF4 with fragments of *Halobia cordillerana.*on the bedding plane. Sample is from BH-22-2-2.50 from Brown Hill, 48 m above base. Note that this sample occurs above the first appearance of *Eomonotis.* This species survived into the *Eomonotis* interval (McRoberts, 2010; 2011).

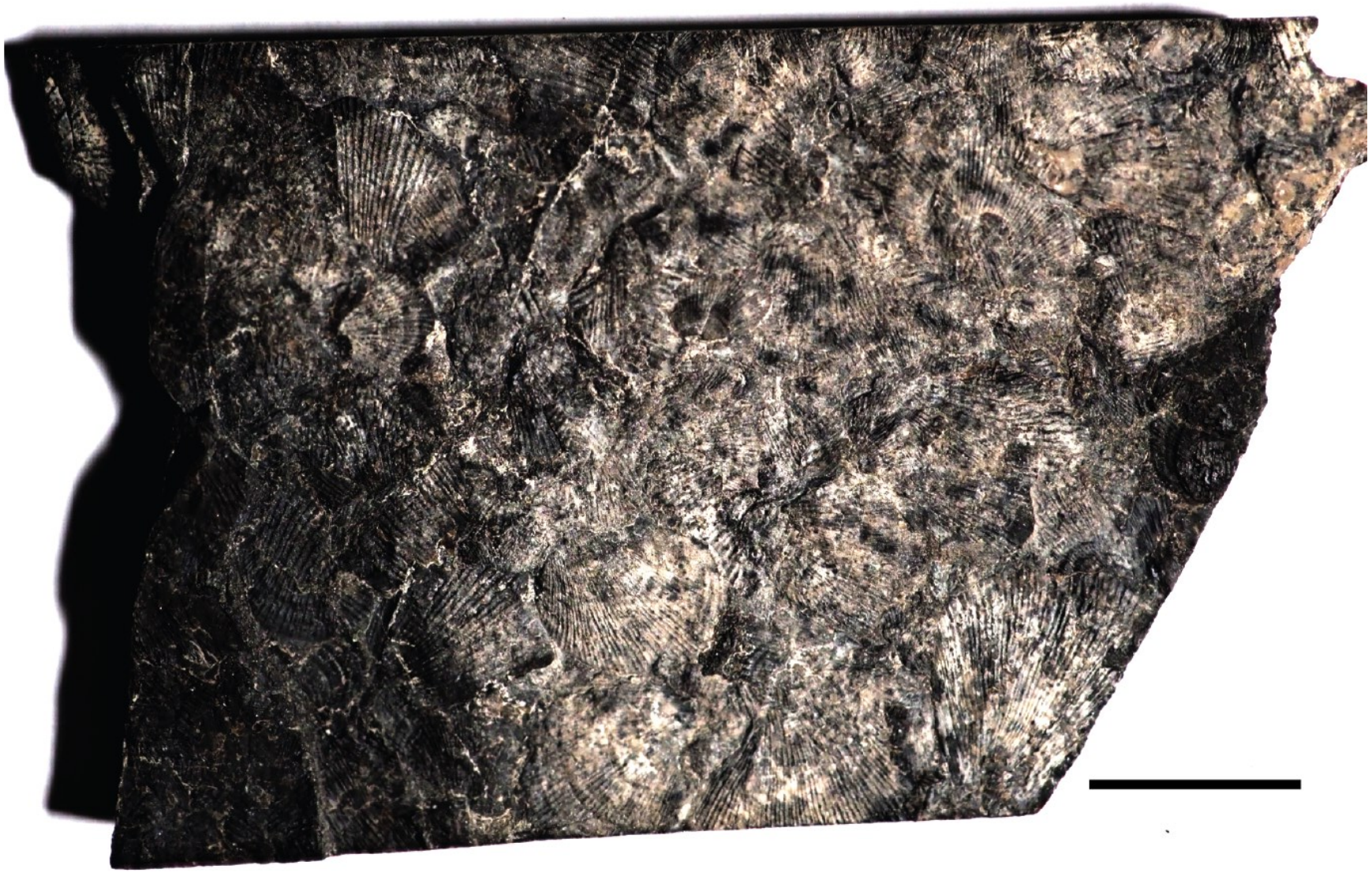

Figure 2.23: BF4 with abundant monotids. These shells are much smaller than expected for monotids, however, this sample is from about 30 m above the last appearance of *Eomonotis pinensis* at Black Bear Ridge, 9 m below the top. Scale is 1 cm.

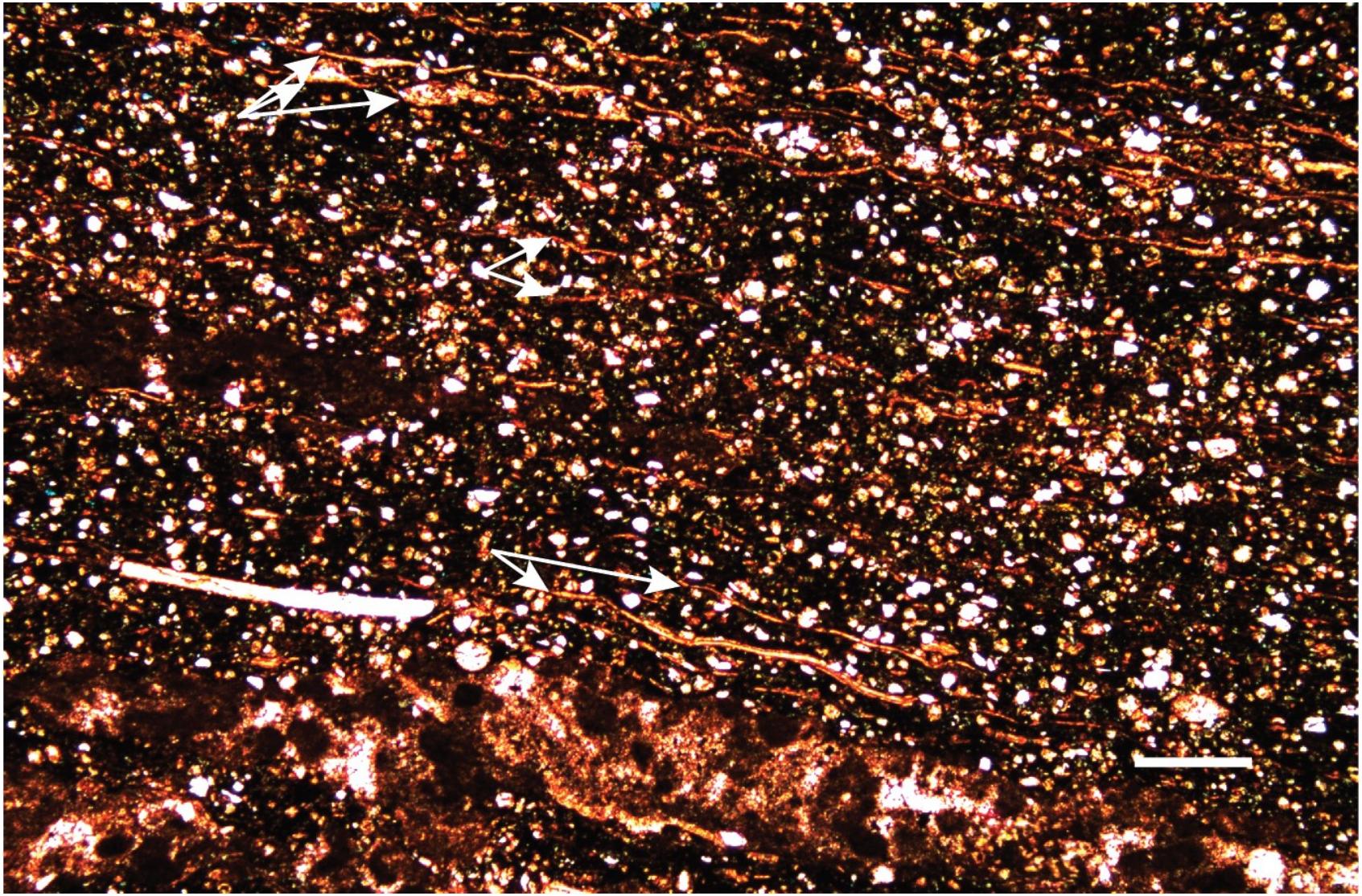

Figure 2.24: Thin section photomicrograph of BF4. White arrows indicate shells fragments of *Halobia sp.* Note that there is much more detritus when compared to thin sections of the other facies. Sample SA-1605-BBR-081 from Black Bear Ridge, 116.1 m above the base. Scale is 500 µm.

BF5

BF5 includes prominent floatstone units that preserve adult-size monotid bivalves in 3-dimensions that occur convex-up on bedding planes (Figs 2.26, 2.29). BF5 commonly breaks on bedding planes which expose lags of smaller shells (Figs 2.27, 2.28, 2.30). Both large and small shells are typically deposited concordant to bedding. The matrix of this facies is a silty carbonate mud (Figure 2.32). BF5 is typically sharply overlying or underlying BF2 or BF6. BF5 is more difficult to identify in the *Halobia* (lower) interval but could be identified from samples taken from beds stratigraphically lower than the intervals analyzed for geochemistry in this study (Figs 2.30, 2.31). BF5 is typically well cemented and prominent in outcrop (Figs 2.25, 2.33).

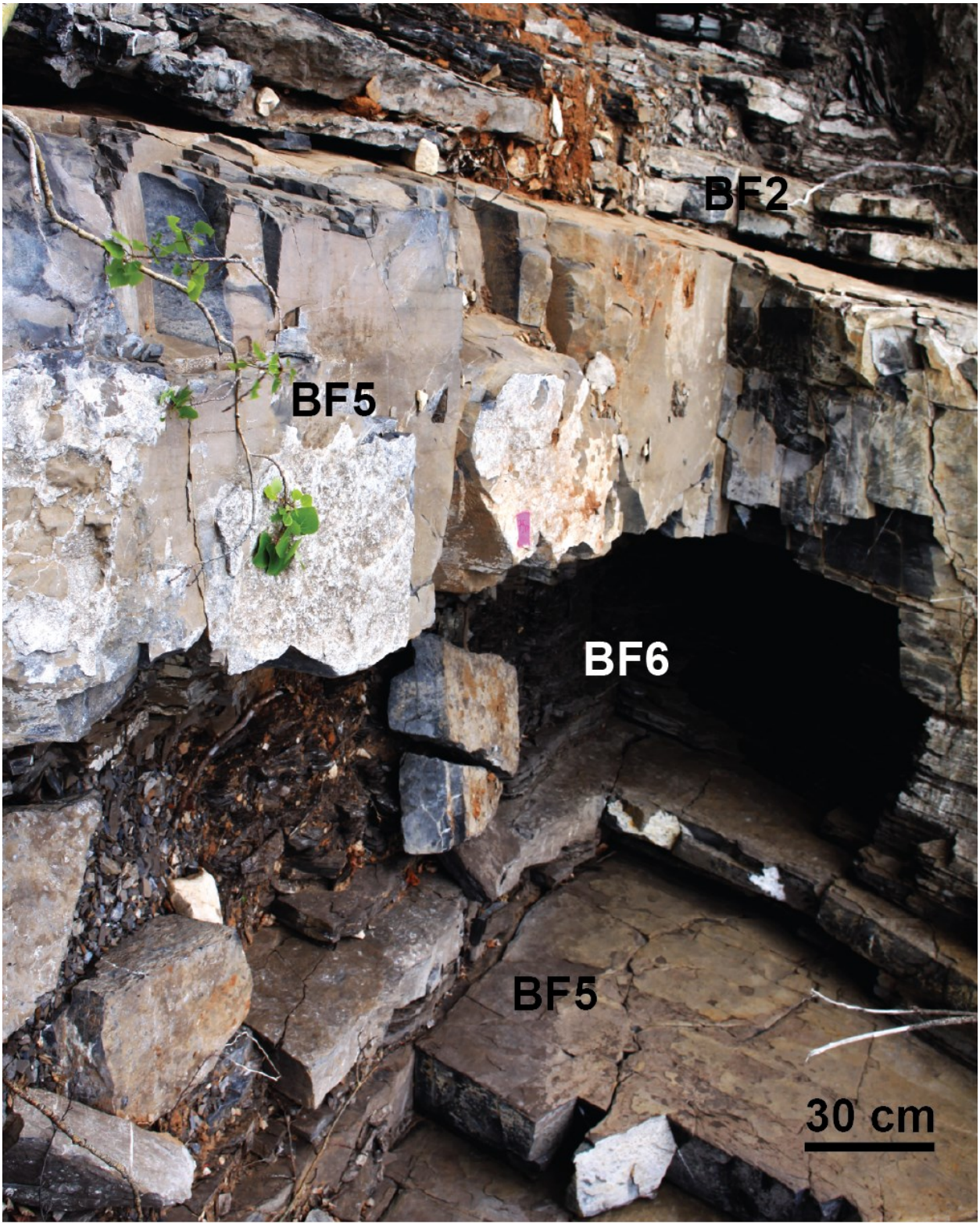

Figure 2.25: BF5 in outcrop at Brown Hill, 59.5 m above the base. Recessive beds in between are the only example of BF6 observed outside of the upper portion of Black Bear Ridge. BF2 overlays.

Figure 2.26: *Monotis subcircularis* preserved in 3 dimensions on a bedding plane in BF5. Photograph taken at Black Bear Ridge. 11.6 m below the top. Scale is 5 cm.

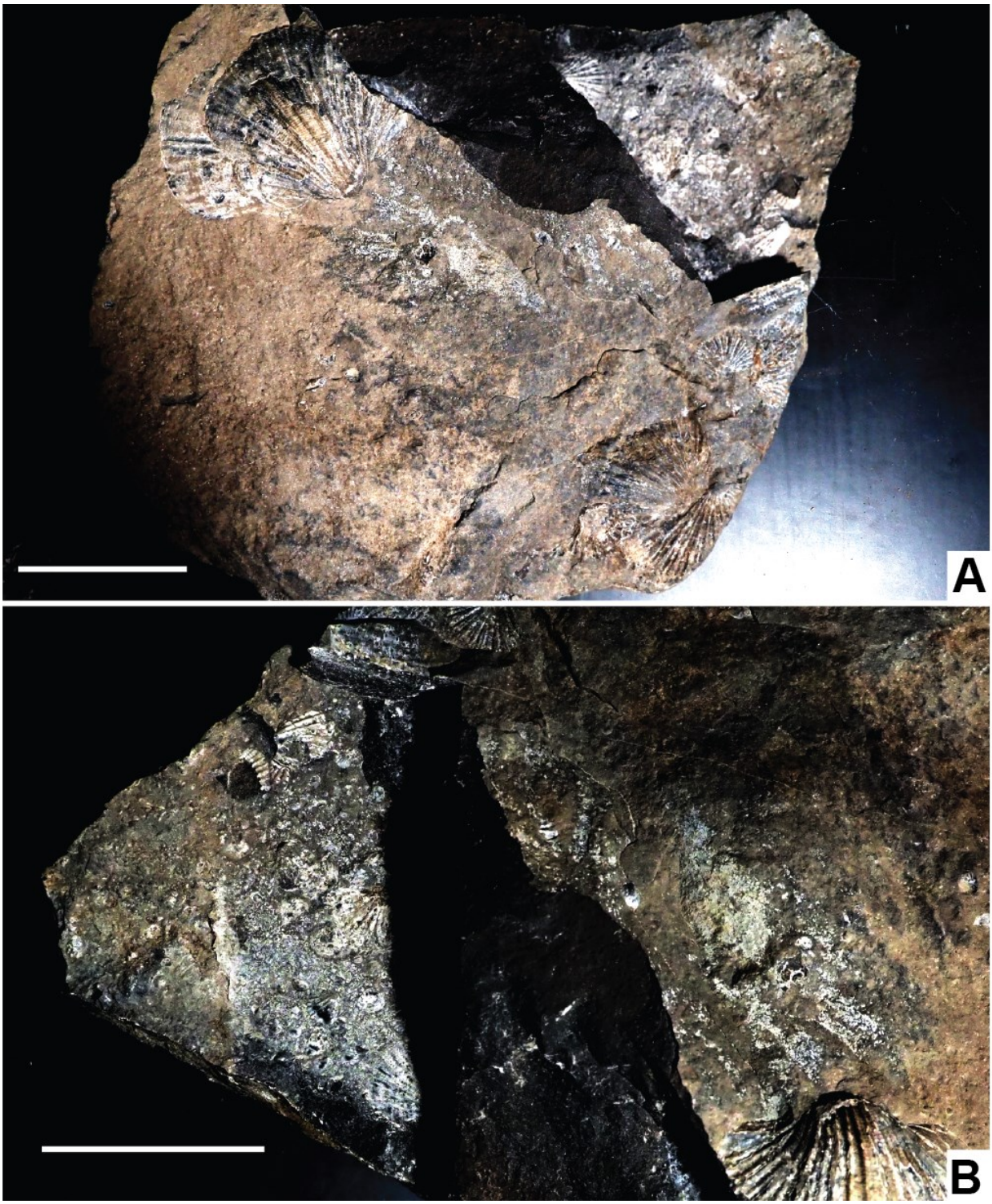

Figure 2.27: Sample BBR-22-2-40.95F from Black Bear Ridge, 11.6 m below top.: *Monotis subcircularis* in BF5. Scale is 5 cm. A) One large isolated shell in 3 dimensions on the bedding plane and several larger shells exposed towards the bottom of the photograph. B) Exposed on a lower bedding plane is a lag of very small individuals.

Figure 2.28: Concentration of small *Monotis subcircularis* exposed on a bedding plane in BF5. Photograph taken at Brlack Bear Ridge, 16. 2 m below the top. Scale card is 7 cm.

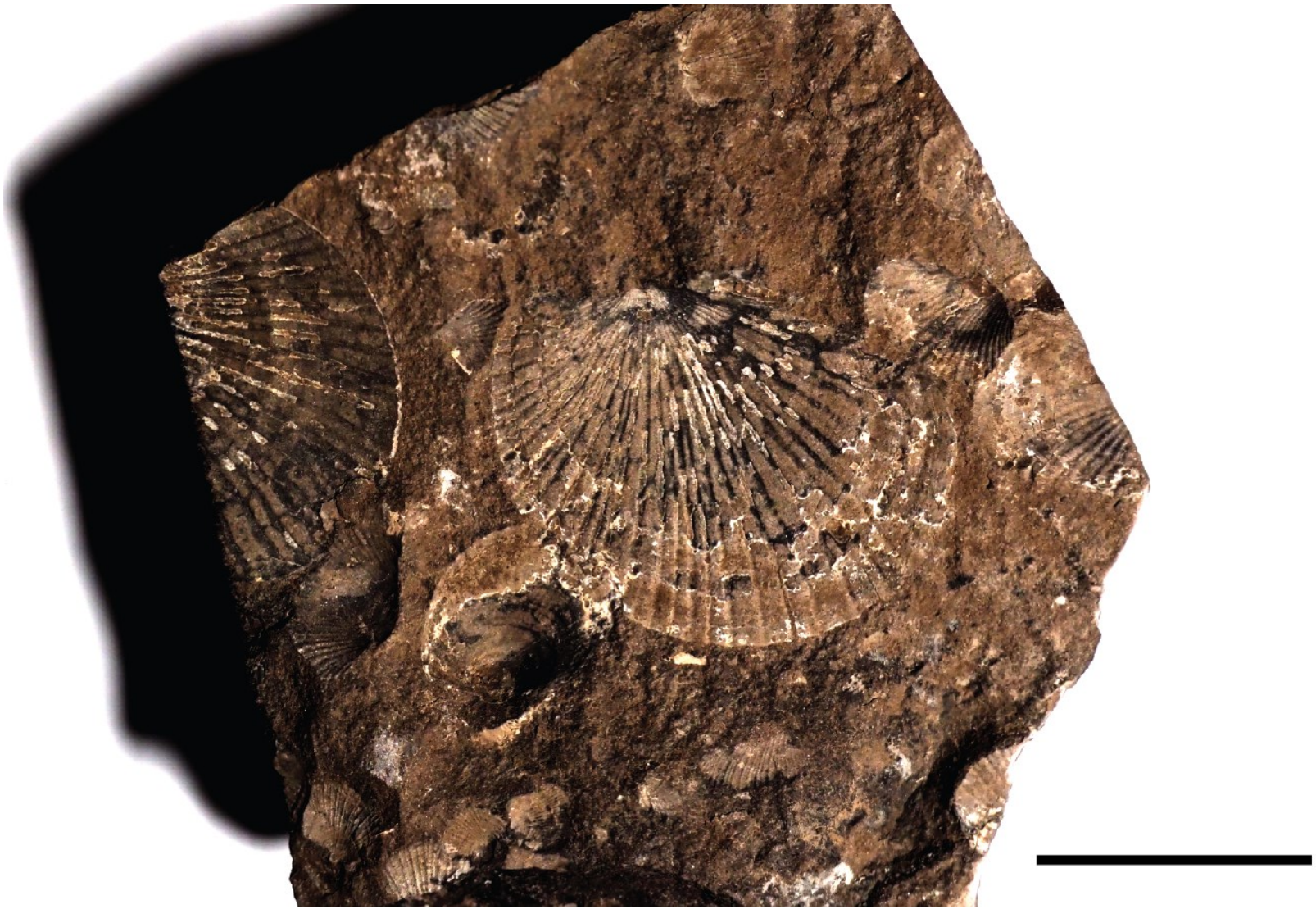

Figure 2.29: Impression of *Eomonotis pinensis* on the sole of bed, BF5. Note the variability in size and dominantly convex-up orientation. Sample BH-22-2-11.65F from Brown Hill, 57.2 m above the base. Scale is 3 cm.

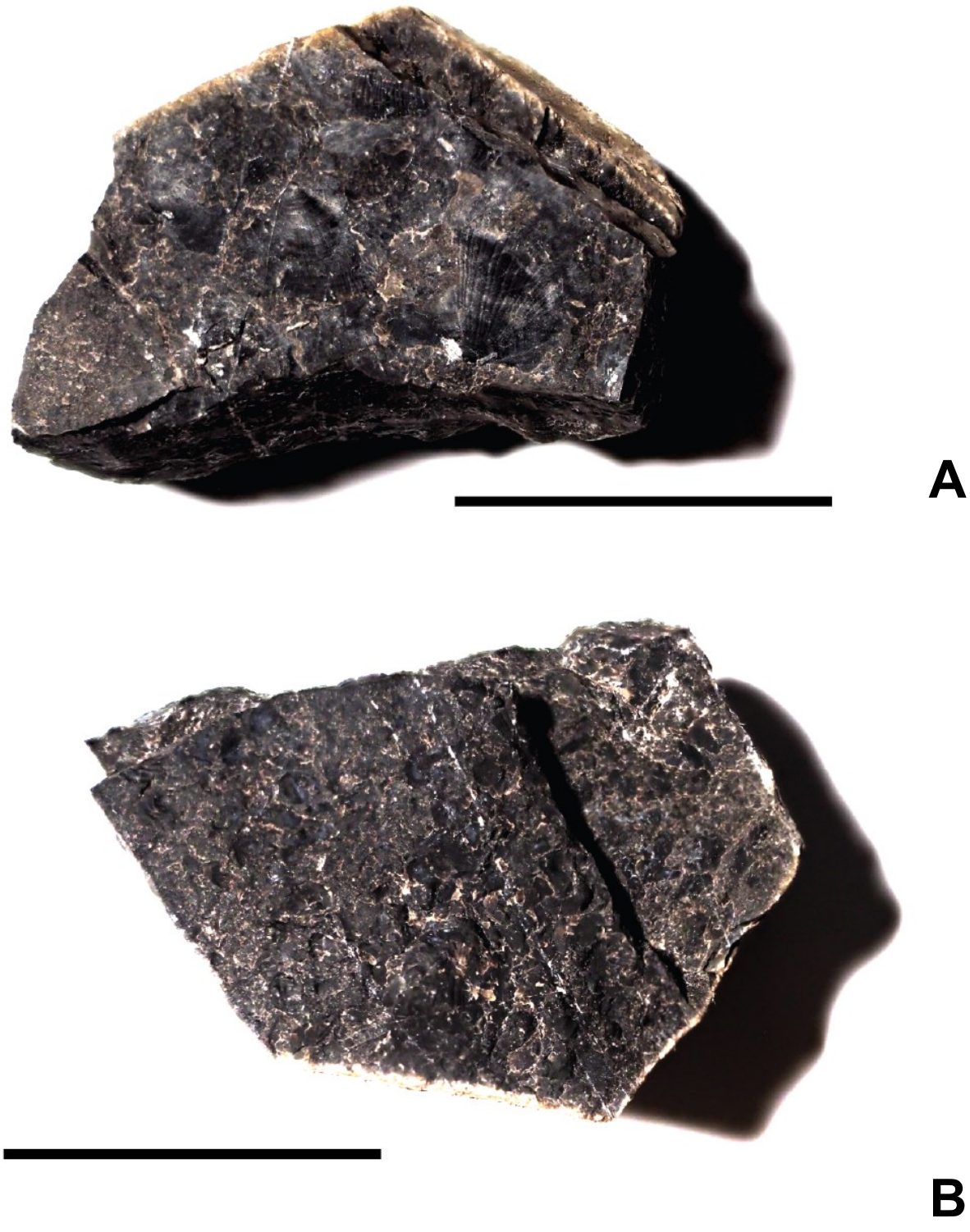

Figure 2.30: Sample PH-22-2-5.00F from Juvavites Cove, 5 m above creek (UTM: 49772 E, 6213150 N, 10V). Scale is 1 cm. A) *Halobia sp.* is apparent on upper bedding plane and resembles the expression of BF2 in the *Halobia* interval (Figure 2.10). B) Impressions of small *Halobia* on the sole of the sample. This sample establishes a criterion of recognition of BF5 in the *Halobia* interval.

Figure 2.31: Sample SA-BH-1605-015 from Brown Hill, 45.3 m above the base. This sample is an example of how BF5 can be expressed in the Halobia interval. A) *Halobia sp.* is obviously abundant in this sample. Note the inflation preserved in the umbo area (black arrow) Scale is 3 cm. B) Thin-section photomicrograph shows that shell is, in fact, not the dominant the dominant component of this rock. Scale is 500 μm.

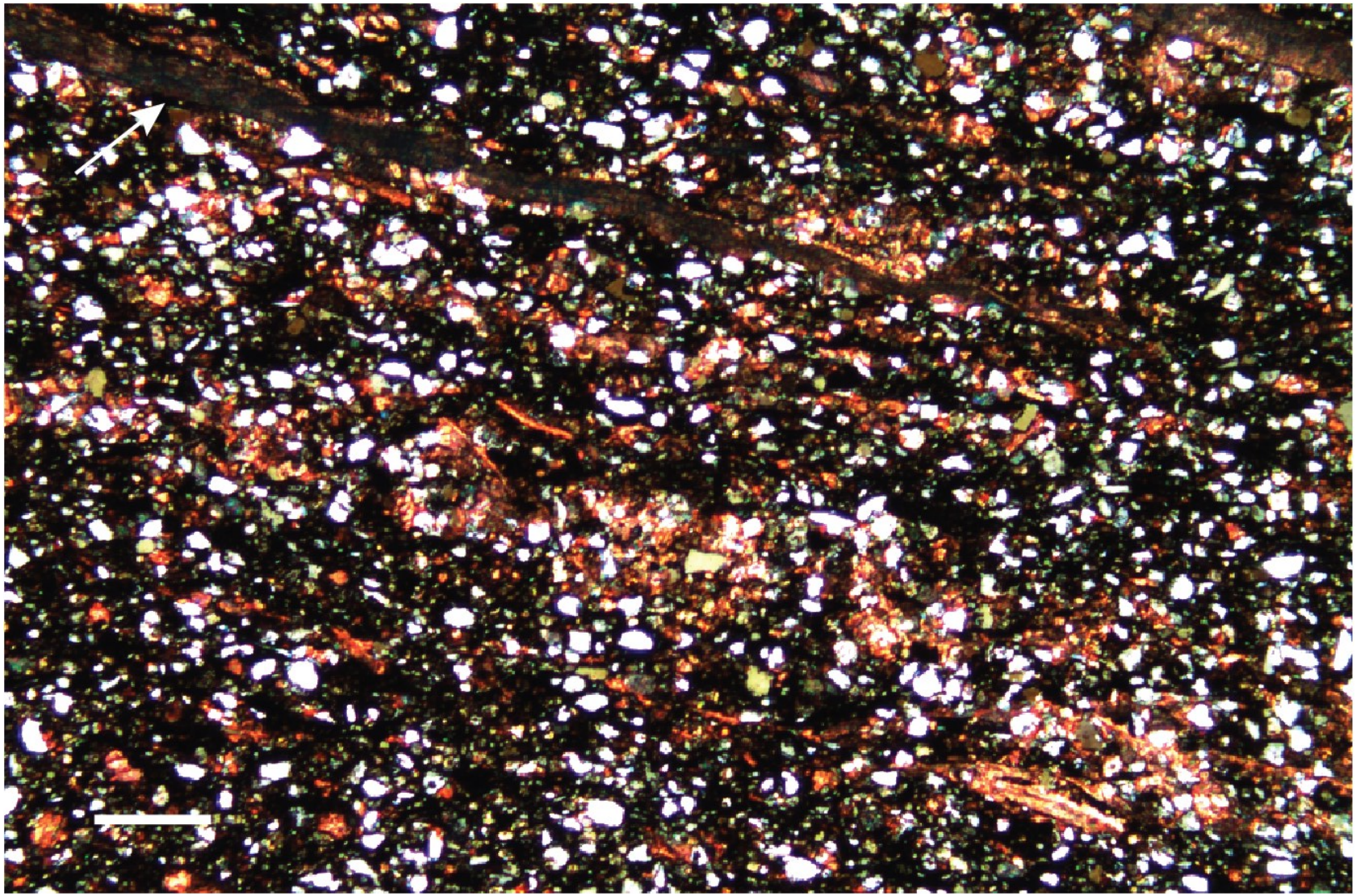

Figure 2.32: Thin-section photomicrograph of BF5. Note the single large *Monotis sp.* shell (white arrow) and the large silt grain size compared to other thin sections. Sample SA-1605-BH-019 from Brown Hill, 65.5 m above base. Scale is 500 µm.

BF6

BF6 is a thinly-bedded, dark grey to black wackestone to floatstone with small and fragmentary monotids (Figs 2.33-2.37). Larger shells typically occur concordant to bedding but the smallest size fraction can occur in random orientations. In thin section, it was observed that BF6 contains less silt and more organic matter and pyrite when compared with the other facies (Figure 2.38). BF6 was only observed toward the top of the Black Bear Ridge section with the exception of a single bed at about 59.5 m above the basal contact with the Baldonnel formation at Brown Hill (Figure 2.25). In the top of the Black Bear Ridge section, BF6 is broken up by beds of BF4 and BF5.

Figure 2.33: BF6 in outcrop. Prominent bed stratigraphically underlying is BF5. Photograph taken at Black Bear Ridge, 20.3 m below the top. Ruler is 150 cm in length.

Figure 2.34: BF6 in outcrop, bedding-plane view. Abundant but small *Monotis sp.* exposed. In contrast to BF5, no adult size shells are observed. Photograph taken at Black Bear Ridge, 17.5 m below top. Segments on Jacob's staff are 10 cm.

Figure 2.35: BF6 in outcrop, bedding-plane view. Solitary, juvenile monotid. Photograph taken at Black Bear Ridge, 18.7 m below top. Scale card is 7 cm.

Figure 2.36: BF6 in outcrop. Abundant shell fragments on bedding plane. Photograph taken at Black Bear Ridge, 7 m below the top. Scale card is 7 cm.

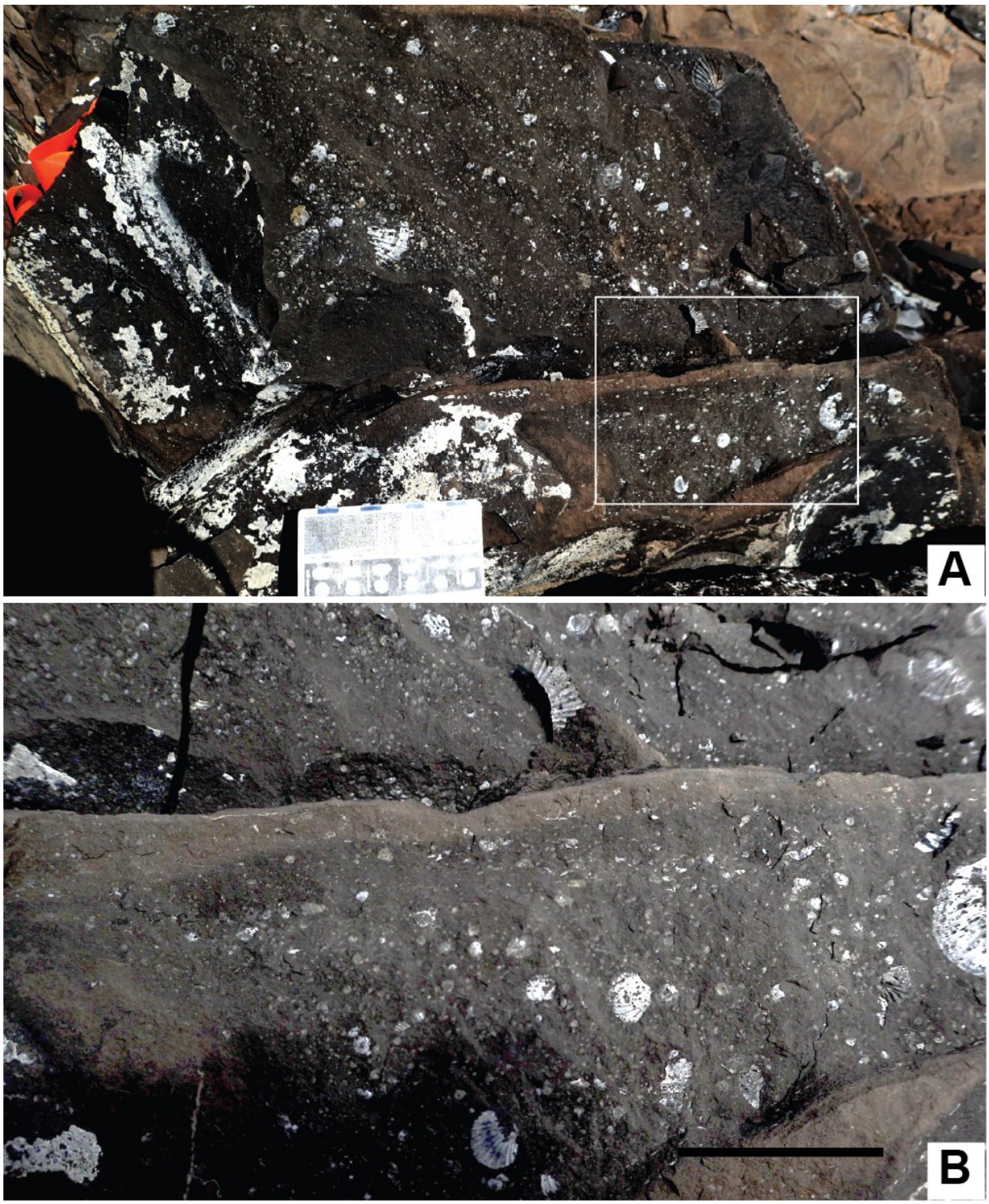

Figure 2.37: BF6 in outcrop, Black Bear Ridge, 7 m below the top. A) Scattered shell material on bedding planes. White box is the location of B. Scale card 7 cm. B) Shell material is fragments or small individuals. Scale 3 cm.

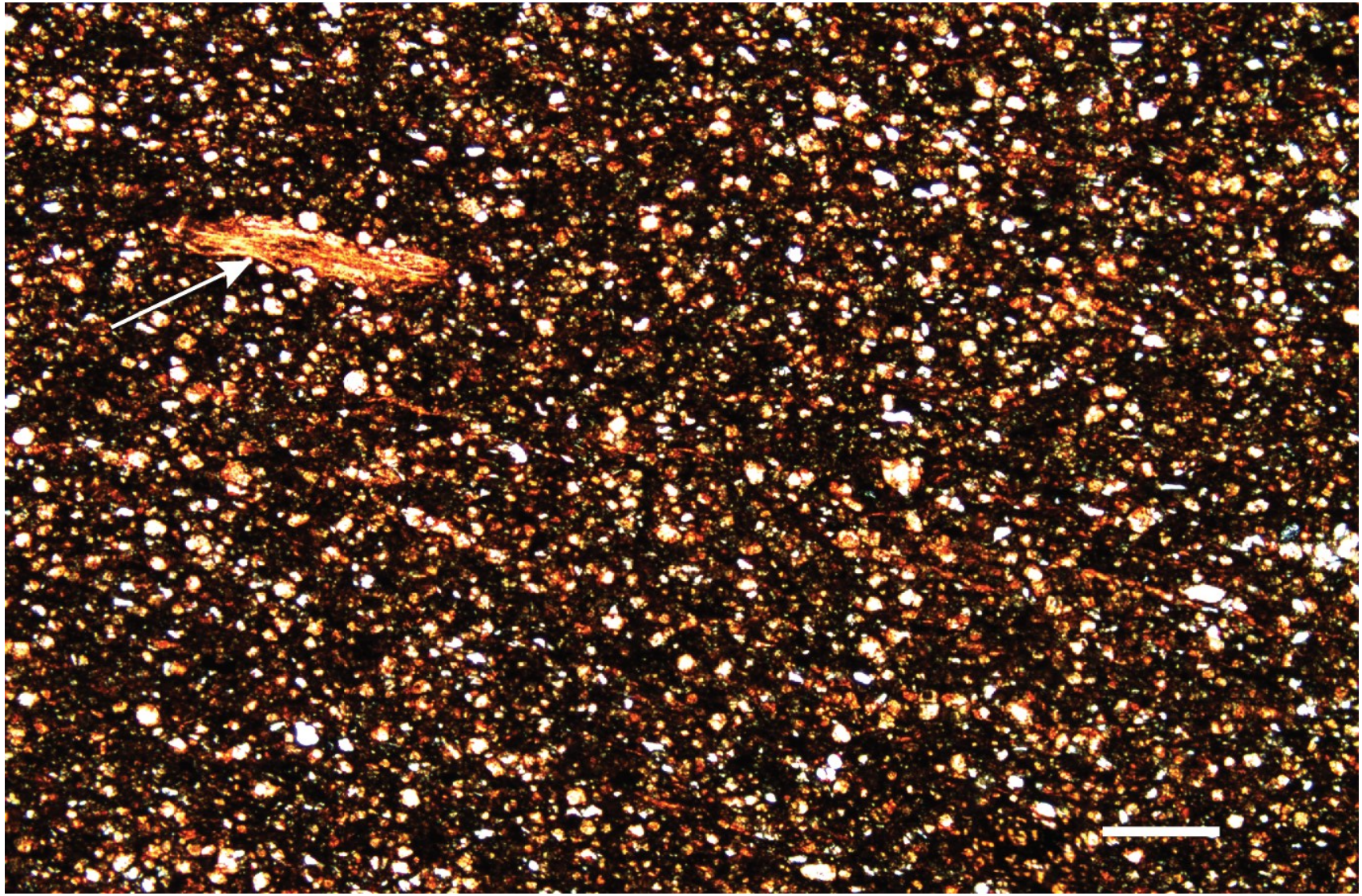

Figure 2.38: Thin-section photomicrograph of BF6. Single shell fragment indicated by white arrow. The rock is dominantly composed of fine-grained silt, carbonate, and organic matter. Sample SA-1605-BBR-090 from Black Bear Ridge, 88.9 m above the base. Scale is 500 µm.

Results

Framboid data

Comparing framboid size-distributions between facies reveals that BF4 and BF6 are characterized by a smaller average framboid size than the other facies (medians=4.00 μm, 4.06 μm respectively; Figure 2.39A-B). Framboids from BF5 display the highest averages (median=5.30 μm). BF2 and BF3 display somewhat moderately sized framboid distributions (medians=4.57 μm, 4.08 μm). BF1 also displays low average framboid sizes (median=4.29 μm). Sample variances compliment these patterns very well. BF2, BF3, and BF5 have the highest variances (medians=2.41 μm, 2.54 μm, 4.11 μm respectively) while BF1, BF4, and BF6 have the lowest variances (medians=1.65 μm, 1.87 μm, 1.43 μm respectively).

Trace Metal Data

U shows enrichment in BF2, BF3, BF4, and BF6 (means=8.2, 9.9, 12.6, 9.3 ppm respectively; Figure 2.39C; Table 2). U_{XS} in BF1 and BF5 is also elevated but less so (means= 5.7, 5.7 ppm respectively). Mo shows moderate values in BF1, BF2, BF3 and BF5 (means=17.8, 27.1, 18.9, 17.4 ppm respectively) and strongly enriched in BF4, and BF6 (means= 87.9, 88.0 ppm respectively; Figure 2.39D). All facies displayed high V/Cr ratios, means ranging from 10.30 to 40.31 (Table 2). V/(V+Ni) ratios are also high, ranging from 0.64-0.99 across all samples.

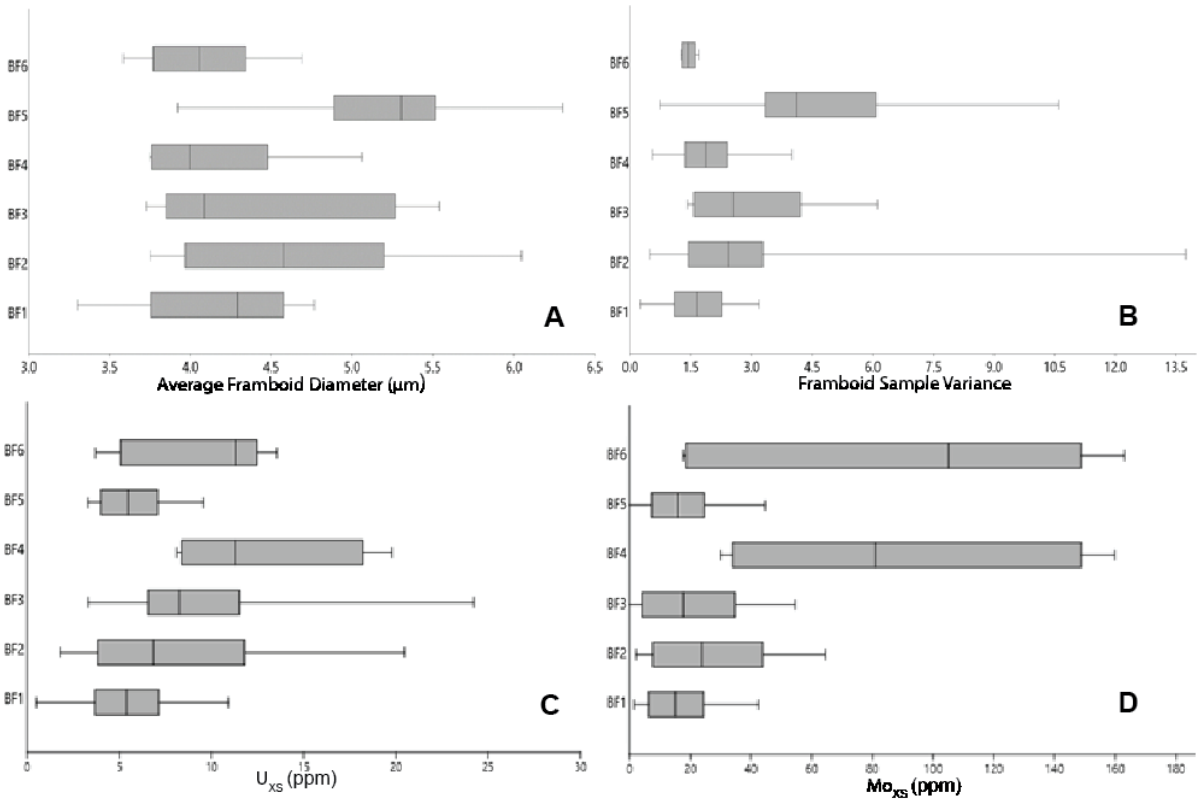

Figure 2.39: Box and whisker plots comparing redox proxy data between the 6 facies. A) Box and whisker plots represent the distribution of the average framboid diameter calculated for each sample. B) Box and whisker plots display the distribution of the variance in framboid diameter calculated for each sample. C) U_{XS} distributions are plotted for each facies. D) Mo_{XS} distributions shown for each facies.

Proxy	SEM		Framboid diameter (µm)					ICP	U_{xs} (ppm)			
Stat	# of samp	n=	Mean	SD	Min	Max	Degree of modification	n=	Mean	SD	Min	Max
BF1	13	328	4.17	1.39	1.23	10.46	High	13	5.68	3.53	0.50	10.91
BF2	15	479	4.53	1.93	1.20	22.58	High	18	8.19	5.86	1.80	20.47
BF3	12	317	4.58	1.93	1.04	14.81	High	10	9.93	6.61	3.31	24.22
BF4	8	339	4.17	1.42	1.47	10.89	Low	4	12.61	7.19	8.12	19.78
BF5	8	370	4.91	2.12	1.81	19.37	Moderate	10	5.72	2.93	3.31	9.56
BF6	6	202	4.02	1.26	1.32	10.08	Low	5	9.26	5.69	3.70	13.56

Proxy	ICP	Mo_{XS} (ppm)				V/Cr				V/(V+Ni)			
Stat	n=	Mean	SD	Min	Max	Mean	SD	Min	Max	Mean	SD	Min	Max
BF1	13	17.76	14.03	1.55	42.44	40.32	22.76	14.36	81.02	0.90	0.05	0.79	0.97
BF2	18	27.06	21.36	2.09	64.49	31.60	24.94	5.12	96.48	0.88	0.06	0.76	0.96
BF3	10	18.88	20.86	-16.5	54.61	27.21	44.84	1.55	153.14	0.87	0.10	0.64	0.99
BF4	4	87.93	57.40	29.92	159.82	10.30	1.14	9.06	11.81	0.88	0.04	0.84	0.93
BF5	10	17.45	13.95	-0.75	44.66	22.16	23.53	9.65	87.00	0.86	0.04	0.80	0.93
BF6	5	87.96	67.90	17.64	163.06	14.30	2.37	10.84	17.49	0.90	0.03	0.87	0.93

Table 2: Statistics of geochemical redox-proxies for each facies. Note that framboid statistics are calculated for the whole data set for each facies rather than from the average of each sample.

CHAPTER 3: PALEO-REDOX CONDITIONS OF THE PARDONET FORMATION

Discussion

Analysis from framboid images indicates that the sections studied were deposited during a long-sustained period of anoxic to euxinic conditions on the deep ocean floor. In all analyzed samples from all facies, 30 framboids could be identified within a reasonably short period of time. This alone suggests that the seafloor consistently experienced reducing conditions throughout deposition of the study interval. It is possible that better oxygenated periods occurred, but H_2S must have at least episodically been free in the water column to explain the abundance of framboids in the sediment (eg. Wilkin et al., 1996). Any such variations occurred on timescales short enough that fully oxygenated facies never developed. Euhedral pyrite is also ubiquitous in all samples. During periods of anoxia, the redox boundary likely laid below the sediment-water interface which allowed framboids to continue to grow within the sediment pile (Wilkin et al., 1996, Wu et al., 2023). This also allowed other diagenetic effects such as overgrowth by diagenetic pyrite or sphalerite, calcite replacement, or the formation of 'polyframboids' (Wignall & Newton, 1998). Qualitative observations of these features were consistent with size distributions (Table 2). Samples with larger and more variable framboid sizes also displayed more diagenetic alteration of framboids. Table 2 summarizes the statistics for all measurements for each facies, however, Figure 2.39 A and B are based on the distribution of averages and variance, respectively, calculated from the measurements from each sample. This method of analysis was used because it draws greater attention to the differences in distributions between the six facies.

For this study, U and Mo were the key elements of interest. The covariance of molybdenum and uranium is a useful tool to gain insight into paleo-redox conditions (Zheng et

al., 2002; Algeo & Tribovillard, 2009; Tribovillard et al., 2012). U(VI) exists in seawater as a highly soluble ion but is reduced to U(IV) at approximately the same redox potential required to reduce Fe(III) to Fe(II). U(IV) is insoluble so U will precipitate into the sediment by forming organic-metal ligands in humic acids or crystalline uraninite (UO_2) (Klinkhammer & Palmer, 1991; Zheng et al., 2002; Algeo & Tribovillard, 2009; Tribovillard et al., 2012). Enrichment in U, therefore, can be used as a proxy for oxygen depletion. Under an oxic water column, [U] has been shown to remain below 5 ppm in modern sediments (Morford et al., 2009). Mo, similarly, begins to enrich in sediments when dissolved O_2 becomes depleted but in the presence of H_2S, Mo precipitation is accelerated by the conversion of molybdate (MoO_4^{2-}) to thiomolybdates ($MoO_xS^{2-}_{(4-x)}$, x=0 to 3) (Zheng et al., 2000; Algeo & Tribovillard, 2009; Tribovillard et al., 2012). This is because thiomolydbates can be captured by both iron sulfides and sulfurized organic matter (Tribovillard et al., 2004). Sediments in anoxic basins have been consistently shown to have Mo concentrations of 20-160 ppm compared to 1-2 ppm in crustal background levels (Zheng et al., 2000). When applying these proxies, paired U and Mo enrichment indicates suboxic to anoxic conditions and strong Mo enrichment relative to U indicates euxinic conditions.

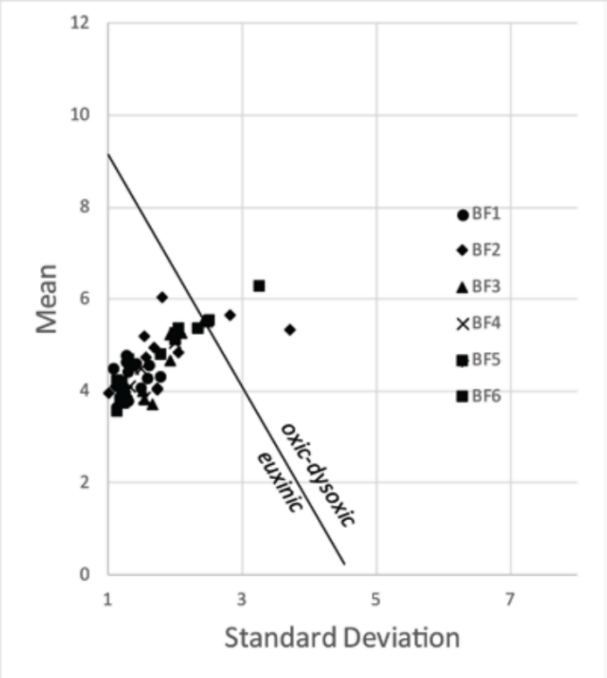

Figure 3.1: Mean versus standard deviation cross-plot of framboid distributions per sample. Euxinic-dysoxic boundary defined following Wilkin et al. (1996). The two parameters are dependant on each other, resulting in the linear relationship, however, if either parameter exceeds a defined threshold, the sample did not form in euxinic conditions.

During euxinic periods, the redox boundary was above the sediment-water interface so framboids quickly fell to the sediment surface resulting in an overall small size distribution with low variance. BF4 and BF6 display framboid distributions with lower averages and variances suggesting deposition in euxinic conditions (Figure 2.39A, B). Mo becomes exceedingly enriched in BF4 and BF6 with moderate U enrichment which fits with the expectation of euxinic sediments (Zheng et al., 2000; 2002; Algeo & Tribovillard, 2009; Tribovillard et al., 2012). BF2, BF3, and BF5 display more moderate U and Mo concentrations and framboid distributions with higher averages and variances so can be interpreted as representing suboxic conditions. Enrichment in U and Mo coupled with the persistent presence of pyrite framboids throughout the studied intervals suggests benthic oxygen was constantly limited. Sample means were plotted against the standard deviations of each individual sample in order to observe the combined effect of the two measures (Figure 3.1). The linear relationship is attributed to the dependence of standard deviation on the sample mean but this allows a discrete boundary defined from modern anoxic basins to be drawn between euxinic and oxic to dysoxic conditions (Wilkin et al., 1996). The majority of the data from the Pardonet formation falls on the euxinic side further emphasizing the persistence of anoxic conditions during the Norian of Western Canada.

The ratio between V and Cr can be used as a redox indicator using a value of 2 as a cutoff (Dill, 1986). V is considered an authigenic redox proxy while Cr represents the detrital component so values less than 2 are considered oxic while values greater than 2 are considered anoxic (Dill, 1986; Wignall et al., 2007; Onoue et al., 2016). Average values across all facies in this study were greater than 10. While this is consistent with the strongly reducing conditions interpreted from all the other redox proxies applied, the V/Cr seem to be anomalously high. There could be an external factor at play causing depletion of Cr or this is possibly an effect of

carbonate dilution which would impact authigenic elements more than detrital element. V/(V+Ni) is another index which has been applied to interpret redox conditions. Values greater than 0.84 are taken to indicate euxinic conditions, values less than 0.60 are considered suboxic, and intermediate values between the two limits are considered anoxic (Hatch & Leventhal, 1992; Wignall et al., 2007; Onoue et al., 2016). Samples from all facies averaged greater than 0.84, adding more evidence of persistent euxinia throughout the studied interval. These two indices taken together with the framboid data would actually suggest all facies formed in somewhat euxinic conditions. V/Cr an V/(V+Ni) are generally regarded, however, as being better interpreted from stratigraphic trends rather than adhering to strict cutoffs (Wignall et al., 2007; Onoue et al., 2016). The U and Mo data seems to record more subtle variations which are hopefully associated with the redox boundary moving from within the sediment pile to above the sediment-water interface. Only the latter condition is relevant to epibenthic fauna such as the flat clams which are the focus of this study.

The distributions of the trace metal data for BF1 and BF5 span the thresholds of 5 ppm U and 20 ppm Mo which is the only indication that oxic conditions may have occurred in these 2 facies. The interpretation of BF1 is less conclusive from the redox proxies. Framboids are generally small but typically appear to have been replaced by calcite. U and Mo concentrations are both relatively low. The fact that BF1 shows good evidence of being formed by gravity flows transporting material from shallower water makes the explanation complicated because the clasts in the flow are unrelated to the redox conditions of where they came to rest. Since BF1 can be safely interpreted as the most proximal facies, better oxygenation would make sense, however, its formation is likely independent of redox conditions where the flow settled. If material was shed from shallow water into deeper euxinic waters, that could explain the incorporation of small

framboids that possibly remineralized in the presence of oxygen carried from shallow water along with the flow. Oxygenated turbidity currents could also account for the lower concentrations of U and Mo in BF1 and BF5. Proxy data shows good agreement with facies interpretations because facies with anoxic to euxinic signatures appear to lack *in situ* shell material.

It is acknowledged that the turbidity events described in Chapter 2 could likely remobilize trace metals, thus skewing the concentrations preserved. However, it is much more likely that currents would remove redox-sensitive trace elements rather than concentrating them because authigenic elements are generally associated with the fine-grained fraction (Sageman & Lyons, 2003). For that reason, where enrichment is observed it is more likely to underestimate the degree of oxygen depletion rather than imply depletion where fully oxygenated sediments existed if current alteration is truly a concern. The above interpretations of paleo-redox conditions thus remain valid. The same can be said for pyrite framboids. It can be imagined that pyrite framboids could be winnowed out of the sediments, however, that is a process that would be unlikely to concentrate a framboid population with small sizes and low variance. The fact that framboids are still present in facies deposited under higher energy conditions demonstrates that they are likely not transported. They may, however, better reflect conditions following event deposition rather than during the event itself.

When plotted against stratigraphic height, the applied redox proxies show good agreement with each other (Figs 3.2, 3.3). That is to say that U_{XS}, Mo_{XS}, V/Cr, and V/(V+Ni) all

Figure 3.2: Brown Hill section litholog demonstrating stratigraphic distribution of observed facies aligned with multiple geochemical logs of redox proxy data. 0 m on the logs is 45.5 m above the basal contact with the Baldonnel formation. The top is the end of outcrop exposure at Brown Hill. Timescale on left calibrated with conodont and bivalve sample identifications, ammonoid zones assumed based on previously published correlations to conodont and bivalve zonations.

Middle Norian
Upper Norian
II
III
IV
Columbianus
Cordilleranus
p.
serrulata
bidentata
H.
Eomonotis
Monotis
FA1
FA2
FA1
0
5
10
15
20
Gamma
0
50
100
150
Fram Average (µm)
Fram Variance
0.0
5.0
10.0
Uks
0
20
40
Moxs
1
10
100
Mo/U
0.3
0.9
2.7
8.1
V/Cr
0
50
100
V/(V+Ni)
0.7
0.8
0.9
1

Middle Norian
Upper Norian
II Columbianus
III
IV
Halobia
Eomon.
postera
serrulata
Cordilleranus
bidentata
Monotis
FA1
FA2
FA1
FA3
Gamma
Fram Average (um)
Fram Variance
Uxs
Moxs
Mo/U
V/Cr
V/(V+Ni)

Figure 3.3: Black Bear Ridge section litholog demonstrating stratigraphic distribution of observed facies aligned with multiple geochemical logs of redox proxy data. 0 m on the logs is 52.5 m below the top contact with the Fernie formation (top of logs). Timescale on left calibrated with conodont and bivalve sample identifications, ammonoid zones assumed based on previously published correlations to conodont and bivalve zonations. Note that the vertical scale is much larger than in Figure 3.2 and sample density is less.

show high values at the same heights corresponding to low framboid diameters and variances. shifts in the geochemical proxy data can also be correlated with lithology changes, however, the trace metal proxies could change in relative proportions due to differences in rock composition, sedimentation rate, or overall detrital material rather than lithology changing in response to paleo-redox conditions. Framboid distributions are certainly not affected by such variables and the chosen trace metal proxies are intended to account for variability in detrital material so it is interpreted that lithology is indeed changing in response to paleo-redox conditions.

To help put the results in context, Mo_{XS} was plotted against U_{XS} (Figure 3.4) so they could be compared with datasets from other modern and ancient sediments (Algeo and Tribovillard, 2009; Tribovillard et al., 2012). Although this method was developed using enrichment factors, the important factors that the cross-plot draws attention to is the ratio of Mo to U and the slope of the best-fit line relative to the baseline ratio found in seawater of about 3.1:1 (Algeo & Tribovillard, 2009) so it is believed that plotting excess values rather than enrichment factors is still useful. The plot is based on trends observed in data from modern sediments in anoxic basins (Algeo and Tribovillard, 2009). In open marine oxygen minimum zones, Mo_{EF}:U_{EF} follows a trend consistent with the average ratio of Mo:U found in seawater with both elements increasing in enrichment with increasingly reducing conditions. In euxinic conditions, Mo_{EF}:U_{EF} increases as the presence of H_2S accelerates Mo precipitation (Zheng et al., 2000; Algeo & Tribovillard, 2009). Other data plots are much higher than the expected Mo:U ratio due to the influence of an "Mn-shuttle" in moderately restricted basins or much lower in strongly restricted basins due to Mo depletion in the deep-water mass (Algeo & Tribovillard,

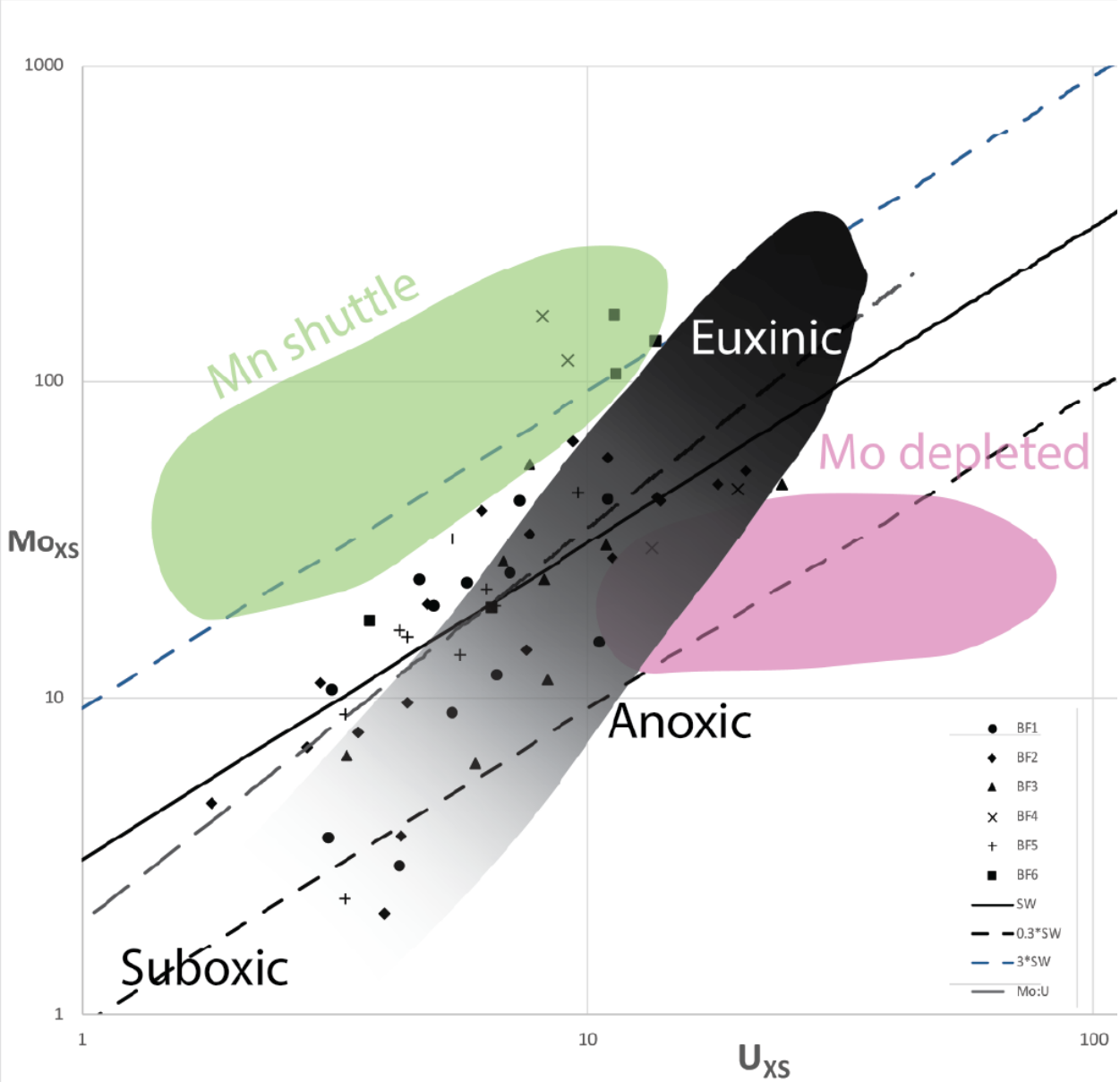

Figure 3.4: Cross-plot of U_{XS} against Mo_{XS}. Data shows an increasing Mo:U ratio relative to the ratio observable in modern open marine sea-water. Fields outlined define the expected ranges data should fall in based on degree of basin restriction. Sea-water ratios and data fields defined after Algeo & Tribovillard (2009) and Tribovillard et al. (2012).

2009). Our data plots within the field defined for open marine shelves, spanning the range from suboxic to euxinic. Consistent with the interpretations already discussed, data points from BF4 and BF6 plot in the euxinic range and even a little above the open marine trend (Mo_{XS}:U_{XS} is greater). The Mo_{XS}:U_{XS} ratio for most of the data points is in the range of typical Mo:U ratios in modern seawater (Algeo & Tribovillard, 2009). The dataset as a whole gives a trendline with a

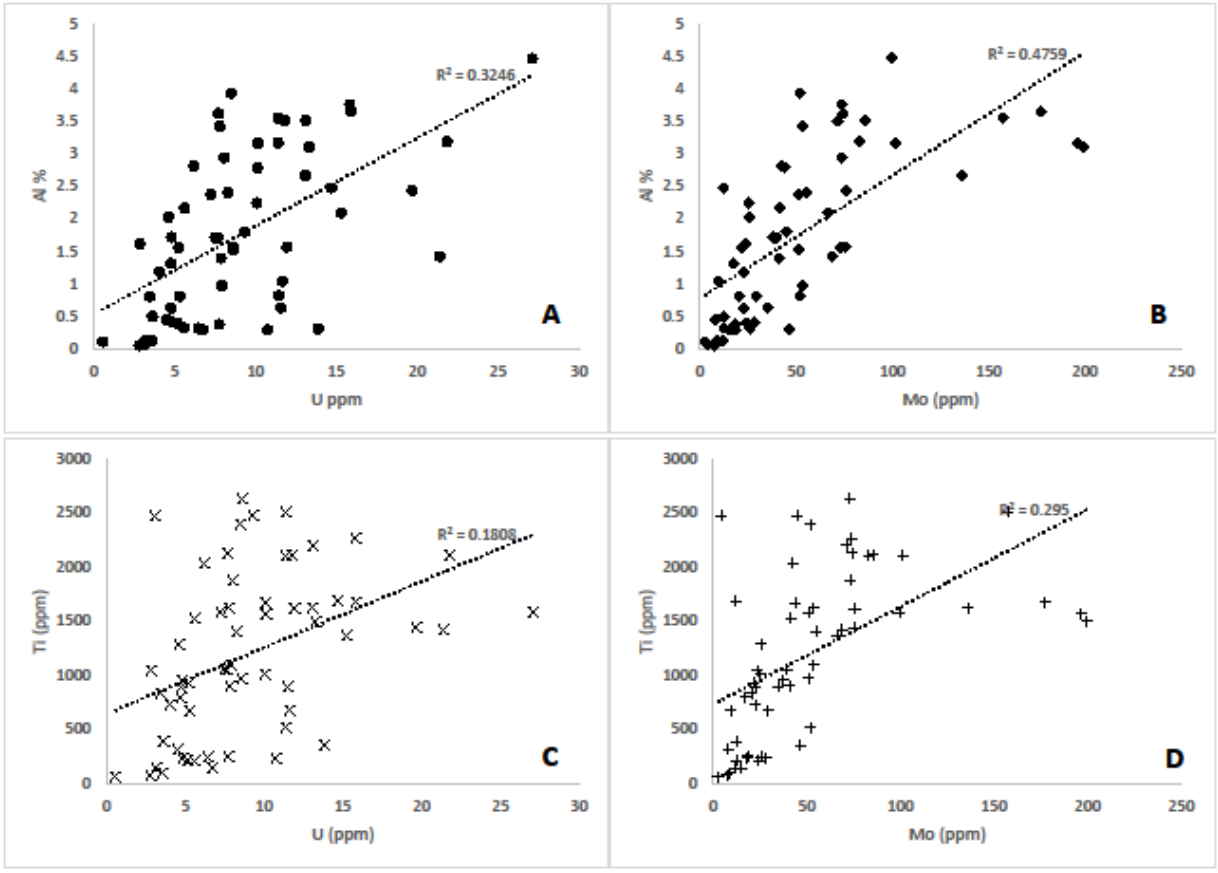

Figure 3.5: Redox sensitive trace metals, U (A, C) and Mo (B, D) plotted against detrital proxies, Al (A, B) and Ti (C, D). R^2 values indicated next to line-of-best-fit.

slope higher than that of seawater meaning Mo_{XS}:U_{XS} increases with increasing enrichment of both elements independently. This places the Pardonet formation in analogy with the Eastern Tropical Pacific margin and some Mesozoic organic-rich Tethyan shale (Algeo & Tribovillard, 2009; Tribovillard et al., 2012).

An attempt was made to interpret the results presented herein by calculating enrichment factors rather than normalizing with the excess method because many of the studies referenced utilize enrichment factors. It quickly became apparent that that method could not be reliably used to interpret this dataset. This is because of the high variability in carbonate content between facies which impacts the enrichment factor value calculated more than the trace metal of interest. This was most obvious for BF1 and BF2 which contain a particularly high proportion of

carbonate. Calculating enrichment factors for samples from these facies yielded anomalously high values with high variance for U in particular. This is because high carbonate results in proportionally low detrital content which inflates the enrichment factor and its sensitivity to variability in detrital content (Van der Weijden, 2002). U was more susceptible to this phenomenon than Mo because, although both are considered authigenic trace metals, U has a weaker association to Al than Mo (Pearson's correlation coefficient of 0.58 compared to 0.72 for Mo in this dataset; Figure 3.5). Steinmann et al. (2020) also observed a strong correlation between Mo and Al. This pattern may have led Del Piero et al. (2020) to erroneously suggest that the Quatsino formation formed in a restricted basin. Had their sample size been larger, they may have noticed this problem as well.

Aside from providing insight into the paleoenvironment of the Pardonet formation, these results draw attention to difficulties in applying trace metal methods to carbonate rocks. This gap has been acknowledged previously (Steinmann et al., 2020) and since then a standard has been introduced which is more appropriate for carbonate rocks (Birdwell & Wilson, 2021). Using enrichment factors was introduced to alleviate concerns of sedimentation rate and dilution from carbonate or biogenic silica (Tribovillard et al., 2006). This method is usable in shale with minor amounts of carbonate or intervals with consistently high carbonate content (Steinmann et al., 2020). In the case of the Pardonet formation, high variability in detrital content between facies makes meaningful comparison between them difficult. This is especially true when [Al] values become very low increasing the EF's sensitivity to variability in [Al] (Van der Weijden, 2002). A separate method of normalization applicable for carbonates would be very useful. For example, normalizing with an element associated to the carbonate fraction rather than the detrital fraction.

Relatively few studies have attempted to apply geochemistry in the interpretation of the Pardonet formation. Those that have focussed on stable carbon and oxygen isotope perturbations across the Carnian-Norian boundary at Black Bear Ridge (Williford et al., 2007; Onoue et al., 2016; Sun et al., 2020; Lei et al., 2021), the Triassic-Jurassic boundary (Wignall et al., 2007; Greene et al., 2012), or total organic carbon (TOC) (Riediger et al., 2004; Williford et al., 2007). Of these, only two applied trace-metal redox-proxies (Wignall et al., 2007; Onoue et al., 2016). Both of these studies used V/(V+Ni) and V/Cr indices as paleo-redox proxies rather than Mo/U but also concluded that the Pardonet formation was deposited during prolonged anoxic to euxinic conditions. Wignall et al. (2007) also analyzed pyrite framboids which indicated periodic oxygenation events which is consistent with our results. High TOC values reported from the Pardonet formation also support the interpretation of deposition in reducing conditions (Riediger et al., 2004; Williford et al., 2007). The Carnian-Norian boundary is much lower in the Black Bear Ridge section than the interval sampled for this study (Zonneveld et al., 2010) so our results cannot be directly compared to the Carnian-Norian studies. Samples were, however, taken up to the last *Monotis* beds before the Triassic-Jurassic boundary such that the top of our section overlaps with the base of Wignall et al. (2007)'s Black Bear Ridge section. This is worth noting because the top portion of the Black Bear Ridge accounts for the most clearly euxinic samples in this study (Figure 3.3). This could be why Wignall et al. (2007) declared the Pardonet formation a record of prolonged euxinia while Onoue et al. (2016) interprets their samples from the Carnian-Norian boundary as suboxic-anoxic.

The Pardonet formation shares characteristics with black shale formations associated with Ocean Anoxic Events (OAE's) during the Jurassic and Cretaceous such as high TOC, laminated fabric, and thin bedding (Tyson & Pearson, 1991; Leckie et al., 2002; Riediger et al., 2004;

Zonneveld et al., 2004; 2010; Tribovillard et al., 2012; others). Oxygen Minimum Zones (OMZ's) have commonly been invoked to explain OAE's, partly because OMZ's are the most common cause of organic rich sediments in modern open oceans (Tyson & Pearson, 1991; Algeo & Tribovillard, 2009).

For most Mesozoic OAE's, a model of seasonal water column stratification in epeiric seas may better explain the variability between events, locations, and the degree of anoxia within individual formations (Tyson & Pearson, 1991). Evidence of brief periods of oxic recovery are observable in Mesozoic black shale formations and such a condition has been proposed for the Pardonet formation as well (Tyson & Pearson, 1991; Wignall et al., 2007), partly in explanation of the facies occurrence of flat clams (McRoberts, 2010). Anoxic conditions are believed to have persisted on the tropical western margin of Pangaea throughout the Triassic (Davies 1997a; Wignall & Twitchett, 2002). Climatic modelling shows that ocean circulation during the Norian would have been favourable to the development of upwelling along the Western North American margin (Golonka et al., 1994). This is further supported by direct evidence of arid conditions on the continent during the Late Triassic in the form of evaporite and aeolian dune facies in the Carnian Charlie Lake formation (Davies, 1997a; Zonneveld et al., 2004; Booker et al., 2008).

In the modern world, arid regions are commonly associated with upwelling zones offshore (Logan, 1960; Dupont et al., 2005). Upwelling, combined with transgression (Zonneveld et al., 2004), and a hot climate in the mid to late Norian (Jaraula et al., 2013; Sun et al., 2020), would lead to intensification of the OMZ and a longer sustained anoxic season (Tyson & Pearson, 1991). There is evidence that there were episodes of ocean euxinia reaching into the photic zone leading up to and through the late Norian extinction event associated with a hot-house climate (Jaraula et al., 2013). This both helps explain the persistent deep-water euxinia

demonstrated in the Pardonet formation and suggests the upper Pardonet could be an important interval to research as an analog when trying to predict how modern climate change may impact deep-water ecosystems. These evidences retain the Eastern tropical Pacific margin as a good modern analog for the Western tropical margin of Pangaea during the Norian which explains the pattern in the Mo:U plot (Figure 3.4; Algeo & Tribovillard 2009).

Since the Pardonet formation has long been believed to have formed under anoxic-euxinic conditions, it has been suggested that it may have formed in a partly restricted basin (Gibson, 1993). Giving consideration to modern analogs and models of black shale deposition, it is concluded that basin restriction is not required to explain euxinia in the Pardonet formation (Tyson & Pearson, 1991; Algeo & Tribovillard, 2009; Tribovillard et al., 2012). It is widely acknowledged that the Peace River Embayment strongly affected the accommodation available for Triassic sedimentation in the Williston Lake area (Gibson & Edwards, 1990; Davies, 1997a; 1997b; Zonneveld et al., 2010). Additionally, the presence of the Ludington formation as a lateral equivalent to the Liard, Charlie Lake, and Baldonnel formations suggests differential subsidence within the basin (Gibson & Edwards, 1990; Davies, 1997a; Zonneveld et al., 2010). Such a scenario also explains the thickening of the Pardonet formation at Black Bear Ridge resulting in the Carnian-Norian boundary occurring within the lower Pardonet rather than the upper Baldonnel (Zonneveld et al., 2004; 2010; Orchard, 2007; Wignall et al., 2007; Williford et al., 2007; Onoue et al., 2016; Sun et al., 2020; Lei et al., 2021). Black Bear Ridge could, therefore, represent a sub-basin with higher subsidence that developed more permanent anoxia resulting in thick anoxic sequences (Tyson & Pearson, 1991; Zonneveld et al., 2010). This would explain the greater dominance of facies deposited in euxinic conditions in the Black Bear Ridge section compared to the Brown Hill section that was observed in this study (Figs 3.2, 3.3).

Facies Association 1 - Proximal bioclastic turbidites.

Facies within the Pardonet formation can be organized into a succession analogous to the classic Bouma sequence of siliciclastic turbidites (Figure 4.1; Bouma 1962). This succession begins (I) with a traction carpet composed of ooids that overlies a surface scoured by the current carrying the ooids. Ooids are known to form inorganically in the presence of sea-water highly saturated with regard to $CaCO_3$ that agitates the seafloor with sufficient frequency to facilitate concentric accretion of carbonate to sediment grains (Davies et al., 1978; Rankey & Reeder, 2011). In other words: ooids are common in shallow tropical seas so their presence among otherwise clearly deep-water sediments in the Pardonet indicates they were transported a great distance (McIlreath & James, 1984). The ooids form the base of a bed containing scattered and broken but sometimes semi-articulated ichthyosaur bone in a carbonate mud matrix (Figure 4.1II). This bed is

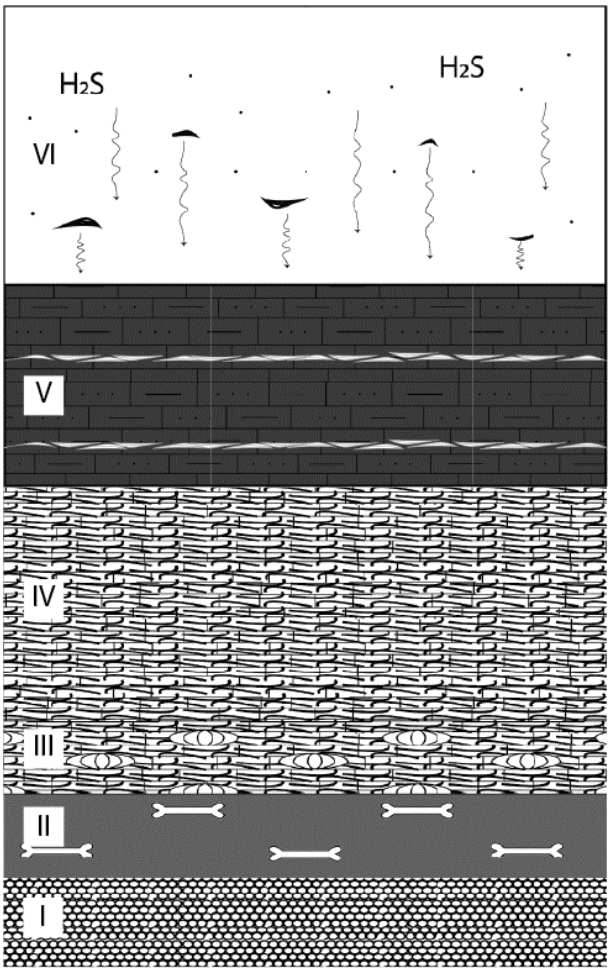

Figure 4.1: Cartoon illustrating the idealized sequence of facies produced by the interpreted carbonate turbidites. Sequence grades from FA1, proximal carbonate turbidites, to FA3, distal carbonate turbidites in euxinic bottom waters. I) Traction carpet composed of ooids. Common at bases of BF1. II) Ichthyosaur bone in silty micrite matrix. An expression of BF1. Other clasts also common. III) Abundant ammonoids and dense bivalves. An expression of BF1. IV) Bivalve laminite, BF2. V) Detritus rich, dark-gray limestone with abundant small and fragmentary bivalves, BF4. VI) Pelagic settling of small shell material, organic matter, and fine-grained sediment with H_2S present in the water column, BF6.

sometimes topped with echinoid spines, gastropod shells, bivalves and/or ammonoids (first expression of BF1). This basal component of the succession is best interpreted as a bioclastic debrite that graded into a turbidite. Since the larger clasts in a debris flow are supported by the cohesive strength of the matrix and buoyancy, the large bioclasts came to rest supported by the fine-grained matrix (Nardin et al., 1979; Cook et al., 1983; Cook & Mullins, 1983). The momentum of the debris flow transferred to the overlying water column initiating a turbidity flow which resulted in the deposition of more organized beds atop the debrite (Davies, 1977). The next member of the succession, 'III' in Figure 4.1, is dominated by flat-clams and ammonoids all deposited concordant to bedding. The better sorting and preferential orientation of clasts in this facies (second expression of BF1) suggest it is a true turbidite. From that perspective, BF1 can be seen as analogous to a Bouma A while BF2 then represents a Bouma B. As the current lost energy, larger clasts were left behind while fine-grained sediment remained suspended such that bivalve shells were nearly the exclusive sedimentary grains in BF2 (Figure 4.1IV).

BF2 has no known analog from modern oceans or other geological time periods. It does, however, have equivalents in Triassic successions of basins globally yet a satisfactory explanation of these facies has not been provided (Jefferies & Minton, 1965; Gruber, 1976; Tozer, 1982b; Ando, 1987; Wignall & Simms, 1990; Campbell, 1994; Davies, 1997a, 1997b; McRoberts, 1997, 2010, 2011; Del Piero et al., 2020). In the Ordovician of Ohio, flattened brachiopods occur in thin shell pavements that superficially resemble facies of the Pardonet in bedding-plane view (Dattilo et al., 2008, fig. 10A). These shell pavements were interpreted as the first post-storm colonizers preserved due to burial in muds deposited in a subsequent storm (Dattilo et al., 2008). Dattilo et al., (2008) acknowledged that multiple of these shell beds with

close vertical spacing could be winnowed by a more erosive event to form a single thicker shell bed. This is analogous to the scenario envisioned for the formation of BF2 except that in the Pardonet formation, hostile water chemistry (discussed in detail in Chapter 4) never allowed subsequent ecological tiers to be established regardless how much time separated events. Also, turbidity currents, rather than storms, are invoked as the process that facilitated winnowing for consistency with the interpretation that the setting is below storm-wave base (Gibson, 1993; Davies, 1997b; Zonneveld et al., 2004; 2010). Clearly, several cycles of recolonization and sediment removal must have occurred to achieve the thicknesses observed in outcrop. McRoberts (2011) noted that BF2 (Type 2 shell beds therein) is often a composite of multiple accumulations separated by thin sediment layers. That observation is consistent with the interpretation of stacked event concentrations. McRoberts (2011) also interpreted BF2 to result from episodes of high population density and thus represent a census assemblage (*sensu* Kidwell & Bosence, 1991). Contrarily, episodic stacking of generations which did not live simultaneously would indicate that these beds are time-averaged (Kidwell & Bosence, 1991). It is interpreted here that BF2 is formed in an area of fine-grained sediment bypass. This unusual expression of such conditions was caused by the presence of effectively two sediment size classes in the system: silt to mud sized and shells greater than 1 cm. In the zone of formation of BF2, currents removed the first class and left the latter. In that way, shells of BF2 are autochthonous despite the involvement of turbidity current in its formation. The shells are preserved in pristine condition because they themselves were not transported and existed on a dominantly composed of carbonate grains that were too soft to abrade the shells while being carried by a current.

Further slowing of the currents allowed the deposition of significantly transported shell material along with coarser silt and carbonate grains (Figure 4.1V). The poor sorting of BF4 may

indicate that it formed from high-density turbidity currents where significant grain-grain contact inhibited grain-size segregation (Eberli, 1987). Interlaminations of shell and detrital material were caused by alternations in current energy. Siliciclastic laminites (*sensu* Lombard, 1971) can develop from contour current reworking of material transported basinward by turbidity currents (Bouma, 1973). As such, BF4 is interpreted to have been deposited by high-density turbidity currents that brought in fragmented shell material, then reworked by contour currents that segregated fine-grained detritus from bedding-concordant shell material (Bouma, 1973; Eberli, 1987). Similar to turbidites in siliciclastic settings, the facies of FA1 interbed in grading sequences that may or may not preserve all facies.

Facies Association 2 - Distal bioclastic turbidites into suboxic bottom waters.

During quiescent periods, dysoxia-tolerant taxa such as halobiids or monotids dominated the seafloor where other benthos could not colonize due to oxygen stress. Turbidity flow events disturbed the local population by winnowing out the underlying pelagic sediment, probably overturning adults, and entraining juveniles. The resulting substrate would be composed of generations of stacked adult size shells, represented by BF2, on top of which, pelagic sedimentation continued and a new generation of bivalves colonized.

Further basinward, the turbidity currents lost much of their energy, becoming low-density and carrying dominantly sediment of coarse silt size or less (Eberli, 1987). Relavively few adult size shells are found in BF5 with a much higher count of small shells which could probably be representative of a population of r-selected species such as halobiids and monotids at any given moment in time (Kidwell & Bosence, 1991; McRoberts, 2011; Del Piero et al., 2020). For that reason, these shell beds are considered census assemblages meaning all individuals on the substrate likely perished in a single event. The smaller shells in BF5 are interpreted to be

juveniles of the same population rather than a dwarfed fauna because there are no examples of a dwarfed fauna *in situ* in any of the facies described. Relating BF5 to the turbidity events is complicated by the occurrence of smaller shells in lags separate from adult size shells which are typically isolated on bedding planes. Calcium carbonate shells differ greatly from siliciclastic sediments on which turbidite facies models were based (Bouma, 1962; Stow et al., 1984; Eberli, 1987). Specifically, the difference in density, internal porosity, and shape increase the buoyancy of shell clasts compared to siliciclastic grains of the same size (Stow et al., 1984; Vigorito et al., 2005). Shape is thought to be especially important for flat-clam shells which have high surface area to mass ratios owing to their flattened morphology. It is speculated that this may have been enough for juveniles in the population to be mobilized by currents that would otherwise be too weak to move grains of their size. They likely traveled a very short

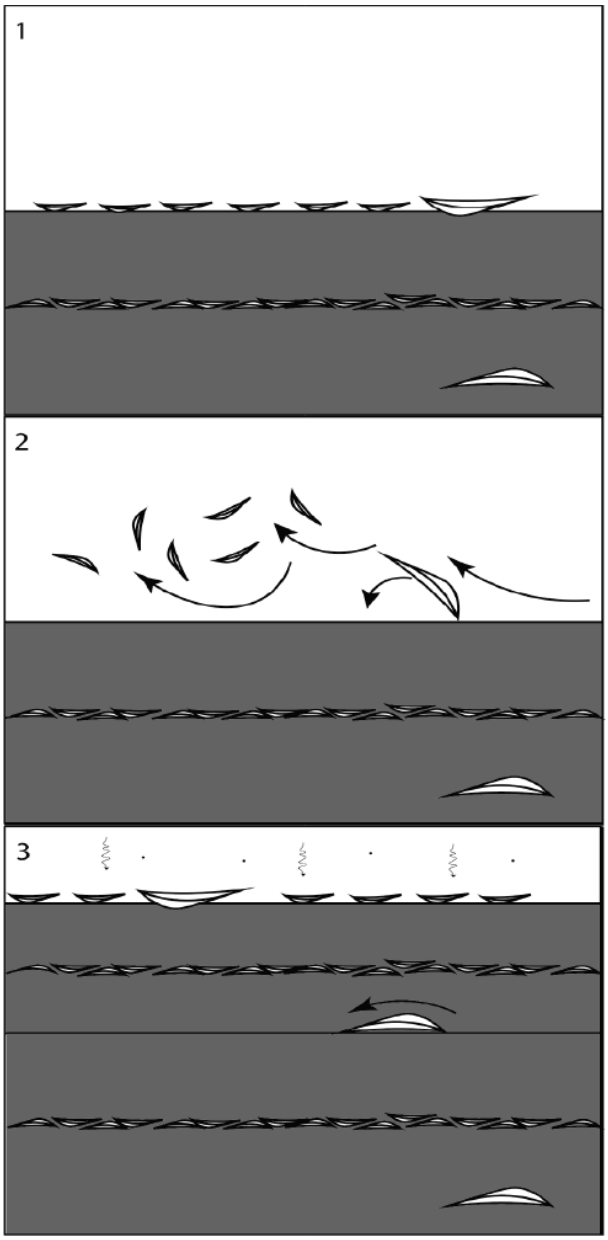

Figure 4.2: Illustration of the sequence of events interpreted to lead to the formation of BF5. 1) A population of flat-clams live on a soupy, fine-grained substrate. Being r-selected taxa, the population is dominated by juveniles with relatively few adult-sized individuals. 2) A waning turbidity current passes over the substrate. The flattened morphology of the juveniles allows them to be entrained by the current while adults are overturned into a more hydrodynamically stable position. 3) Adults are buried by fine-grained sediment carried by the turbidity current. Juveniles are deposited in a lag as the current loses energy and are in turn buried by more fine-grained sediment. Once the current has settled a new population is established on top of the fine-grained sediment. In the absence of passing currents, pelagic deposition dominates and most flat-clams reach adult size, allowing the formation of BF3.

distance, then were deposited in a lag as the flow waned. The current also may have been able to overturn adults to a more hydrodynamically stable convex-up orientation (Figure 4.2). The substrate underlying the bivalve population likely also experienced some remobilization in this case but, for the formation of BF5, currents must have been at an energy level that was net depositional with regard to the fine-grained sediment found in the matrix. Overall, the lack of obvious scour in this BF5 can be accounted for by the fact that turbidity flows carrying carbonate sediment are less erosive than their siliclastic counterparts (Stow et al., 1984; Eberli, 1987; Uchman, 2007). After disrupting the local bivalve population, the turbidity currents deposited massive mudstone. Sedimentary structures were not preserved as they are commonly not in low-density carbonate turbidites (Stow et al., 1984; Eberli, 1987; Vigorito et al., 2005). BF5 is the most puzzling of the facies described above and, admittedly, this interpretation lack supporting evidence. In the future, more field work should be done to analyze these beds in detail for evidence of current modification or evidence that can reject the interpretation herein.

Where the turbidity currents no longer reached with appreciable energy, a stable bivalve population existed living on a slowly agrading hemipelagic ooze. This environment allowed the formation of BF3. BF3 is interpreted to be hemipelagic sediments deposited in distal settings. The quartz silt that is ubiquitous in the Pardonet formation indicates that none of the sediments were purely pelagic, hence hemipelagic (McIlreath & James, 1984). It has been suggested that the silt is aeolian in origin (Davies, 1997b). Bivalves are believed to be *in situ* because of the condition of the shells and the lack of sorting or preferential orientation of shells. McRoberts, (2011) noted right and left valve pairs preserved with their hingelines aligned in a 'butterfly' orientation in Type 1 shell beds which are considered equivalent to this facies. Likewise, close association of left and right valves were observed in BF3 (Figure 2.16). This indicates very little

post-mortem reworking of the valves. The dominance of adult shells approximates a census assemblage which indicates that the majority of individuals survived into adulthood which can be accounted for by the absence of predation and competition and lack of environmental disturbance (Kidwell & Bosence, 1991; Powell & Stanton, 1996; McRoberts, 2011). Overall, shells in BF3 are considered to most accurately reflect the local bivalve population at the time of deposition.

Facies Association 3 - Distal bioclastic turbidites into anoxic to euxinic bottom waters.

During some periods of time, the deep seafloor oxygen concentration dipped below the tolerance of the local halobiids and monotids. As turbidity currents settled into the more distal, euxinic zones in which BF4 and BF6 formed, fragmented shell material was deposited in amalgamating lags separated by fine-grained silt and carbonate debris (Figure 4.1V). Carbonate sediments are much more prone to dispersing into the overlying water column above the final resting place of turbidites due to their greater buoyancy and lesser development of electrostatic surface charges that would cause flocculation (Stow et al., 1984; Vigorito et al., 2005). These sediments that escape the turbidity current mix with pelagic sediments and settle slowly (Stow et al., 1984). In the case of BF6, that mixture included small shell material, mud-sized carbonate, organic matter, and lesser amounts of fine quartz silt (Figure 4.1VI).

In outcrop, BF6 strongly resembles BF3 but differs notably in the size and preservation of bivalves. This implies that these facies represent similar hydraulic conditions but BF6 formed in environments that were inhospitable to the bivalves in the system. BF6 fits the definition of the Type 3 shell bed of McRoberts, (2011) which is interpreted to be consist primarily of transported shells in a within-habitat, time-averaged assemble *sensu* Kidwell & Bosence, (1991). paucity in full-sized shells and fragmentary shells are consistent with that interpretation. Assuming a

relatively slow sedimentation rate based on small overall grain size and thin bedding, shells on the sediment surface at any given time probably displayed some amount of time averaging. BF6 is also similar to BFC 3 of Del Piero, (2020). In the Quatsino formation, small and juvenile *Halobia* in BFC 3 were interpreted to develop from planktonic larvae that settle in anoxic to euxinic bottom-waters then only reach moderate sizes before perishing because of the oxygen stress. This interpretation could be applied to BF6 but the context of the other facies and fragmentary shells favour the interpretation of the shell material as being transported. These assemblages are not interpreted to represent a dwarfed fauna as Del Piero, (2020) interpreted in their rocks because they are not *in situ.* This means they are true juveniles that were transported from better oxygenated water while adults were left behind. BF6 is dominantly associated with BF4 and BF5. The matrix of BF6 is notably darker than the other facies which likely reflects a higher concentration of preserved organic matter.

Discussion

Comparison to previous work

Overall, the unique nature of the clasts in this system seem to mask the expression of classic Bouma sequences. All lithofacies of the Pardonet formation have previously been interpreted broadly as turbidites and hemipelagic deposition (Zonneveld et al., 2004) but detailed descriptions of the nuances of the interval have not been previously published. It is likely that the relationship of some of the facies to the turbidite system has long been overlooked due to the lack of preservation of sedimentary structures which are diagnostic of certain facies in the Bouma sequence. Many facies described herein were previously assumed to be pelagic deposits due to the absence of physical sedimentary structures (Davies, 1998a, 1998b; Zonneveld et al., 2004). Structureless fine-grained facies can be explained by the differences in physical and

electrostatic properties of fine-grained carbonate versus aluminosilicate clays (Stow et al., 1984). The presence of shelly benthos, such as flat-clams, in deeper water further complicates the story because they introduce large, unrounded clasts into the system at depths where such immature clasts would never reach in the siliciclastic world. This is particularly complicated in the case of these flattened bivalves whose fluid dynamics are strongly influenced by the large surface-area to mass ratio of their valves. Their shells were possibly mobilized by currents depositing much finer sediment rather than being buried in place. This also illustrates how quiet the water must have been in the case of BF3 for flat clams to be found in life position.

Zonneveld et al. (2004) described 4 lithofacies observed in the Pardonet formation all grouped into one facies association which was interpreted to represent pelagic deposition with minor bioclastic turbidites in proximal to distal offshore settings. Compared to the facies scheme presented herein, Zonneveld et al. (2004)'s BP-IX and BP-XI are equivalent to BF1 and BF2 respectively. BP-X is described as "thinly interbedded carbonate mudstone and bivalve laminite" (Zonneveld et al., 2004) and so is probably equivalent to BF4 which appears similar in outcrop scale to BF2 but slight alternation between shell material and fine-grained detritus can be observed at a finer scale. BP-VIII probably encompasses BF3, BF5, and BF6 because Zonneveld et al. (2004) was a sedimentological study and did not describe the size distributions used herein to distinguish these three facies. Contrary to Zonneveld et al. (2004), the Pardonet formation is interpreted herein to represent the deposits of multiple aspects of a bioclastic turbidite complex rather than being dominated by hemipelagic deposition.

Lithofacies described in Zonneveld et al. (2004) were reassessed in consideration of the shell-bed types defined by McRoberts (2011) and observations of lithology and shell preservation in the definition of the facies scheme presented herein. Type 1 shell beds are

represented in the present study by BF3. BF2 is equivalent to Type 2 shell beds, however, some expressions of BF1 may also fit the definition of Type 2 because McRoberts (2011) did not discuss the occurrence and significance of other associated bioclastic material such as other bivalve taxa, cephalopods and vertebrates. BF4, BF5, and BF6 all fit the definition of Type 3 shell beds because of the presence of small and fragmentary shells in more random orientations. Lithological differences and geochemical data helped in differentiating these facies.

The facies described for this study are much easier to distinguish in the *Eomonotis* and *Monotis* intervals than the earlier *Halobia* interval. This is because the younger, bigger bivalves are easier to observe in hand samples but also because the size disparity between adult and juvenile shells is larger for the taxa that reach greater adult size. BF5 specifically depends on this size disparity for adults and juveniles to be sorted onto separate bedding planes. The current velocity thresholds for the formation for each facies is dependent on the size of the bivalves present because it is interpreted that hydraulic sorting is responsible for differentiating most of the facies. Theoretically, however, those thresholds should still exist for all bivalve species in the system. Examples of BF5 and BF6 were not, in fact, demonstrated in the *Halobia* intervals of the sections studied. To test the robustness of the facies scheme presented, it would be interesting to replicate this study focussing on the lower parts of the Black Bear Ridge and Brown Hill sections in the *Halobia* biozone. Other localities on Williston Lake could be included in such a study including Pardonet Hill or East Carbon Creek where *Gryphaea* co-occurs with *Halobia*. The first test would be to try to identify all six facies where only smaller bivalves are present.

Stratigraphic Context

Data presented in this study is likely insufficient to meaningfully interpret overarching Transgression-Regression (T-R) cycles as is common in chemostratigraphic studies, (eg, Playter

et al., 2018; LaGrange et al., 2020). However, the facies scheme presented may be useful in interpreting higher resolution sequence stratigraphy in the Pardonet going forward. The facies presented are dominantly controlled by two factors: the distance from the source of the turbidite system and paleo-redox conditions. Both of these factors can be associated with relative sea-level, although they are not directly controlled by sea-level. Carbonate turbidite systems can commonly develop much more laterally continuous facies belts than their siliciclastic counterparts owing to an entire carbonate margin sourcing material rather than a single point-source (Schlager & Chermak, 1979; Crevello & Schlager, 1980; Cook & Mullins, 1983; notable exception: Payros et al., 2006). The facies of the Pardonet are therefore likely to be laterally continuous, and they appear to be in outcrop (Davies, 1997b; Zonneveld et al., 2004; McRoberts 2011), but, with only two sections in the present study, no conclusions can be made about if facies can be mapped. Even if facies associations are laterally continuous, there is likely internal variability depending on where turbidity flows were active at any given time. The preceding discussion on proximal versus distal facies likely applies both with reference to relative distance from the sediment source as well as distance from the axis of an active turbidite channel (Vigorito et al., 2005). For that reason, assignment of facies associations should be based on relative proportions of beds fitting descriptions of BF1 and BF2 compared to BF3 or BF6. Such lateral variability may also account for the difference between FA2 and FA3. For example, if the chemocline were constant, FA2 could've formed on the overbank while FA3 formed at the toe of the slope.

At Brown Hill, the base of the studied section is assigned to FA1 and is characterized by relatively strongly reducing conditions (Figs 3.2, 4.3). At about 8 m height, FA2 is observed overlying and is characterized by more oxidizing conditions. At about 15.5 m, prominent

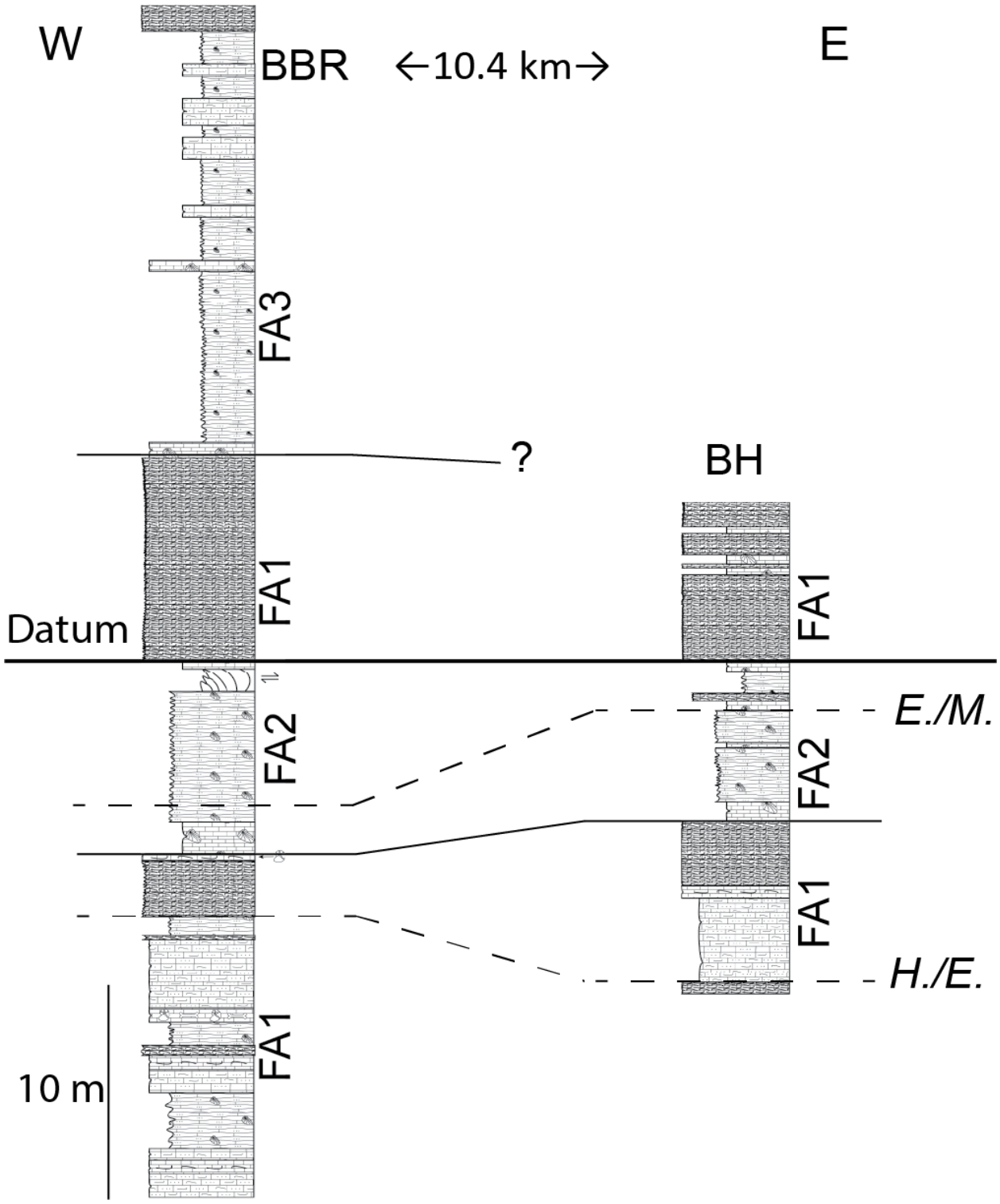

Figure 4.3: Correlation between Black Bear Ridge (BBR) and Brown Hill (BH). Solid lines mark boundaries between facies associations. Two of these surfaces can be correlated between the two sections. Datum is arbitrarily picked on one of these surfaces (29 m below the top of the Pardonet at BBR; 60.9 m above the top of the Baldonnel formation at BH). Dashed lines indicate biostratigraphic turnovers between *Halobia* and *Eomonotis (H./E.)* and *Eomonotis* and *Monotis (E./M.)*.

Monotis laminites (BF2, FA1) occur and seem to record the return of stronger reducing conditions but a few distinctly better oxygenated horizons can be identified. A similar progression of facies was observed at Black Bear Ridge. FA1 can be observed at the base of the study inteval and is also characterized by relatively strongly reducing conditions (Figs 3.3, 4.3). FA2 overlies and is more oxidizing and is in turn overlain by prominent *Monotis* laminites. Above these beds, FA3 is present and displays the most consistent and strong reducing conditions observable. At the very top of the Black Bear Ridge section, another few meter thick *Monotis* laminite exists and the highest sample taken from these beds suggests a return of more oxidizing conditions.

During the falling stage systems tract (FSST) the highest dominance of grainflows and high-density turbidites should be observable (De Gasperi & Catuneanu, 2014; Catuneanu 2019). Grainflows were not interpreted in this study, however, the debrites and high-density turbidites of FA1 are taken to represent the FSST. During lowstand and early transgression, low-density turbidity flows became more common. Low-density turbidity flows continued into early transgression, then hemipelagic deposition became dominant during late transgression and highstand (De Gasperi & Catuneanu, 2014; Catuneanu, 2019). Generally, it is thought that reduced benthic oxygen is associated with high relative sea-level (Tyson & Pearson, 1991; Leckie et al., 2002), but this may not necessarily be true in basins restricted from the open ocean (Harris et al., 2018). La Grange et al. (2020) summarized that redox proxies decrease during transgression in restricted settings due to increased exchange with the open ocean (Turner et al., 2016), but increase in open-ocean settings due to greater separation between the photic zone and benthic environment (Harris et al., 2018). As discussed in Chapter 3, the trace metal data supports open oceanographic conditions for the Pardonet so it may be fair to assume that euxinic

facies occur within the transgressive systems-tract (TST) or highstand systems-tract (HST). Redox proxies presented in Figures 3.2 and 3.3 display a trend from stronger reducing conditions toward the base to better oxygenated condtions, then returning to strongly reducing, euxinic conditions towards the top of the Black Bear Ridge section. This can be explained with a regression followed by transgression. Considering sedimentological and geochemical evidence in conjunction concludes a tentative interpretation for the studied interval of FSST (FA1) followed by LST (FA2), then TST (FA1-FA3) (Figure 4.3) although stratigraphic surfaces probably occur within facies associations rather than at their contacts. The Pardonet formation as a whole represents the deep-water component of a large scale TST (Davies, 1997b; Zonneveld et al., 2004) which may be responsible for the persistence of reduced oxygen conditions throughout Pardonet deposition. An overall deepening trend in the formation explains the greater reducing signal from the upper Pardonet (Sephton et al., 2002; Riediger et al., 2004; Wignall et al., 2007; the present study) compared to that of the Carnian-Norian boundary interval (Zonneveld et al., 2010; Onoue et al., 2016; Lei et al., 2021)

Orchard et al. (2001a) interpreted the upper portion of Black Bear Ridge, the portion which is one of our studied sections, as the third of four third-order sequences which the entire Black Bear Ridge succession is divided into. This sequence is divided into an LST, then TST, followed by an HST. The LST corresponds roughly with the lower occurrence of FA1 denoted on Figure 4.3. The TST spans FA2, the first prominent *Monotis* laminites (BF2) and into the euxinic facies (BF6). Finally, the HST is composed of FA3. Generally, this fits with the expectations outlined above reasonably well. In order to refine these interpretations, criteria should be defined to identify maximum regressive and maximum flooding surfaces. For example, maximas and minimas respectively in detrital proxies could be applied (La Grange et

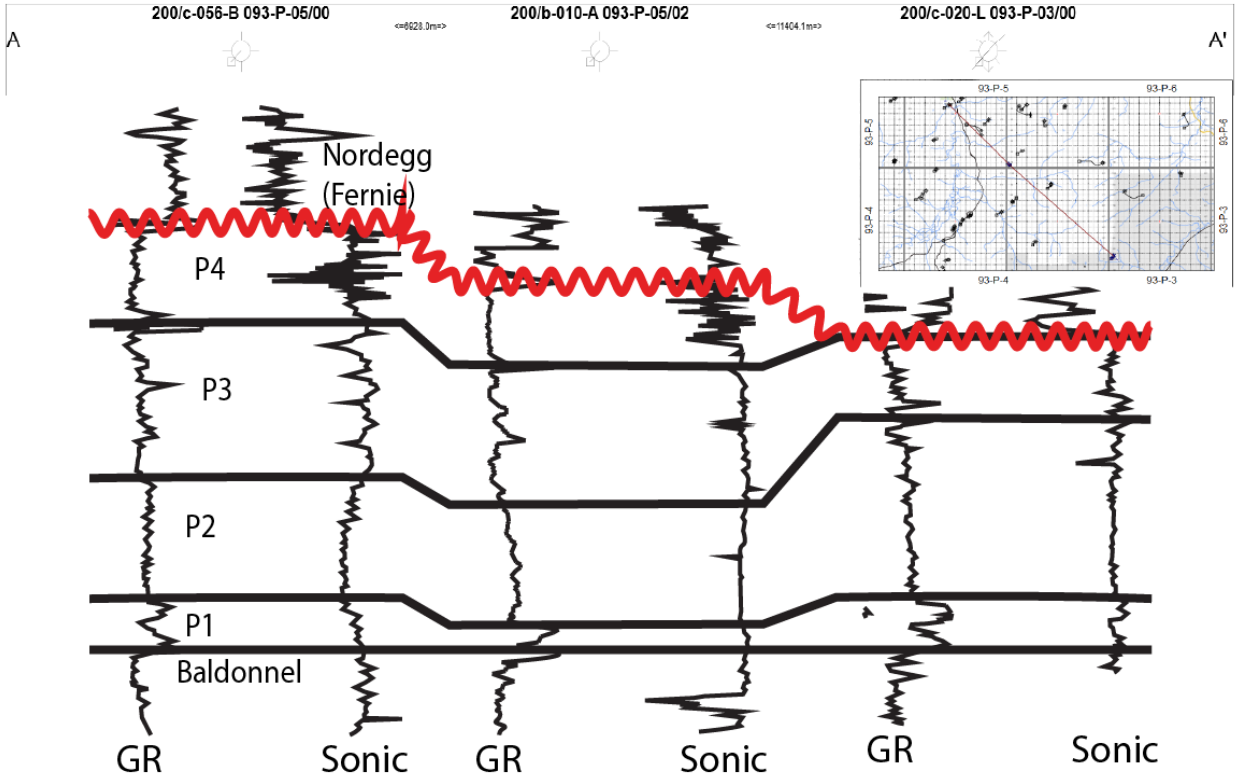

Figure 4.4: Three well cross-section of the Pardonet formation in the subsurface Southeast of Williston Lake. Datum is the top of the Baldonnel formation. The Pardonet can be divided into four units in the subsurface based on log responses. P1 is identified by the high-gamma response. P2 has a lower and more constant log signature. P3 appears less organized with a low but serrated signature and, finally, P4 is identified by the chaotic appearance of the sonic log. P4 is truncated by the sub-Jurassic unconformity to the East. After Barss & Montandon (1981).

al., 2020). No attempt was made here to interpret such geochemical features because of expected differences in detrital content between facies independent of changes in systems tracts and a lack of the necessary data density. A larger scale, higher resolution study could help resolve the sequence stratigraphy.

In the subsurface of Northeast British Columbia, the Pardonet is subdivided into four lithological units based on gamma and sonic log responses (Barss & Montandon, 1981). It is likely that those four units correspond to low-resolution systems-tracts within the Pardonet (Figure 4.4). For example, the high gamma signature of P1 is attributed to proportionally high uranium concentration in the rocks which may be due to abundant phosphate in the form of both

authigenic phosphate and bone concentrations and to the high organic content of theses rocks. Both phosphates and organic matter could have been concentrated by a combination of stratigraphic condensation and reducing conditions during transgression (Loutit et al., 1988; Zheng et al., 2002; Harris et al., 2018; La Grange et al., 2020). P2, therefore, would represent the HST, clean limestone of P3 could be formed from an increase of high-density turbidites during FSST, and the lowstand systems-tract (LST) represented by P4. A detailed core study would be required to confirm these predictions. Two lithological surfaces can be correlated between Brown Hill and Black Bear Ridge (Figure 4.3). The first marks a lateral shift from FA1, which was deposited in a more proximal setting, to FA2, which was deposited in a distal, hemipelagic setting. The second is recognized by FA2 sharply overlain by bivalve laminite which is assigned to FA1. This is tentatively interpreted as a transgression followed by regression. In order to develop a more robust stratigraphic framework for the Pardonet formation, other outcrop sections such as Pardonet Hill, Juvavites Cove, East Carbon Creek, and the lower portions of Brown Hill and Black Bear Ridge should be revisited with the purpose of assessing facies relationships to sea-level fluctuations. All of these sections expose the lower part of the formation and so fell outside of the scope of the present study.

An alternative interpretation may be that FA1 is associated with the HST because carbonate sedimentation is highest when the carbonate factory is most productive (Catuneanu, 2006). In this case, FA2 may be associated with the LST and FA3 may develop due to anoxia driven by transgression. The highstand-shedding model, however, works best for fully developed rimmed-platforms in tropical oceans (Schlager, 2005, Catuneanu, 2006; James & Jones, 2016). The Pardonet formation was deposited basinward of a carbonate ramp, assuming the depositional setting of the Baldonnel formation existed somewhere landward (Zonneveld et al., 2004).

Despite developing near tropical latitudes (Golonka, 2007), that system never developed reefs to the same degree that as in the Devonian or in modern oceans (Davies, 1997b; Zonneveld et al., 2004; MacNeil & Jones, 2006; Puga-Bernabéu et al., 2011). The Upper Triassic depostional system of western Canada much better fit the concept of a C-factory (*sensu* Schlager, 2005) so a model of greatest sediment input during lowstand is favoured (Schlager, 2005; Catuneanu, 2006). The Pardonet formation shows no real evidence of unconformities and they are not expected. The Pardonet represents a deep-water system that would never be subaerially exposed nor develop drowning unconformities because the system is always fed some sediment shed from the carbonate ramp or, at the very least, background pelagic deposition. One could also interpret that the studied sections were deposited during two transgression-regression cycles. The first resulting in FA1 at low sea-level overlain by FA2 at high sea-level, then the return of FA1 at a second lowstand, and finally FA3 at the second highstand (Figure 4.3). In this scenario, the second highstand reached a higher relative sea-level or some external factor could account for the development of euxinia during the second highstand.

Implications to halobiid and monotid paleoecology

Halobiids or monotids have previously been interpreted to be benthic recliners (McRoberts, 2010, 2011; Del Piero et al., 2020), which is consistent with the emplacement of many specimens in BF3. To expand on that, their flattened morphology and regular association with pelagic deposits may suggest they employ a 'snowshoeing' strategy similar to what has been interpreted for strophomenid brachiopods which also display flattened morphologies (Rhoads, 1970). In the case of the Pardonet formation, the bivalves rested atop a soupy mixed carbonate and quartz silt ooze substrate during quiescent periods, and avoided sinking into the substrate due to their large surface area, and relatively low mass-surface area ratio.

If this interpretation is true, then the paleo-redox proxies employed in this study indicate that these halobiids and monotids were indeed living in oxygen-diminished waters as previously speculated (McRoberts, 2010). Taken together with the facies occurrences, the redox proxies also demonstrate that there was a degree of reducing conditions which were outside the tolerance of these bivalves, as was previously demonstrated for *Halobia cordillerana* (Del Piero et al., 2020). Our results indicate that Del Piero et al. (2020)'s conclusion that *Halobia cordillerana* could colonize suboxic bottom waters to the exclusion of other benthos can be expanded to include other late-Triassic flat-clams. Del Piero et al. (2020)'s BFC 2 is analogous to BF2 herein and BFC 3 is likely comparable to BF6. In the Quatsino formation, Del Piero et al. (2020) was able to place their BFC 3 in the dysoxic-oxic range based on the presence of simple bioturbation. No equivalent facies was identified in the Pardonet formation. The only known trace fossils found in the Pardonet formation are borings in bivalve shells that occurred in event beds and were interpreted to have been transported from shallow water (Zonneveld & Bistran, 2013) and a single surface trace interpreted as a fish feeding pit (Zonneveld, unpublished data). The absence of trace fossils is thought to also be the result of limited oxygen in the benthic environment. Oxygen stress has been shown to reduce the size, complexity, and diversity of trace fossils, however, traces are typically not entirely excluded until the dissolved oxygen concentration drops below some threshold between 1.0-0.5 mL/L (Savrda & Bottjer, 1986; Tyson & Pearson, 1991). Trace makers may have been present, with their traces not preserved for the same reasons discussed in the previous section for physical sedimentary structures. Alternatively, endobenthos may have been excluded by the presence of dense flat-clam populations that were more competitive at low oxygen-levels. Unlike the Quatsino formation, evidence in this study suggests that Pardonet deposition was characterized by insufficient oxygenation to support a combined

community of infauna and epifauna. Opportunistic populations that colonize event beds in the deep ocean have patchy distributions by nature (Gage, 1996). It is common for local populations to be monotypic for a long period following an event due to the scarcity of resources in the deep sea (Gage, 1996; Wetzel & Uchman, 2001). In the Pardonet formation, however, the entire Peace River foothills region displayed a monotypic assemblage at any point in time (Westerman, 1964; Davies, 1997b; Orchard et al., 2001a; 2001b; Zonneveld et al., 2004; 2010) with few exceptions (e.g. *Gryphaea* at East Carbon Creek; McRoberts, 2011). This suggests that oxygen stress was the primary factor driving down diversity in the region.

Although they do not occur in such impressive thicknesses, earlier Triassic flat-clams, such as *Claraia, Peribositra, Enteropleura* and *Daonella,* also occurred in episodic, monospecific shell-beds (McRoberts, 2010). Aside from a few examples (Ando, 1987; Campbell, 1994), flat-clams appear to have occurred mainly in deep-water environments throughout the Triassic and around the globe (McRoberts, 2010). Turbidity-flow-mediated concentration of shells is an interpretation that could likely be applied to many deep-water occurrences of flat-clam shell-beds. Tolerance to sub-oxic conditions is insufficient to explain dense, monospecific accumulations because not all occurrences are in oxygen-restricted basins like the Western Canadian examples. For example, the Hallstatt facies in the Northern Calcareous Alps of Austria are interpreted as pelagic deposits in a fully oxygenated basin (McRoberts et al., 2008). Overall, Triassic flat-clams were likely r-selected generalists with wide environmental tolerances such that they could survive in otherwise unfavourable environments and reach a global distribution. For the same reason, they likely quickly colonized the seafloor following turbidity events that wiped out competition and were concentrated into shell-beds by subsequent flows. This affinity for episodic depositional systems could also explain their high

origination and extinction rates. Although this strategy is uncommon for shelly benthos, it has been demonstrated that r-selected burrowers colonize the tops of turbidite beds in well oxygenated (Tunis & Uchman, 1996) and poorly oxygenated (Uchman 1992) settings. The dense, but low-diversity assemblages flat clams tend to be found in is also consistent with an opportunistic strategy (Ekdale, 1985).

There is no known modern analog for Triassic flat-clams with regard to the fact that they were shelly fauna that colonized deep, sometimes suboxic water in high densities (McRoberts, 2010). Part of the reason they may have held such a peculiar niche may have been related to their appearance in the aftermath of the end-Permian extinction event. Most families of shelly marine fauna experienced heavy losses at the end of the Permian which left many ecological niches unoccupied. This event also marked the beginning of Class Bivalvia's dominance over Class Brachiopoda (Sepkoski, 1981). Although most investigations of biotic recovery after the end-Permian extinction have focussed on Lower Triassic successions, biodiversity never reached pre-extinction levels until the mid-Jurassic (Sepkoski, 1981; Zonneveld et al., 2007a; Greene et al., 2011). Additionally, and more relevant to this study, a second major extinction event occurred at the end of the Norian stage (Sepkoski, 1981; Jaraula et al., 2013). Evidence from Williston Lake has indicated that the late Triassic extinction resulted from the combined effects of multiple events (Sephton et al., 2002; Wignall et al., 2007). The timing of some of these events, specifically the Norian-Rhaetian boundary which is marked by the extinction of most *Monotis* species (McRoberts et al., 2008), might coincide with the formation of the Manicouagan impact crater in Quebec, Canada (Hodych & Dunning, 1992; Sephton et al., 2002). This impact is not clearly correlated with $\delta^{13}C_{org}$ and $\delta^{15}N_{org}$ perturbations across the boundary (Sephton et al., 2002), but it was nonetheless speculated that global warming in the aftermath of the impact may

have promoted ocean anoxia by drawing a parallel to the Cretaceous Chicxulub impact event (O'Keefe & Ahrens, 1989; Sephton, et al., 2002). The Manicouagan impact has yet to be demonstrated as a direct cause of the Late Triassic extinctions.

The end-Permian extinction coincided with an intense and widespread anoxic event which persisted in the eastern Panthalassa Ocean into the Anisian, broken up by minor oxygenated intervals (Wignall & Twitchett, 2002; Zonneveld et al., 2007a). This period in the early Triassic set a stage where it became advantageous for even shallow water fauna to develop resistance to oxygen depletion. Zonneveld et al. (2007a) showed that lingulide brachiopods became very abundant in the Middle Triassic of western Canada and interpreted that lingulides are ecological opportunists that were able to reach high abundances in the absence of competition in optimal marine settings. The flat-clams may have arisen and diversified because they are also ecological opportunists. Del Piero et al. (2020) noted that *Halobia* did occur in better oxygenated facies with other shelly fauna and bioturbation present but only achieved high abundance in dysoxic-anoxic facies that excluded other benthos. This also makes the connection to the above discussion that while flat-clams are not exclusive to anoxic, deep-water facies, they certainly seem to achieve greater dominance in stressed conditions.

The hypotheses presented herein and elsewhere to explain the life mode and facies occurrences of flat clams, should be tested using models in simulated environments. 3-D printed models have been used to test the life mode, habitat, and feeding strategies of various brachiopods (Garcia et al., 2018; Dievert et al., 2019; Dievert et al., 2021). 3-D printed models would be ideal for such testing on flat clams because the thin shells are usually impossible to completely remove from their matrix without damaging the fossil. Such models could then be placed on simulated substrates to determine if benthic reclining on a fine-grained, soupy

substrate is plausible. Multiple models could also be placed in high density in a flume to understand how they respond to various levels of turbid current energy (Vogel & LaBarbera, 1978). If facies can be replicated forming in the fashion described above, this would support our interpretations. Otherwise, more work would need to be done to try to explain the unique facies occurrences displayed by flat clams.

Biostratigraphy

At Brown Hill, the coinciding last appearance of *Halobia* and first appearance of *Eomonotis* was observed at 46.3 m above the basal contact of the Pardonet formation with the Baldonnel formation below the top contact of the Pardonet formation with the base of the Fernie formation. The conodont sample from the horizon was assigned to the *postera* Zone. The last clear *Eomonotis* occurred at 58.9 m and the first clear *Monotis* occurred at 60.75 m. Fossils within this interval were too poor for field identification. Both horizons were therefore sampled for conodonts Later reassessment of fossil samples justified the placement of the *Eomonotis-Monotis* boundary at the last *Eomonotis*. The condonts at that horizon were place in the *bidentata* Zone while the sample from 60.75 m could not be classified with better resolution than Late Norian-Rhaetian. The occurrence of *Monotis subcircularis* several meters above the sample rules out Rhaetian age for the conodonts. The *Halobia-Eomonotis* turnover was observed 51.7 m below the top contact of the Pardonet formation with the base of the Fernie formation at the top of the last dense *Monotis* beds, marked by a granule lag (Orchard et al., 2001a; 2001b; Wignall et al., 2007; Greene et al., 2012). and the corresponding conodont sample was assigned to the *postera* Zone. *Monotis* replaced *Eomonotis* at 35.85 m below the top but no conodonts could be recovered from the conodont sample taken from this horizon.

Bivalve and conodont zonations have both been calibrated to Tozer (1982a; 1994)'s ammonoid biostratigraphy of the Upper Triassic of the region (Orchard et al., 2001a; 2001b; McRoberts, 2010). The Columbianus Zone largely correlates with the last *Halobia* species. The appearance of *Eomonotis* roughly corresponds with the boundary between the Columbianus III and IV subzones. The top of the *postera* Zone correlates with the boundary between the Columbianus II and III subzones. The Columbianus III and IV subzones correlate with the *serrulata* Zone. Therefore, *Eomonotis* is expected to appear later in the *serrulata* Zone. The fact that our conodont sample from the approximate first appearance of *Eomonotis* was placed in the *postera* Zone means the Columbianus III subzone must be strongly reduced at Williston Lake in order to place the top of *postera* close to the base of *Eomonotis* (Figs 3.2, 3.3). This is consistent with published biostratigraphic logs of Black Bear Ridge (Orchard et al., 2001a; 2001b). The base of Cordilleranus, *bidentata,* and *Monotis* are all correlated and define the base of the upper Norian. At Brown Hill, the conodont sample and 58.9 m was placed in the *bidentata* zone confirming that *Eomonotis* observed at that horizon were the last appearance as that horizon approximates the middle-upper Norian boundary. Conodonts were not successfully extracted from the sample from the first *Monotis* horizon at Black Bear Ridge but it can be assumed based on the intercalibration of biostratigraphic schemes and correlation with Brown Hill that the horizon represents the base of *bidentata* conodont zone, Cordilleranus ammonoid zone, and thus the base of the upper Norian. Although some ammonoids were recovered from the field, not enough specimens were of identifiable quality to make any meaningful placement in any ammonoid faunas. Published intercalibrations do, however, allow correlations to ammonoid zones defined for the area. Ichthyolith biozones were also defined for northeastern British Columbia but no zone could be defined for the upper Norian strata (Johns et al., 1997). These

strata are dominated by the actinoptyerigian *Birgeria* with few other taxa identified (Orchard et al., 2001a).

CONCLUSIONS

This study has confirmed a long-held hypothesis that the Pardonet formation was deposited in deep, anoxic waters, at least the upper portion that was the focus of this study. Application of geochemistry also demonstrated the subtle variability in redox conditions during the deposition of the studied intervals. It was previously assumed on the lack of sedimentary structures, and shell beds containing little non-shell sediment that the Pardonet was deposited by very slow pelagic deposition. Application of paleontological and geochemical evidence allowed an alternative interpretation which emphasizes the importance of turbiditic processes over quiet pelagic processes while also emphasizing that the bivalves are indeed found in the sediments they occupied in life. Refining previous observations of lithofacies and shell-bed types into a comprehensive facies scheme allowed a better understanding of the influence of redox conditions on the distribution of flat-clams by aiding in the understanding of which facies do and do not contain *in situ* shells. Applying paleo-redox proxies also provided further evidence that *Halobia* could tolerate suboxic conditions as well as demonstrating that *Eomonotis* and *Monotis* replaced *Halobia* in this niche by occupying the same facies with the same paleo-redox conditions. Understanding the depositional environment of the Pardonet will also aid in investigations of the paleoecology of the bivalves contained within it. It may also aid in interpreting other flat-clam-rich deposits in other basins.

It is argued that the upper Pardonet formation was deposited during a regression followed by transgression on the basis of sedimentological and geochemical evidence. Interpretations presented will aid in putting the studied interval in the context of broader scale sequence stratigraphy and earlier Norian stratigraphy, however, more work is needed to make these

connections Further testing of the relationships between paleo-redox conditions, facies, and bivalve distributions will create opportunity to interpret the stratigraphy of other localities where the Pardonet formation outcrops. It may be possible to predict stratigraphic trends based on sedimentological and paleontological features that can be observed in the field before undertaking expensive geochemical analyses.

Applying paleo-redox proxies also allowed the conclusion that the northwestern margin of Pangaea was open to the ocean during the Norian stage, although, the influence of tectonics on the deposition of late Triassic sediments in Western Canada cannot be denied. It was also inferred that the persistent reducing conditions in the offshore benthic environment during the Norian was the result of the interplay of upwelling ocean currents and a hot global climate. Finally, this study demonstrated some of the difficulties of interpreting geochemical data in rocks with highly variable amounts of carbonate between facies and the need to develop better methods for applying geochemical proxies in limestone.

BIBLIOGRAPHY

- ALGEO, T. J., TRIBOVILLARD, N. 2009. Environmental analysis of paleoceanographic systems based on molybdenum-uranium covariation. Chemical Geology, v. 268, p. 211-225.
- AMATI, L., FELDMANN, R. M., ZONNEVELD, J.-P. 2004. A new family of Triassic lobsters (Decapoda: Astacidea) from British Columbia and its phylogenetic context. Journal of Paleontology, v. 78, p. 150-168.
- ANDO, H. 1987. Paleobiological study of the Late Triassic bivalve *Monotis* from Japan. The University Museum, The University of Tokyo, Bulletin, v. 30, p. 1-110.
- BARSS, D. L., MONTANDON, F. A. 1981. Sukunka-Bullmoose gas fields: Models for a developing trend in the southern foothills of Northeast British Columbia. Bulletin of Canadian Petroleum Geology, v. 29, p. 293-333.
- BERANEK, L. P. MORTENSEN, J. K. 2011. The timing and provenance record of the Late Permian Klondike orogeny in northwestern Canada and arc-continent collision along western North America. Tectonics, v. 30, TC5017. https://doi.org/10.1029/2010TC002849.
- BIRDWELL, J.E., WILSON, S.A. 2021 Geochemical and mineralogical properties of Boquillas Shale geochemical reference material ShBOQ-1. Fact Sheet, USGS Numbered Series. U.S. Geological Survey, 4 p.
- BLAKE, D. B., ZONNEVELD, J.-P. 2004. *Carniaster orchardi* new genus and species (Echinodermata: Asteroidea), The first Triassic asteroid from the western hemisphere. Journal of Paleontology, v. 78, p. 723-730.
- BOUMA, A. H. 1962.Sedimentology of some flysch deposits. A graphic approach to facies interpretation. Elsevier, Amsterdam, 167 p.
- BOUMA, A. H. 1973. Contourites in Niesenflysch, Switzerland. Eclogae Geologicae Helvetiae, v. 66, p. 315-323.
- BRUMSACK, H.-J. 2006. The trace metal content of recent organic carbon-rich sediments: Implications for Cretaceous black shale formation. Palaeogeography, Palaeoclimatology, Palaeoecology, v. 232, p. 344-361.
- CALVERT, S. E., PEDERSEN, T. F. 1993. Geochemistry of Recent oxic and anoxic marine sediments: Implications for the geological record. Marine Geology, v. 113, p. 67-88.
- CAMPBELL, H.J. 1994. The Triassic bivalves *Halobia* and *Daonella* in New Zealand, New Caledonia, and Svalbard. Institute of Geological & Nuclear Sciences Monograph, v. 4, p. 1-166.
- CATUNEANU, O. 2006. Principles of Sequence Stratigraphy. Elsevier. 388 p.
- CATUNEANU, O. 2019. Model-independent sequence stratigraphy. Earth-Science Reviews, v. 188, p. 312-388.
- COLQUHOUN, D. J. 1960. Triassic stratigraphy of Western Central Canada. Doctoral Thesis, University of Illinois.
- COOK, H. E., HINE, A. C., MULLINS, H. T. (eds) 1983. Platform Margin and Deep Water Carbonates. SEPM Short Courses no. 12.

- COOK, H. E., MULLINS, H. T. 1983. Basin margin environment. *In* SCHOLLE P. A., BEBOUT, D. G., MOORE, C. H. (eds) Carbonate Depositional Environments, AAPG Memoir 33, p. 539-617.
- CREVELLO, P. D., SCHLAGER, W. 1980. Carbonate debris sheets and turbidites, Exuma Sound, Bahamas. Journal of Sedimentary Petrology, v. 50, p. 1121-1147.
- DATTILO, B. F., BRETT, C.E., TSUJITA, C. J., FAIRHURST, R. 2008. Sediment supply versus storm winnowing in the development of muddy and shelly interbeds from the Upper Ordovician of the Cincinnati region, USA. Canadian Journal of Earth Sciences, v. 45, p. 243-265.
- DAVIES, P. J., BUBELA, B., FERGUSON, J. 1978. The formation of ooids. Sedimentology, v. 25, p. 703-730.
- DAVIES, G. R. 1977. Turbidites, debris sheets, and truncation structures in upper Paleozoic deep-water carbonates of the Sverdrup basin, Arctic Archipelago. *In* COOK, H. E., ENOS, P. (eds) Deep-Water Carbonate Environments. SEPM Special Publication, no. 25, p. 221-247.
- DAVIES, G.R. 1997a. The Triassic of the Western Canada Sedimentary Basin: tectonic and stratigraphic framework, paleogeography, paleoclimate and biota. Bulletin of Canadian Petroleum Geology, v. 45, p. 434-460.
- DAVIES, G.R. 1997b. The Upper Triassic Baldonnel and Pardonet formations, Western Canada Sedimentary Basin. Bulletin of Canadian Petroleum Geology, v. 45, p. 643-674.
- DE CAPOA BONARDI, P. 1984. *Halobia* zones in the pelagic Late Triassic sequences of the central Mediterranean area. Bollettino della Società Paleontologica Italiana, v. 23, p. 91-102.
- DE GASPERI, A., CATUNEANU, O. 2014. Sequence stratigraphy of the Eocene turbidite reservoirs in Albacora field, Campos Basin, offshore Brazil. AAPG Bulletin, v. 98, p. 279-313.
- DEL PIERO, N., RIGAUD, S., TAKAHASHI. S, POULTON, S. W., MARTINI, R. 2020. Unravelling the paleoecology of flat clams: New insights from an Upper Triassic halobiid bivalve. Global and Planetary Change, v. 190, p. 1-17.
- DIEVERT, R. V., BARCLAY, K. M., MOLINARO, D. J., LEIGHTON, L. R. 2019. Evaluation the effects of morphology and orientation on feeding in atrypide brachiopods using 3-D printed models. Palaeogeography, Palaeoclimatology, Palaeoecology, v. 527, p. 77-86.
- DIEVERT, R. V., GINGRAS, M. K., LEIGHTON, L. R. 2021. The functional performance of productidine brachiopods in relation to environmental variables. Lethaia, v. 54, p. 806-822.
- DILL, H. 1986. Metallogenesis of early Paleozoic graptolite shales from the Graefethal Horst (northern Bavaria-Federal Republic of Germany). Economic Geology, v. 81, p. 889-903.
- DUPONT, L. M., DONNER, B., VIDAL, L., PÉREZ, E. M., WEFER, G. 2005. Linking desert evolution and coastal upwelling: Pliocene climate change in Namibia. Geology, v. 33, p. 461-464.
- EBERLI, G. P. 1987. Carbonate turbidite sequences deposited in rift-basins of the Jurassic Tethys Ocean (eastern Alps, Switzerland). Sedimentology, v.34, p. 363-388.

- EDWARDS, D. E., BARCLAY, J. E., GIBSON, D. W., KVILL, G. E., HALTON, E. 1994. Triassic strata of the Western Canada sedimentary basin. *In* Mossop, G. D., Shetsen, I. (eds.) Geological atlas of the Western Canada sedimentary basin. Canadian Society of Petroleum Geologists and Alberta Research Council, Calgary. p. 259-271.
- EKDALE, A. A. 1985. Paleoecology of the marine endobenthos. Palaeogeography, Palaeoclimatology, Palaeoecology, v. 50, p. 63-81.
- ENDERS, A., LEHMANN, J. 2012. Comparison of wet-digestion and dry-ashing methods for total elemental analysis of biochar. Communications in Soil Science and Plant Analysis, v. 43, p. 1042-1052. doi: 10.1080/00103624.2012.656167
- FERRI, F., ZONNEVELD, J.-P. 2008. Were Triassic rocks of the Western Canada Sedimentary Basin deposited in a foreland? Reservoir, v. 35, p. 12-14.
- GAGE, J. D. 1996. Why are there so many species in deep-sea sediments? Journal of Experimental Marine Biology and Ecology, v. 200, p. 257-286.
- GARCIA, E. A., MOLINARO, D. J., LEIGHTON, L. R. 2018. Testing the function of productide brachiopod spines on arenaceous substrates using 3D printed models. Palaeogeography, Palaeoclimatology, Palaeoecology, v. 511, p. 541-549.
- GIBSON, D. W. 1971. Triassic stratigraphy of the Sikanni Chief River-Pine Pass region, Rocky Mountain Foothills, northeastern British Columbia. Geological Survey of Canada, Paper 70-31.
- GIBSON, D. W. 1975. Triassic rocks of the Rocky Mountain Foothills and Frontranges of northeastern British Columbia and west-central Alberta. Geological Survey of Canada, Bulletin 247, 61p.
- GIBSON, D. W., EDWARDS, D. E. 1990 An overview of Triassic stratigraphy and depositional environments in the Rocky Mountain Foothills and Western Interior Plains, Peace River Arch area, northeastern British Columbia. Bulletin of Canadian Petroleum Geology, v. 38A, p. 146-158.
- GIBSON, D. W. 1993. Triassic. *In* Stott, D. F., Aitken, J. D. (eds.) Sedimentary cover of the craton in Canada, p. 294-320. Ottawa: Geological Survey of Canada, Volume 5.
- GOLONKA, J., ROSS, M. I., SCOTESE, C. R. 1994. Phanerozoic paleogeographic and paleoclimatic modeling maps. *In* EMBRY, A. F., BEAUCHAMP, B., GLASS, D. (eds.) Pangea: Global environments and resources. Canadian Society of Petroleum Geologists, Special Publication, Memoir 17, p. 1-47.
- GOLONKA, J. 2007. Later Triassic and Early Jurassic palaeogeography of the world. Palaeogeography, Palaeoclimatology, Palaeoecology, v. 244, p. 297-307.
- GREENE, S. E., BOTTJER, D. J., HAGDORN, H., ZONNEVELD, J.-P. 2011. The Mesozoic return of Paleozoic faunal constituents: A decoupling of taxonomic and ecological dominance during the recovery from the end-Permian mass extinction. Palaeogeography, Palaeoclimatology, Palaeoecology, v. 308, p. 224-232.
- GREENE, S. E., BOTTJER, D. J., CORSETTI, F. A., BERELSON, W. M., ZONNEVELD, J.-P. 2012. A subseafloor carbonate factory across the Triassic-Jurassic transition. Geology, v. 40, p. 1043-1046.

- GRUBER, B. 1976. Neue Ergebnisse auf dem gebiete der Ökologie, Stratigraphie und Phylogenie der Halobien (Bivalvia). Mitteilungen der Gesellschaft der Geologie und Bergbaustudented in Österreich, v. 23, p. 181-198.
- HARRIS, N. B., MCMILLAN, J. M., KNAPP, L. J., MASTALERZ, M. 2018. Organic matter accumulation in the Upper Devonian Duvernay formation, Western Canada Sedimentary Basin, from sequence stratigraphic analysis and geochemical proxies. Sedimentary Geology, v. 376, p. 185-203.
- HATCH, J. R., LEVENTHAL, J. S. 1992. Relationship between inferred redox potential of the depositional environment and geochemistry of the Upper Pennsylvanian (Missourian) Stark Shale Member of the Dennis Limestone, Wabaunsee County, Kansas, U.S.A. Chemical Geology, v. 99, p. 65-82.
- HODYCH, J. P., DUNNING, G. R. 1992. Did the Manicouagan impact trigger end-of-Triassic mass extinction? Geology, v. 20, p. 51-54.
- HUNT, A. D., RATCLIFFE, J. D. 1959. Triassic Stratigraphy, Peace River Area, Alberta and British Columbia, Canada. AAPG Bulletin, v. 43, p. 563-589.
- IRVING, E. 1977. Drift of the major continental blocks since the Devonian. Nature, v. 270, p. 304-309.
- JAMES, N. P., JONES, B. 2016. Origin of Carbonate Sedimentary Rocks. John Wiley & Sons Ltd. 446 p.
- JARAULA, C. M. B., GRICE, K., TWITCHETT, R. J., BÖTTCHER, M. E., LEMETAYER, P., DASTIDAR, A. G., OPAZO, L. F. 2013. Elevated pCO2 leading to Late Triassic extinction, persistent photic zone euxinia, and rising sea levels. Geology, v. 41, p. 955-958.
- JEFFERIES, R.P.S., MINTON, P. 1965. The mode of life of two Jurassic species of '*Posidonia'* (Bivalvia). Palaeontology, v. 8, p. 156-185.
- JOHNS, M. J., BARNES, C. R., ORCHARD, M. J. 1997. Taxonomy and biostratigraphy of middle and late Triassic elasmobranch ichthyoliths from northeastern British Columbia. Geological Survey of Canada, Bulletin, v. 502, 235 p.
- KIDWELL, S. M., BOSENCE, D. W. J., 1991. Taphonomy and time-averaging of marine shelly faunas. *In* ALLISON, P. A. AND BRIGGS, D. E. G. (eds.) Taphonomy: Releasing data locked in the fossil record. Topics in Geobiology, Plenum Press, New York, v. 9, p. 115-209.
- KLINKHAMMER, G. P., PALMER, M. R. 1991. Uranium in the oceans: Where it goes and why. Geochimica et Cosmochimica Acta, v. 55, p. 1799-1806.
- KONHAUSER, K. O. 2007. Introduction to Geomicrobiology. Blackwell, Malden, Massachusetts.
- LAGRANGE, M. T., KONHAUSER, K. O., CATUNEANU, O., HARRIS, B. S., PLAYTER, T. L. GINGRAS, M. K. 2020. Sequence stratigraphy in organic-rich marine mudstone successions using chemostatigraphic datasets. Earth Science Reviews, v. 203, 103147. DOI: https://doi-org/10.1016/j.earscirev.2020.103137.
- LECKIE, R. M., BRALOWER, T. J., CASHMAN, R. 2002. Oceanic anoxic events and plankton evolution: Biotic response to tectonic forcing during the mid-Cretaceous. Paleoceanography and Paleoclimatology, v. 17, p. 13-1-13-29. DOI: https://doi-org.login.ezproxy.library.ualberta.ca/10.1029/2001PA000623

- LEI, J. Z. X., HUSSON, J. M., GOLDING, M. L., ORCHARD, M. J., ZONNEVELD, J.-P. 2021. Stable carbon isotope record of carbonate across the Carnian-Norian boundary at the prospective GSSP section at Black Bear Ridge, British Columbia, Canada. Albertiana, v. 46, p. 1-10.
- LOGAN, R. F. 1960. The central Namib Desert, South West Africa. Publ. nat. Acad. Sci. 758, 1-141.
- LOMBARD, A. 1971. La Nappe du Niesen et son Flysch. Matériaux pour la carte géologique de la Suisse, v. 141, p. 252.
- LOUTIT, T. S., HARDENBOL, J., VAIL, P. R., BAUM, G. R. 1988. Condensed sections: The key to age determination and correlation of continental margin sequences. *In* WILGUS, C. K., HASTINGS, B. S., KENDALL, C. G. S., POSAMENTIER, H. W., ROSS, C. A., VAN WAGONER, J. C. Sea Level Changes - An integrated approach. Society of Economic Paleontologists and Geologists, Special Publication, v. 42, p. 183-213.
- MACNEIL, A. J., JONES, B. 2006. Sequence stratigraphy of a Late Devonian ramp-situated reef system in the Western Canadian Sedimentary Basin: Dynamic responses to sea-level change and regressive reef development. Sedimentology, v. 53, p. 321-359.
- MARTINDALE, R. C., ZONNEVELD, J.-P., BOTTJER, D. J. 2010. Microbial framework in Upper Triassic (Carnian) patch reefs from Williston Lake, British Columbia, Canada. Palaeogeography Palaeoclimatology Palaeoecology, v. 297, p. 609-620.
- MCGOWAN, C. 1991. An ichthyosaur forefin from the Triassic of British Columbia exemplifying Jurassic features. Canadian Journal of Earth Sciences, v. 28, p. 1553-1560.
- MCILREATH, I. A., JAMES, N. P. 1984. Carbonate Slopes. *In* WALKER, R. G. Facies Models, Second Edition. Geoscience Canada. P. 245-257.
- MCLEARN, F. H. 1930. A preliminary study of the faunas of the Upper Triassic Schooler Creek formation, western Peace River, British Columbia. Transactions of the Royal Society of Canada, v. 24, p. 13-19.
- MCLEARN, F. H. 1940. Note on the geography and geology of the Peace River Foothills. Transactions of the Royal Society of Canada, 3rd series, v. 34, p. 63-74.
- MCLEARN, F. H. 1941. Triassic stratigraphy of Brown Hill, Peace River Foothills, B. C. Transactions of the Royal Society of Canada, series 3, section 4, v. 55, p. 93-104.
- MCLEARN, F. H. 1947. The Triassic *Nathorstites* fauna in northeastern British Columbia. Geological Survey of Canada, Paper 47-24, 27p.
- MCLENNAN, S.M., 2001. Relationships between the trace element composition of sedimentary rocks and upper continental crust. Geochemistry, Geophysics, Geosystems 2
- MCROBERTS, C.A. 1997. Late Triassic North American halobiid bivalves: stratigraphic distribution, diversity trends, and their circum-Pacific correlation, *in* DICKINS, J. M., YANG, Z., YIN, H., LUCAS, S G., ACHARYYA, S.K. (eds) Late Paleozoic and Early Mesozoic circum-Pacific events and their global correlation. Cambridge University Press, World and Regional Geology, v. 10, p. 198-208.
- MCROBERTS, C.A., KRYSTYN, L., & SHEA, A. 2008. Rhaetian (Late Triassic) *Monotis* (Bivalvia: Pectinoida) from the eastern Northern Calcareous Alps (Austria) and the end-Norian crisis in pelagic faunas. Paleontology, v. 51, p.571-535.

- MCROBERTS, C.A. 2010. Biochronology of Triassic bivalves, *in* Lucas, S. G. (ed.) The Triassic Timescale. Geological Soceity, London, Special Publications, v. 334, p. 201-219.
- MCROBERTS, C.A. 2011. Late Triassic Bivalvia (chiefly Halobiidae and Monotidae) from the Pardonet formation, Williston Lake area, Northeastern British Columbia, Canada. Journal of Paleontology, v. 85, p. 613-664.
- MORFORD, J. L., MARTIN W. R., CARNEY, C. M. 2009. Uranium diagenesis in sediments underlying bottom waters with high oxygen content. Geochimica et Cosmochimica Acta, v. 73, p. 2920-2937.
- MORRISON, J. M., CODISPOTI, L. A. SMITH, S. L., WISHNER, K., FLAGG, C., GARDNER, W. D., GAURIN, S. NAQVI, S. W. A. MANGHANI, V. PROSPERIE, L., GUNDERSEN, J. S. 1999. The oxygen minimum zone in the Arabian Sea during 1995. Deep-Sea Research II, Topical Studies in Oceanography, v. 46, p. 1903-1931.
- NARDIN, T. R., HEIN, F. J., GORSLINE, D. S., EDWARDS, B. D. 1979. A review of mass movement processes, sediment and acoustic characteristics, and contrasts in slope and base-of-slope systems versus canyon-fan-basin floor systems. *In* DOYLE, L. J., PIKEY, O. H. (eds) Geology of Continental Slopes. SEPM Special Publication, no. 27, p. 61-73.
- NICHOLLS, E. L. MANABE, M. 2001. A new genus of ichthyosaur from the Late Triassic Pardonet formation of British Columbia: Bridging the Triassic-Jurassic gap. Canadian Journal of Earth Sciences, v. 38, p. 983-1002.
- NICHOLLS, E. L. MANABE, M. 2004. Giant ichthyosaurs of the Triassic-A new species of *Shonisaurus* from the Pardonet formation (Norian: Late Triassic) of British Columbia. Journal of Vertebrate Paleontology, v. 24, p. 838-849.
- O'Keefe, J. D., Ahrens, T. J. 1989. Impact production of CO_2 by the Cretaceous-Tertiary extinction bolide and the resultant heating of the Earth. Nature, v. 388, p. 247-249.
- ORCHARD, M. J., ZONNEVELD, J.-P., JOHNS, M. J., MCROBERTS, C. A., SANDY, M. R., TOZER, E. T., CARRELLI, G. G. 2001a. Fossil succession and sequence stratigraphy of the Upper Triassic of Black Bear Ridge, northeast British Columbia, a GSSP prospect for the Carnian-Norian boundary. Albertiana, v. 25, p. 10-22.
- ORCHARD, M. J., MCROBERTS, C. A., TOZER, E. T., JOHNS, M. J., SANDY, M. R., SHANER, J. S. 2001b. An intercalibrated biostratigraphy of the Upper Triassic of Black Bear Ridge, Williston Lake, northeast British Columbia. Current Research, 2001-A6, Geological Survey of Canada.
- ORCHARD, M. J. 2007. A proposed Carnian-Norian Boundary GSSP at Black Bear Ridge, Northeast British Columbia, and a new conodont framework for the boundary interval. Albertiana, v. 36, p. 130-141.
- ONOUE, T., ZONNEVELD, J.-P., ORCHARD, M. J., YAMASHITA, M., YAMASHITA, K., SATO, H., KUSAKA, S. 2016. Paleoenvironmental changes across the Carnian/Norian boundary in the Black Bear Ridge section British Columbia, Canada. Palaeogeography, Palaeoclimatology, Palaeoecology, v. 441, p. 721-733.
- PAYROS, A., PUJALTE, V., ORUE-ETXEBARRIA, X. 2006. A point-sourced calciclastic submarine fan complex (Eocene Anotz formation, western Pyrenees): facies architecture, evolution and controlling factors. Sedimentology, v. 54, p. 137-168.

- PLAYTER, T., CORLETT, H., KONHAUSER, K., ROBBINS, L., ROHAIS, S., CROMBEZ, V., MACCORMACK, K., ROKOSH, D., PRENOSLO, D., FURLONG, C. M., PAWLOWICZ, J., GINGRAS, M. K., LALONDE, S., LYSTER, S., ZONNEVELD, J.-P. 2018. Clinoform identification and correlation in fine-grained sediments: A case study using the Triassic Montney formation. Sedimentology, v. 65, p. 263-302.
- POLUBOTKO, I.V., 1986. Zonal complexes of the Late Triassic halobiids in the northeastern USSR, *in* Yanshin, A.L., Dagys, A.S. (eds) Mesozoic biostratigraphy of Siberia and the Far East. Transactions of the Institute of Geology and Geophysics, Novosibirsk, v. 648, p. 118-126.
- POWELL, E. N., STANTON JR., R. J. 1996 The application of size-frequency distribution and energy flow in paleoecological analysis: An example using parautochthonous death assemblages from a variable salinity bay. Palaeogeography, Palaeoclimatology, Palaeoecology, v. 124, p. 195-231.
- PUGA-BERNABÉU, Á., WEBSTER, J. M., BEAMAN, R. J., GUILBAUD, V. 2011. Morphology and controls on the evolution of a mixed carbonate-siliciclastic submarine canyon system, Great Barrier Reef margin, northeastern Australia. Marine Geology, v. 289, p. 100-116.
- RANKEY, E. C., REEDER, S. L. 2011. Tidal sands of the Bahamian Archipelago. *In* Principles of Tidal Sedimentology. Springer, Dordrecht, 538-565.
- REVSBECH, N. P., LARSEN, L. H., GUNDERSEN, J., DALSGAARD, T., ULLOA, O., THAMDRUP, B. 2009. Determination of ultra-low oxygen concentrations in oxygen minimum zones by the STOX sensor. Limnology and Oceanography: Methods, v. 7, p. 371-381.
- RHOADS, D. C. Mass properties, stability, and ecology of marine muds related to burrowing activity. Geological Journal, Special Issue, 1970, v. 3, pp. 391-406.
- RIEDIGER, C., CARRELLI, G. G., ZONNEVELD, J.-P. Hydrocarbon source rock characterization and thermal maturity of the Upper Triassic Baldonnel and Pardonet formations, northeastern British Columbia, Canada. Bulletin of Canadian Petroleum Geology, v. 52, p. 277-301.
- ROHAIS, S., CROMBEZ, V., EUZEN, T., ZONNEVELD, J.-P. 2018. Subsidence dynamics of the Montney formation (Early Triassic, Western Canada Sedimentary Basin): insights for its geodynamic setting and wider implications. Bulletin of Canadian Petroleum Geology, v. 66, p. 128-160.
- SAGEMAN, B. B., LYONS, T. W. 2003. Geochemistry of Fine-grained Sediments and Sedimentary Rocks. *In* HOLLAND, H. D., TUREKIAN, K. K. (eds.) Treatise on Geochemistry, v. 7, p. 115-158.
- SAVRDA, C. E., BOTTJER, D. J. 1986. Trace-fossil model for reconstruction of paleo-oxygenation in bottom waters. Geology, v. 14, p. 3-6.
- SCHLAGER, W., CHERMAK, A. 1979. Sediment facies of platform-basin transition, Tongue of the Ocean, Bahamas. *In* PILKEY, O. H., DOYLE, L. S. (eds) Geology of continental slopes. SEPM Special Publication no. 27, p. 193-208.
- SCHLAGER, W. 2005. Carbonate Sedimentology and Sequence Stratigraphy. Concepts in Sedimentology and Paleontology #8, SEPM. 200 p.

- SEPHTON, M. A., AMOR, K., FRANCHI, I. A., WIGNALL, P. B., NEWTON, R., ZONNEVELD, J.-P. 2002. Carbon and nitrogen isotope disturbances and an end-Norian (Late Triassic) extinction event. Geology, v. 30, p. 1119-1122.
- SEPKOSKI JR., J. J. 1981. A factor analytic description of the Phanerozoic marine fossil record. Paleobiology, v. 7, p. 36-53.
- STANLEY, G. D., ZONNEVELD, J.-P. 2011. The occurrence of the hydrozoan genus Cassianastraea from Upper Triassic (Carnian) rocks of Williston Lake, British Columbia, Canada. Journal of Paleontology, v. 85, p. 29-31.
- STEINMANN, J. W., GRAMMAR, G. M., BRUNNER, B., JONES, C. K., RIEDIGER, N., 2020. Assessing the application of trace metals as paleoproxies and a chemostatigraphic tool in carbonate systems: A case study from the "Mississippian Limestone" of the midcontinent, United States. Marine and Petroleum Geology, v. 112, 104061. https://doi.org/10.1016/j.marpetgeo.2019.104061.
- STOW, D. A. V., WEZEL, F. C., SAVELLI, D., RAINEY, S. C. R., ANGELL, G. 1984. Depositional model for calcilutites: Scaglia Rossa limestones, Umbro-Marchean Apennines *in* STOW, D. A. V., PIPER, D. J. W. (*eds*) Fine-grained sediments: Deep-water processes and facies, Geological Society, London, Special Publications, v. 15, p, 223-241.
- SUN, Y. D., ORCHARD, M. J., KOCSIS, Á. T., JOACHIMSKI, M. M. 2020. Carnian-Norian (Late Triassic) climate change: Evidence from conodont oxygen isotope thermometry with implications for reef development and Wrangelian tectonics. Earth and Planetary Science Letters, v. 534, 116082. https://doi.org/10.1016/j.epsl.2020.116082.
- TOZER, E. T. 1982a. Late Triassic (upper Norian) and earliest Jurassic (Hettangian) rocks and ammonoid faunas, Halfway River and Pine Pass map areas, British Columbia. Geological Survey of Canada Paper, v. 82 p. 843-876.
- TOZER, E. T., 1982b. Marine Triassic faunas of North America; their significance for assessing plate and terrane movements. Geologische Rundschau, v. 7, p. 1077-1104.
- TOZER, E. T. 1984. The Trias and its ammonoids: The evolution of a time scale. Geological Survey of Canada, Miscelaneous Report 35, 171 p.
- TOZER, E. T. 1994. Canadian triassic ammonoid faunas. Geological Survey of Canada Bulletin 467. 663 p.
- TRIBOVILLARD, N., RIBOULLEAU, A., LYONS, T., BAUDIN, F. 2004. Enhanced trapping of molybdenum by sulfurized marine organic matter of marine origin in Mesozoic limestones and shales. Chemical Geology, v. 213, p. 385-401.
- TRIBOVILLARD, N., ALGEO, T. J., LYONS, T., RIBOULLEAU, A. 2006. Trace metals as paleoredox and paleoproductivity proxies: An update. Chemical Geology, v. 232, p. 12-32.
- TRIBOVILLARD, N., ALGEO, T. J., BAUDIN, F., RIBOULLEAU, A. 2012. Analysis of marine environmental conditions based on molybdenum-uranium covariation: Applications to Mesozoic paleoceanography. Chemical Geology, v. 324-325, p. 46-58.
- TUNIS, G., UCHMAN, A. 1996. Ichnology of Eocene flysch deposits of the Istria Peninsula, Croatia and Slovenia. Ichnos, v. 5, p. 1-22.

- TURNER, B. W., TRÉANTON, J. A. SLATT, R. M. 2016. The use of chemostratigraphy ro refine ambiguous sequence stratigraphic correlations in marine mudrocks. An example from the Woodford Shale, Oklahoma, USA. Journal of the Geological Society, v. 173, p. 854-868.
- TYSON, R. V., PEARSON, T. H. 1991. Modern and ancient continental shelf anoxia: An overview. Geological Society, London, Special Publications, v. 58, p. 1-24.
- UCHMAN, A. 1992. An opportunistic trace fossil assemblage from the flysch of the Inoceramian beds (Campanian-Palaeocene), Bystrica Zone of the Magura Nappe, Carpathians, Poland. Cretaceous Research, v. 13, p. 539-547.
- UCHMAN, A. 2007. Deep-sea trace fossils from the mixed carbonate-siliciclastic flysch of the Monte Antola formation (Late Campanian-Maastrichtian), North Apennines, Italy. Cretaceous Research, v. 28, p. 980-1004.
- VAN DER WEIJDEN, C. H. 2002. Pitfalls of normalization of marine geochemical data using a common divisor. Marine Geology, v. 184, p.167-187.
- VIGORITO, M., MURRU, M., SIMONE, L. 2005. Anatomy of a submarine channel system and related fan in a foramol/rhodalgal carbonate sedimentary setting: A case history from the Miocene syn-rift Sardinia Basin, Italy.
- VOGEL, S., LaBarbera, M. 1978. Simple flow tanks for research and teaching. Bioscience, v. 28, p. 638-643.
- VON GUNTEN, K. ALAM, M. S., HUBMANN, M., OK, Y. S., KONHAUSER, K. O., ALESSI, D. S. 2017. Modified sequential extraction for biochar and petroleum coke: Metal release potential and its environmental implications. Bioresource technology, v. 236, p. 106-110. doi: 10.1016/j.biortech.2017.03.162
- WETZEL, A., UCHMAN, A. 2001. Sequential colonization of muddy turbidites in the Eocene Beloveža formation, Carpathians, Poland. Palaeogeography, Palaeoclimatology, Palaeoecology, v. 168, p. 171-186.
- WHITEAVES, J. F. 1889. On some fossils from the Triassic rocks of British Columbia. Contributions to Canadian Palaeontology, Geological Survey of Canada, v. 1, p. 127-149.
- WIGNALL, P.B., SIMMS, M.J. 1990. Pseudoplankton. Paleontology, v. 33, p. 359-378.
- WIGNALL, P.B., NEWTON, R. 1998. Pyrite framboid diameter as a measure of oxygen deficiency in ancient mudrocks. American Journal of Science, v. 298, p.537-552.
- WIGNALL, P. B., TWITCHETT, R. J. 2002. Extent, duration, and nature of the Permian-Triassic superanoxic event. In Koeberl, C., MacLeod, K. C. (*eds.*) Catastrophic events and mass extinctions: Impacts and beyond. Geological Society of America, Special Paper, v. 356, p. 395-413
- WIGNALL, P. B., ZONNEVELD, J.-P., NEWTON, R. J., AMOR, K., SEPHTON, M. A., HARTLEY, S. 2007. The end Triassic extinction record of Williston Lake, British Columbia. Palaeogeography, Palaeoclimatology, Palaeoecology, v. 253, p. 385-406.
- WILKIN, R.T., BARNES, H.L., BRANTLEY, S.L. 1996. The size distribution of framboidal pyrite in modern sediments: An indicator of redox conditions. Geochimica et Cosmochimica Acta, v. 60, p. 3897-3912.
- WILLIFORD, K. H., ORCHARD, M. J., ZONNEVELD, J.-P., MCROBERTS, C. BEATTY, T. W. 2007. A record of stable organic carbon isotopes from the Carnian-Norian boundary

section at Black Bear Ridge, Williston Lake, British Columbia, Canada. Albertiana, v. 36, p. 146-148.

- WU, X., LUO, H., ZHANG, J., CHEN, Q., FANG, X., WANG, W. LI, W., SHI, Z, ZHANG, Y. 2023 Volcanism-driven marine eutrophication in the end-Ordovician: Evidence from radiolarians and trace elements of black shale in South China. Journal of Asian Earth Sciences, v. 253, 105687. DOI: https://doi-org/10.1016/j.jseaes.2023.105687
- YIN, H.F. 2003. Triassic biostratigraphy of China, *in* ZHANG, W., CHEN, P., PALMER, A. R. (eds) Biostratigraphy of China. Science Press, Beijing, p. 379-422.
- ZAKHAROV, V.A., BOGOMOLOV, Y.I., ILYINA, V. I., KONSTANTINOV, A. G., KURUSHIN, N. I., LEBEDEVA, N. K., MELEDINA, S. V., NIKITENKO, B. L., SOBOLEV, E. S., SHURYGIN, B. N. 1997. Boreal zonal standard and biostratigraphy of the Siberian Mesozoic. Russian Geology and Geophysics, v. 38, p. 927-956.
- ZHENG, Y., ANDERSON, R. F., VAN GEEN, A., KUWABARA, J. Authigenic molybdenum formation in marine sediments: a link to pore water sulfide in the Santa Barbara Basin. Geochimica et Cosmochimica Acta, v. 64, p. 4165-4178.
- ZHENG, Y., ANDERSON, R. F., VAN GEEN, A., FLEISHER, M. Q. 2002. Remobilization of authigenic uranium in marine sediments by bioturbation. Geochimica et Cosmochimica Acta, v. 66, p. 1759-1772.
- ZONNEVELD, J.-P. 2001. Middle Triassic biostromes from the Liard formation, British Columbia, Canada: Oldest examples from the Mesozoic of NW Pangea. Sedimentary Geology, v. 145, p. 317-341.
- ZONNEVELD, J.-P., CARRELLI, G.G., RIEDIGER, C. 2004. Sedimentology of the Upper Triassic Charlie Lake, Baldonnel and Pardonet formations from outcrop exposures in the southern Trutch region, northeastern British Columbia. Bulletin of Canadian Petroleum Geology, v. 52, p. 343-375.
- ZONNEVELD, J.-P., BEATTY, T. W., PEMBERTON, S. G. 2007a. Lingulide brachiopods and the trace fossil *Lingulichnus* from the Triassic of western Canada: Implications for faunal recovery after the end-Permian mass extinction. Palaios, v. 22, p. 74-97.
- ZONNEVELD, J.-P., HENDERSON, C., STANLEY, G. D., ORCHARD, M. J., GINGRAS, M. K. 2007b. Oldest scleractinian coral reefs on the North American craton: Upper Triassic (Carnian), northeastern British Columbia, Canada. Palaeogeography Palaeoclimatology Palaeoecology, v. 243, p. 421-450.
- ZONNEVELD, J.-P., BEATTY, T.W., WILLIFORD, K.H., ORCHARD, M.J., MCROBERTS, C.A. 2010. Stratigraphy and sedimentology of the lower Black Bear Ridge section, British Columbia: candidate for the base-Norian GSSP. Stratigraphy, v. 7, p. 61-82.
- ZONNEVELD, J.-P., BISTRAN, R. 2013. Bored bivalves in Upper Triassic (Norian) event beds, Northeastern British Columbia, Canada. Ichnos, v. 20, p. 88-98.
- ZONNEVELD, J.-P., MOSLOW, T. F. Palaeogeographic setting, lithostratigraphy, and sedimentary frameword of the Lower Triassic Montney formation of western Alberta and northeastern British Columbia. Bulletin of Canadian Petroleum Geology, v. 66, p. 93-127.
- ZONNEVELD, J-P. 2022. Triassic sedimentary & stratigraphic framework: Williston Lake, northeastern British Columbia. Solaster Geosciences Inc., St. Albert, Alberta, Canada.